STRUCTURAL CHARACTERIZATION OF ADENO-ASSOCIATED VIRUS SEROTYPES 1 AND 6 GLYCAN INTERACTIONS

By

ROBERT NG

A DISSERTATION PRESENTED TO THE GRADUATE SCHOOL
OF THE UNIVERSITY OF FLORIDA IN PARTIAL FULFILLMENT
OF THE REQUIREMENTS FOR THE DEGREE OF
DOCTOR OF PHILOSOPHY

UNIVERSITY OF FLORIDA

2012

To my parents, family and friends.

ACKNOWLEDGMENTS

I would like to begin by thanking my parents; Ng Mok Meng, and Tan Moei Moei for the sacrifices they made to provide me with great opportunities and I am forever grateful because they continue to love, support, and encourage me. To my brothers (Robin Ng and Ebert Ng) and sisters (Jeny Ng, Helen Ng, and Helni Ng), and grandparents, especially (in loving memory) Tan A Kie for valuable advice and warm companionships. I feel extremely indebted and honored to be mentored by Dr. Mavis Agbandje-McKenna who believes in my abilities and patiently nurture the scientist in me. I am always and forever grateful for the encouragement and opportunities she has provided me and the personal counseling sessions. This dissertation will be impossible to complete without her tremendous assistance. I would also like to thank Dr. Robert McKenna for being a great teacher and fielder of my incessant queries. My committee members, Dr. James B. Flanegan, Dr. Nicholas Muzyczka, Dr. ArunSrivastava and Dr. Richard Snyder have been extremely encouraging and helpful and provided critical inputs. I would also like to thank the collaborators, Dr. Richard Jude Samulski, Dr. Jay Chiorini, Dr. David F. Smith; UF Vector core and the beamline scientists at CHESS for the resources and time invested in my work. I greatly appreciate the help offered by the administrative staff of the IDP, BMB and UF International Center. I am grateful to be a member of ‘The McKenna Lab’ which has been my family away from home. Dr. Lakshmanan Govindasamy, Dr. Hyun-Joo Nam, Dr. Antonette Bennett, Dr. Brittney L. Gurda, Mike DiMattia, and Edward B. Miller deserve special thanks for teaching me the techniques used in the lab and also for invaluable advice; Dr. Art Robbins, Dr. John Domsic, Dr. Katherine Sippel, Dr. Sujata Halder, Dr. Balendu Avvaru, Dr. Balasubramanian Venkatakrisnan, Lawrence Tartaglia, Lauren Drouin, Michelle Zak,

Mayank Aggarwal, Yu-Shan Tseng, Bridget Lins, Harald Messer, Chris Boone, Farzaneh Tondnevis, and Lin-Ya Huang for their help and to share great moments with me. Special thanks to Dr. Sujata Halder, who helped me during this last year in the program and the process of writing this dissertation. I would like to thank the high school, MD, and undergraduate students that I had taught over the years, especially Angela McCall, Yomi Fabunmi, and Jordan Zeldin for being patient with me. For my one-year mentor in Master degree, Dr. Thomas O'Brien, I will never forget his kindness and warmness to share and teach me during my first year in US. I also thank my rotation mentors Dr. Sergei Zolotukhin and Dr. Scott Greishaber who helped and mentored me immensely in my first year in IDP. I am grateful to have been blessed with such an amazing group of friends for being present at all the special events in my life including birthdays, farewells, new years, and always being there when I needed you. Last but not least, my heartfelt thanks to my lovely girl friend, Yue Liu, whose unconditional love, tolerance, and support has helped me tremendously in this memorable journey.

TABLE OF CONTENTS

LIST OF TABLES

LIST OF FIGURES

LIST OF ABBREVIATIONS

AAV	Adeno-associated virus
ADV	Aleutian mink disease virus
BPV1	bovine parvovirus 1
CAR	coxsackie and adenovirus receptor
CFG	consortium for functional glycomics
Cryo-EM	cryo-electron microscopy
CPV	canine parvovirus
DMEM	dulbecco’s modified eagle medium
DNA	deoxyribonucleic acid
EDTA	ethylene diaminetetraacetic acid
EGFR	epidermal growth factor receptor
ELISA	Enzyme-Linked Immunosorbent Assay
EM	electron microscopy
FGFR1	fibroblast growth factor receptor 1
FPV	feline panleukopenia virus
H-1PV	human tumor isolated 1 parvovirus
HBoV	human bocavirus
HEK	Human Embryonic Kidney
HGFR	hepatocyte growth factor receptor
HIV	human immuno-deficiency virus
HS	heparin sulfate
HSPG	heparan sulfate proteoglycan
HSV	herpes simplex virus
ITR	inverted terminal repeats

LamR	laminin receptor
mRNA	messenger ribonucleic acid
Neu5Ac	N-acetylneuraminic acid
NLS	nuclear localization signal
NT	nucleotides
PBS	phosphate buffer saline
PDGFR	platelet-derived growth factor receptor
PEG	polyethylene glycol
PLA_2	phospholipase A_2
PPV	porcine parvovirus
QPCR	quantitative PCR
RFU	relative fluorescence units
RNA	ribonucleic acid
SIA	sialic acid
ssDNA	single-stranded deoxyribonucleic acid
TfR	transferrin receptor
VLPs	virus like particle
VP	viral protein

Abstract of Dissertation Presented to the Graduate School
of the University of Florida in Partial Fulfillment of the
Requirements for the Degree of Doctor of Philosophy

STRUCTURAL CHARACTERIZATION OF ADENO-ASSOCIATED VIRUS SEROTYPES 1 AND 6 GLYCAN INTERACTIONS

By

Robert Ng

August 2012

Chair: Mavis Agbandje-McKenna
Major: Medical Science- Biochemistry and Molecular Biology

Adeno-Associated Viruses (AAVs) are small ssDNA viruses with the ability to package non-genomic DNA for therapeutic gene delivery. Due to their non-pathogenicity and ability to transduce non-dividing and dividing cells, these viruses have generated significant interest in their development as therapeutic vectors. These properties dictate the tissue of choice for a particular gene delivery application. Towards understanding the capsid determinant(s) of these functions, we have employed AAV1 and AAV6, which differ by just 6 of 736 VP residues yet exhibit tissue and transduction differences, as models for receptor attachment site characterization. AAV1 binds sialic acid (SIA), while AAV6 binds both SIA and heparan sulfate (HS).

The crystal structures of AAV1 and AAV6 at 2.5Å and 3.0Å resolution showed 5 of 6 differing AAV1/AAV6 amino acids within the ordered VP structure localized proximal to the icosahedral three-fold axis and identified this capsid region as dictating important functions during infection. A series of reciprocal single residue mutations (AAV1 to AAV6 and AAV6 to AAV1) were thus generated to interrogate the role of the interior and exterior residues in dictating transduction efficiency. Quantitative comparisons of virus titers using ELISA, qPCR, and a HEK293 GFP infectivity assay show no significant

differences in capsid assembly, genome packaging, and cellular transduction, respectively, among recombinant wild-type AAV1 and AAV6 and their mutations. In addition, to structurally characterizing the glycan receptor interaction of AAV1 with SIA,X-ray crystallography was used to map it's binding site on the AAV1 capsid to a region conserved in AAV6, suggesting that these two viruses utilize the same capsid region for this interaction. Site-directed mutagenesis and biochemical studies are underway to confirm this finding. With respect to HS binding, the docking algorithm DOCK6 was used as to localize a potential binding site to a region on the AAV6 capsid that contains an AAV1/AAV6 E531K residue difference consistent with previous mutagenesis and biochemical data. Data arising from these studies will aid the targeting of the AAV capsid to specific tissues or receptor populations for improved targeted gene delivery through recombinant DNA engineering.

CHAPTER 1
BACKGROUND AND INTRODUCTION

Gene Therapy and Gene Delivery Vectors

Gene therapy can be defined as the transfer of new functional genetic material to the cells of an individual resulting in therapeutic benefit (216). Since the first successful gene therapy trial by Rosenberg *et al.* using retrovirus to deliver the genetic marker neomycin into melanoma patients in 1990 (253), gene therapy has developed immensely. Within a decade, there were more than 550 clinical trials underway (http://www.wiley.com/legacy/wileychi/genmed/clinical). In 2012, over 1600 clinical trials had been completed or underway(99). However, there are several challenges remaining that need to be overcome. These include: complexity of multi-gene disorders, the design of an effective delivery vector, tissue specificity, the control of transgene expression, patient immune rejection, and vector pathogenicity(54). In order to overcome these challenges, more efforts are required to understand the basic molecular biology of the vectors which can be used to improve safe and efficiency. One key determinant for the clinical success of gene therapy is the efficiency of gene transfer into the cells of patients. The gene delivery vector must possess special characteristics and mechanisms that allow it to pass through apolar and hydrophobic cellular membranes and be stable enough to deliver its cargo into the nucleus (116). In order, these include engineering the vector from immune rejection in the extracellular milieu, carrying DNA to penetrate through cellular membranes, protecting the DNA from cytoplasmic (enzymatic) degradation factors, and effectively expressing the transgene product in the nucleus. Moreover, host safety and high production yield also play major

roles in the development of a gene therapy system. Generally, gene therapy vector can be divided into non-viral and viral vectors (116).

Non-viral Delivery Vectors

Besides naked DNA injection which is generally facilitated by high pressure injection or electroporation (140, 159), current ongoing non-viral gene delivery involves either a cationic polymer system, a nanoparticle system, lipoplex, or a multifunctional envelope-type nano device (MEND) as which described below (145).

Cationic Polymer System

Based on their natural positively charged properties, various cationic polymers have been shown to effectively condense anion-rich DNA, termed polyplexes, and attach to highly sulfated glycosaminoglycans (GAG) on the cell surface (162). This is then followed by endocytosis and plasmid expression. Examples of cationic polymers used for gene therapy include polyethylenimine (PEI), polypropyleniminedendrimers, poly-L-lysine (PLL), chitosan, and polyethylene glycol (PEG). Since its initial use in 1995, PEI has been the most extensively used cationic polymer system for gene delivery and it performs the best among cationic polymers (40, 162). PEI has a high transfection efficiency that can be attributed to the buffering capacity of its amine groups which are also important for endosomal disruption. The use of PEI results in a “proton-sponge” phenomenon which promotes fusion with PEI containing endosomes (13, 26). However, the tendency of PEI/DNA mixtures to form aggregates and accumulate in lung can cause cellular toxicity which reduces their potential applicability as a gene delivery vector *in vivo* (226). To overcome this setback, various formulations of PEG, amino-acids, cholesterol derivatives, and PEI molecules have been shown to create amphiphilic polymer carriers which result in increase of DNA condensation and

biocompatibility as well as a 3- to 11-fold increase in transfection efficiency (15, 46, 280). Several important factors affecting efficiency/ cytotoxicity of polyplexes are ionic strength, zeta potential molecular weight, degree of branching, and particle size. Efficiency of polymer-DNA condensation depends largely on the +/- charge ratio and zeta potential of the polyplexes. The closer the +/- ratio is to 1, the lower the zeta potential is, indicating an increase in the tendency of aggregation and cellular toxicity. Most PEI formulations studied were prepared using PEI with molecular weight of 10-800 kDa range and consist of linear and branched PEIs (162). In order to improve *in vivo* specific targeting and transgene efficiency, small ligand and glycan modifications (e.g. transferrin and glucose) on the functional group of cationic polymers have been studied (177).

Inorganic Nanoparticles

Recent advances in nanotechnology have inspired the application of nanoparticles (NPs) as gene delivery systems (290). Upon administration, specific proteins attach and adsorb nanoparticles based on their size, hydrophobicity, and surface characteristic. Adsorption of proteins to the nanoparticle surface changes its overall physicochemical properties including hydrodynamic diameter and surface charges (154, 173). These specific proteins may then determine the transfer efficiency of the nanoparticles. Another term used in nanoparticle delivery system is magnetofection which involves subsequent magnetic field exposure of nucleic acids–magnetic nanoparticles (239). This application has allowed for a safe and effective *in vivo* delivery system using superparamagnetic iron oxide nanoparticles (SPIONs) with a combination of polyplexes (SPIONs-PAA-PEI) to treat adenocarcinoma (242). In general, gene delivery using nanoparticles provides several attractive features which are not present in other non-

viral systems. First, nanoparticles provide much lower cytotoxicity, genotoxicity, and immunogenicity. Second, when combined with liposomes, they show much higher gene transfer efficiency than liposomes alone. Third, due to their small size, nanoparticles can travel with blood circulation and pass through the blood-brain barrier. This makes them a perfect vector for central nervous system (CNS) gene delivery. Iron oxide nanoparticles coated with PLL serves as a good example as *in vivo* studies show high gene transfer efficiency for glia and brain targeting following intravenous injection (308). Other examples are calcium phosphate and organically modified silica (ORMOSIL) (33).

Lipids

Similar to polyplexes, this delivery system can self-assembled based on the electrostatic interactions between lipids and DNA, termed lipoplexes. Based on lipid types, formulations of ongoing lipofection studies involve cationic (1,2-dioleoyl-3-trimethylammonium-propane (DOTAP) and 3β-[N-(N',N'-dimethylaminoethane)-carbamoyl] cholesterol (DC-Chol)) and neutral (dioleophosphatidylethanolamine (DOPE)) liposomes (296). Similar to polyplex, various lipid formulations have been shown to affect DNA condensation, packaging size, cellular toxicity, and transfection efficiency. The physicochemical characteristics of lipoplexes range between 190-240mV surface potential and pH 10-11.5. The +/- ratio and zeta potential of lipoplexes should be above 1 (176, 238). While lipofection offers an attractive attribute due to its less limited packaging size, studies have also shown that *in vivo* transfection efficiency is dependent on the liposome's packaging size. Optimal size for *in vivo* and *in vitro* transfection is 40-80nm and 200-400 nm, respectively (322). Studies have shown that PLL or antibody modifications of lipoplex surface will reduce aggregation and improve lipofection efficiency. Lipofection efficiencies depend not only on the cellular plasma

membrane permeability of the liposomes, but also on their endosome destabilizing activity. Certain lipoplexes (glycyrrhizin (GA) and tocopherol ester succinic acid (TS)) are attractive due to their pH-sensitivity which has been shown to improve gene transfer efficiency in CV-1 cells (monkey kidney fibroblast) by 100-fold (64). An example of lipoplexes that is commercially-available is lipofectamine which is widely used in mammalian cell plasmid transfections (277).

Multifunctional Envelope-type Nano Device (MEND)

MEND, introduced by Hideyoshi Harashima (166), is a novel delivery system composed of the condensed core of polyplexes containing nucleic acid which is encapsulated by a lipid envelope (liposome). While *in vivo* reporter gene administration using either positively charged lipoplex or polyplex have demonstrated limited liver delivery efficiency due to high tendency of aggregation and accumulation in lung cells, the MEND delivery system provides a higher level of luciferase activity in liver (314). It is shown that this improved liver delivery profile is attributed to the lower accumulation tendency of the MEND system in lung. Modifications of MEND systems have also been studied which include the incorporation of pH sensitive membrane lytic GALA (Glu-Ala-Leu-Ala) and other cell targeting proteins in the system (257).

Current Progress in Non-viral Gene therapy

Compared to viral gene delivery (described below), non-viral gene delivery offers a more controlled production, relatively safer delivery profile, and low or no immune rejection. In addition, its flexible modifications, highly assorted formulations, and ease of manipulations have resulted in significant increase in cell targeting, endosomal destabilization, and biocompatibility which has drawn huge attention to investigating this system for the development of gene delivery systems (184). However, there is a low

level of transfection efficiency due to structural polymorphism or heterogeneity associated with preparations of lipoplexes and polyplexes. Thus, much effort will be required to attain the high level of transfection efficiency and transgene expression obtainable by viral delivery approaches. Studies have been performed combining these systems with viral proteins which has resulted in a significant increase of transfection efficiency (20, 227, 297), which can be implemented for the development of better and promising approaches for gene delivery.

Viruses as natural nucleic acid delivery systems

Since the first gene transformations in the 1970s using DNA, RNA, or retroviruses (109, 219), these discoveries have inspired researchers to utilize viruses for development as vectors for gene therapy technology. While gene delivery using non-viral vectors has the advantages of larger production yield and low immunogenicity, gene delivery using viral vectors has been shown to have significantly higher transduction efficiency into patient cells. The difference in transduction efficiencies results from the natural life cycle properties of viruses which have evolved to infect and replicate very effectively in their natural specific hosts and cell types (117, 125). Viruses have been defined as obligate intracellular parasites that infect all domains of life, from bacteria and archaea to eukaryotes and may cause severe disease in their host (74, 169). Basic virus structure, called nucleocapsid, consists of the genomic material (DNA or RNA) which is encapsulated and protected by a protein shell (capsid). Some viruses, so called enveloped viruses, have an external lipid membrane envelope to protect the nucleocapsid and carry glycoproteins which serve as the ligand for receptor attachment on cell surfaces. The viral genome encodes various multifunctional regulatory, replication, and assembly viral proteins which are mostly toxic for host cells. Moreover,

in order to undergo efficient replication, most viruses have evolved to exploit host cell machineries for their successful replication.

Viruses can be classified based on their route of transmission, life cycle, genomic structures, and capsid morphologies (74). The most recent International Committee on Taxonomy of Viruses (ICTV) report classifies viruses into 6 orders, 94 families, 395 genera and 2475 identified species, with 72 virus families not assigned to an order (29) (http://www.ictvonline.org/). Despite the differences in life cycle among various species, most viruses are known to share common properties including viral genome packaging, specific host / cell targeting properties, and efficiency of cellular internalization. Hence, the overall idea in viral gene therapy is to genetically engineer viruses to carry therapeutic genes and effectively deliver them into the target cells. This strategy substitutes most of the wild-type viral genome with the gene of interest (including promoter and polyadenylation signals) resulting in the delivery of the target gene into patient cells without viral replication. In the case of recombinant viral vector production, maintenance of *cis*-acting elements (packaging signals and viral specific replication elements) are required for viral replication and are transiently expressed in the packaging cells (117, 125). Currently, there more than 65% of ongoing clinical trials (n=1222/1786 in 2011) utilizing viral vectors as the delivery system, with examples including gammaretrovirus, lentivirus, adenovirus and Adeno-associated virus (AAV) (http://www.wiley.com/legacy/wileychi/genmed/clinical) (Figure 1-1).

Gammaretroviral Vectors

The most clinically utilized prototype of retroviruses is Moloney-murine leukemia gammaretrovirus (MuLV) (118). Due to its natural tropism to cause and infect cancer cells in host (murine) cells, it has gained popularity as a viral vector for human cancer

therapy. MLV is a positive single stranded (ss) RNA enveloped virus with the particle size of approximately ~90nm. MLV infects and replicates within its host cells through reverse transcription to produce double stranded (ds) DNA (provirus), which is then integrated into the host chromosomes. The wild-type gammaretrovirus genome (~9-11kb) consists of three open reading frames (ORF); *gag*, *po*l and *env*, (which code for capsid proteins, reverse transcriptase polymerase, and envelope proteins, respectively) flanked by 3' and 5' long terminal repeats (LTRs). For the design of gammaretroviral vector, the gene of interest can be inserted by removing the three ORFs. However five *cis*-replicating elements are indispensable, the promoter region at the 5' LTR, the primer binding site (PBS), the 5' and 3' splice site, the packaging signal (φ), and the polypurine tract (PPT) in the 3' LTR (listed from the 5' to 3' of the genome). Studies have also shown that several accessory elements can increase the transgene expression and/or regulate neighboring gene expression caused by insertion mutation, e.g. woodchuck hepatitis post-transcriptional regulatory element (WPRE) and removal of the enhancer at the 3'LTR to generate a self-inactivating (SIN) vector.

The production of recombinant retroviral vectors was achieved by transfecting the recombinant plasmid into transformed murine cells expressing retroviral Gag, Pol and Env. Within the packaging cells, the recombinant therapeutic gene, using the packaging signal, is inserted into newly assembly recombinant gammeretroviral virions. Upon administration, these replication-defective virions will release and integrate the therapeutic gene into the host chromosome and express the transgene.

In order to design more improved tissue targeting and specificity, much effort has been put toward the modification of the Env proteins of retroviral vectors. An example is

the VSG-G pseudotype retroviral vector, in which genetically engineered vesicular stomatitis virus (VSV) G protein is used to replace retrovirus Env proteins in the packaging cells, These recombinant virions display VSV-G proteins on their envelope membrane which was shown to have higher tissue transduction efficiency in various cells (9, 317).

Lentiviral Vectors

While gammaretroviral vectors are known to only infect replicating cells, lentiviruses can infect both replicating and non-replicating cell lines (108, 174). This striking feature is attributed to the presence of accessory proteins (integrase, matrix and Vpr) which form a pre-integration complex (PIC) with the nuclear pore (278). Human Immuno-deficiency Virus (HIV) type 1 is the prototype member of Lentivirus genus in *Retroviridae* family. In addition to the ORFs of gammaretrovirus, the HIV-1 genome encodes for two regulatory (Tat and Rev) and four accessory proteins (Nef, Vpr, Vpu and Vif) which are important for the wild-type HIV life cycle. Similar to the design of the gammaretroviral vectors, the production of lentiviral vectors requires the maintenance of *cis*-replicating elements.

Since the first recombinant lentivirus used for *in vivo* gene transduction, there are currently three generations of lentiviral vectors available (267). In the first generation of the HIV delivery system (221), all HIV genes were expressed in the provirus, except for *env* which was complemented by an additional plasmid expressing VSV-G protein. Since the packaging cells express and carry ~80% of the viral genome, this approach raises concerns regarding cellular toxicity during human gene delivery. Hence, second generation vectors were designed by removal of accessory genes; include *vpr*, *vif*, and *nef*, and carried only LTR, *gag*, *pol*, *tat*, and *rev*. However, these vectors still exhibited

cellular toxicity. The current generation of lentiviral vectors are less complex and expresses only three (*gag*, *pol*, and *rev*) out of nine HIV wild-type genes (198) thus offering safer gene delivery.

The most recent progress on the production of lentiviral vector in clinical studies involves transfection of packaging cells with four different plasmids. The first plasmid contains a packaging signal (φ), a therapeutic gene, and a PPT. A self-inactivating feature is added by replacing the 3'LTR with the 5'LTR. The expression of the gene is driven by a heterologous promoter (RSV). The remaining three plasmids encode Gag and Pol, Rev, and VSV-G, respectively. Within the packaging cells, recombinant lentiviral vectors will replicate and package the gene of interest.

Adenoviral Vectors

Adenovirus is a ds DNA (~36kb) non-enveloped isocahedral virus with a particle size of ~90nm in diameter (30, 302). Currently there are more than 100 members of *Adenovirinae* family which infect a broad range of vetebrates, including humans. Fifty seven different serotypes have been isolated from humans and most of these are associated with upper respiratory infections in children. These different serotypes can be classified into 7 subgroups (A-G). Serological studies show that ~60% of children populations are seropositive for *Adenovirus* (Ad) subgroup C (69), and Ad5 (subgroup C) is the most commonly used for gene delivery vector design. Due to its natural host tropism in humans, administration of adenoviral vectors elicits pre-existing cytotoxic T and B cell responses which limits transduction efficiency during gene delivery applications. In order to overcome this barrier, much effort has been directed toward the development of less toxic, low immunogenic and specific cell targeted Ad vectors. The wild-type Ad genome consists of five early transcription units (E1A, E1B, E2, E3 and

E4), two delayed early transcription units (IX and IVa2), and one major late (ML) transcription unit.

In the first generation Ad vectors (81), wild-type Ad E1 and E3 genes were removed from the recombinant virus with the goal to ensure that the adenoviral vector was replication defective and to increase the packaging size to 8.3 kb, respectively. However, *in vivo* administration using this recombinant vector resulted in high inflammatory responses (190). The next generation of Ad vectors, which provided larger packaging size (14kb) by removal of two more genes (E2 and E4), still did not overcome the problem of significant immune response and, moreover, transgene expression using this vector is much reduced compared to the previous E2 or E4 containing vector (293). The current generation of Ad vectors provide the largest packaging size (37kb) and safest delivery vector by replacing the complete genome of Ad virus with therapeutic genes, which are called gutless or gutted vectors (14, 47). During vector production, the replication-defective property of this gutless vector is complemented by the expression of a replication-competent helper vector in the packaging cells (235).

Adeno-associated Viral (AAV) Vectors

Adeno-associated virus is a small ssDNA (~5kb) parvoviruses with a particle size of ~26nm in diameter (31, 42). It belongs to *Dependovirus* genus and requires helper viruses (e.g. Ad virus and Herpes Simplex Virus (HSV)) to undergo successful lytic infection. Since its first discovery as contaminant with an Ad virus preparation in 1965, no disease or pathogenicity has been reported associated with AAV infection. Due to its non-pathogenicity, AAV has drawn huge attention for the development as a gene delivery vector. To date, over 100 gene sequences have been isolated from human/non-human primate tissues and twelve serotypes have been described (AAV1-

AAV12), in which AAV2 is the most clinically utilized serotype (113). However, differential tissue tropism and transduction efficiencies among various serotypes have inspired the development of other serotypes for as more tissue specific vectors (326), AAV1 and AAV6 for muscle and cardiac gene delivery, and AAV9 for brain delivery.

The wild-type AAV genome contains two ORFs; *rep* and *cap*, which encode for viral proteins important for viral replication and capsid assembly, respectively. These ORFs are flanked by two inverted terminal repeats (ITR) which contain hairpin-shaped sequences important for viral replication and genome packaging. These repeats are the only *cis*-acting elements present in AAV.

AAV vectors are generated by co-transfection of two or more plasmids into packaging cells; a common example is transformed HEK293 cells. The first plasmid carries the recombinant therapeutic gene flanked by two ITRs. The other remaining plasmids carry *rep*, *cap*, and Ad helper genes. Recombinant virions produced can be isolated and purified from the cell lysates. Compared to retroviral and adenoviral vectors, AAV vectors show no proto-oncogene / cellular toxicity and relatively less immunogenicity, respectively.

Examples of Viral Vector Mediated Gene Delivery Therapy

By 2012, more than 1200 clinical trials were underway using viral vector gene therapy (http://www.wiley.com/legacy/wileychi/genmed/clinical). There were several issues encountered during these years, e.g., including the death of a patient in the trial using an adenoviral vector to treat ornithine transcarbamylase (OTC) deficit (25, 178, 201), the development of leukemia in two patients treated with gammaretroviral vector for X-linked SCID (51). Despite the problems mentioned, gene therapy has been in the spotlight due to the successful development of treatments for inherited diseases, e.g.

including immuno-deficiency and bone marrow transfer (10). Recently, more and more application oriented AAV vectors have been successfully used for treatment of retinal diseases and several neurodegenerative diseases (32, 50, 250). Since around 2005, the number of gene therapy clinical trials has increased back to ~100 per year worldwide with application to a broader array of diseases including Parkinson's disease, Alzheimer's disease, cancer, retinal degeneration, hemophilia, and cardiovascular diseases. Notably, less than 10% of the trials nowadays are aimed at monogenic inherited disorders, which initially inspired the whole idea of gene therapy (116). The Wiley group (http://www.wiley.com/legacy/wileychi/genmed/clinical) has reported that more than 1780 gene therapy clinical trials have been undertaken worldwide in which ~64% are performed for the treatment of cancer related diseases and that over two thirds of clinical trials are based on viral vector administration.

Gene Therapy for Severe Acquired Disease: Cancer

Currently, the alternatives for the treatment of tumors include the introduction of a tumor suppressor gene for cell apoptosis, the introduction of suicide genes, using anti-angiogenesis factors and immune regulatory genes, or the application of oncolytic viruses.

The most common loss of tumor suppressor activity arises from a defect in p53, RB1, and BRCA1. Previous studies had indicated that reactivation of these tumor suppressors in tumor cells resulted in apoptosis and elimination of tumors; as well as causing the cells to be more sensitive to chemotherapy. An example of a clinical trial for cancer treatment was the administration of an adenoviral vector expressing normal p53 protein into 25 non-small cell lung cancer (NSCLC) patients (279). The outcome of this study was a 28-64% decrease in tumor progression up to 14 months.

Alternative treatments for cancer cells include using a suicide gene. This concept exploits the capability of herpes simplex viral thymidine kinase (HSV-TK) to phosphorylate and convert ganciclovir (GCV) or acyclovir (ACV) into toxic drugs which will terminate DNA replication (241). Selective infection of viral vectors into cancer cells will then eliminate TK+ cancer cells. Examples of viral vectors using this strategy are an AAV vector for bladder cancer, an Ad viral vector for breast and colorectal cancers, a lentiviral vector for prostate cancer, and a HIV vector for T cell leukemia (16, 194, 215, 233, 294).

Immune-regulatory factors also represent good candidates for the treatment of cancer (181, 299). This concept is exploited by gene therapy to inhibit cancer cell differentiation through immune stimulatory factors, for examples cytokine (IL-2, IL-12, GM-CSF), co-stimulatory molecules (B7), major histocompatibility (MHC) (136, 189, 321). Studies have shown that administration of viral vectors resulted in gene modification of tumor cells, stimulation of reactivation of the host's immune system and prevention of tumor recurrence (273). However, this treatment is less effective in later stage cancer patients. This might be due to immunosuppressive factors released by cancer cells to suppress immune response. To overcome this barrier, future progress is directed toward the development of genetically modified dendritic cells (DC) which express higher level of cytokines and promote T-cell activation (104).

The most recent cancer cell killing strategy involves the use of the E1B deficient Ad vector, called ONYX-15 (139, 254). It was reported that the Ad E1B protein can inactivate the p53 tumor suppressor gene which is mutated in most cancer patients. In normal cells, p53 will limit Ad replication through interaction with E1B protein (206).

Using the ONYX-15 Ad vector, selective oncolytic strategy was feasible and resulted in relatively safe and significant (>50%) tumor regression (112, 164, 218). In addition to Ad, several viral vectors which have different oncolytic mechanisms were also studied, e.g. Herpes Simplex Virus (HSV), Newcastle disease virus, Reovirus, and Vesicular Stomatitis Virus (VSV).

Anti-angiogenesis can be defined as the application of specific compound to reduce or eliminate formation of blood vessels (vasculogenesis) (107). Most tumors secrete various growth factors to induce capillary growth in order to support their expansion. Studies have shown that Ad vectors expressing the extracellular domain of human vascular endothelial growth factor receptor (hVEGFR) were able to infect human lung cancer cells and inhibit VEGF-stimulated DNA synthesis. Following the study, *in vivo* administration of treated cells into a mouse model decreased colorectal tumor size 10 days post injection and enhanced apoptosis *in vivo* (259). Another *in vivo* gene delivery using an Adenoviral vector was performed to investigate the treatment of Transitional Cell Carcinoma (TCC) in the bladder of a mouse. This study utilized Ad-mediated an antisense bFGF (bFGF-AS) strategy to reduce microvessel density and enhanced endothelial cell apoptosis (146).

Gene Therapy for Severe Acquired Disease: Acquired Immune Deficiencies Syndrome (AIDS)

One alternative of gene therapy applications for AIDS patients is to generate genetically modified hematopoietic cells that may exhibit intracellular expression of anti-HIV genes to inhibit HIV replication and pathogenicity. To date, most AIDS therapeutic strategies involve anti-HIV drugs that target Gag and Pol. Two regulatory proteins (Tat and Rev) and four accessory proteins (Nef, Vif, Vpu, Vpr) have been identified to be

important for HIV replication (249). Rev responsive element (RRE) transcripts were identified to suppress HIV replication through interaction with Rev. When applied into human CD4+ cells, expression of RRE (RRE decoys) resulted in no detectable HIV replication (19). Other promising approaches as to treat HIV are RNA interference (RNAi) tools which target and breakdown viral RNA coding for accessory proteins (249).

Gene Therapy for Genetic Disorder: Severe Combined Immuno-deficiencies

Severe Combined Immuno-deficiencies (SCID) is a class of inherited immune disorders in which the functions of both T cells and B cells of the adaptive immune response system are impaired. The two most common SCIDs are X-linked SCID and adenosine deaminase (ADA) deficiency. In X-linked SCID patients, mutations in the common gamma chain (γc) gene (located on X chromosome) can result in a non-functional γ chain which is shared by various cytokine receptors. In healthy patients, interactions between cytokines and their receptors trigger cell signaling which are important for T and B cells differentiation. Failure in interleukin signaling will result in low expression or absence of T cells and natural killer (NK) cells and non-functional B cells. In 1990, gene therapy introduced a new era of medicine by using a retroviral vector to deliver the γc gene into patient CD4+ T cells. This resulted in elevated numbers of T, B, and NK cells leading to the recovery of immuno-compromised abnormalities.

The second common SCID is caused by ADA deficiency (281). Adenosine deaminase is a zinc metalloenzyme whose function is important for purine breakdown. In ADA-SCID patients, non-functional ADA results in the accumulation of deoxyadenotide (dATP) which inhibits the activity of ribonucleotidereductase to generate deoxynucleotide (dNTs) (100). Imbalance of dNT synthesis results in limited lymphocyte proliferation causing the immune system to be compromised. Clinical

studies using retroviral vectors have shown long-term (2 years) ADA expression in T and B cells of SCID patients (11).

Gene Therapy for Genetic Disorder: Lysosomal Storage Disease (LSD)

Gaucher disease (GD), named after the founder Phillipe Gaucher in 1882 (115), is the most common type of genetic lysosomal storage disorder (LSD) caused by deficient β-glucocerebrosidase (GCase) gene expression resulting in accumulation of glycolipids (glucocerebroside) in macrophages and enlargement of the liver and spleen (44). To date, researchers have pursued the cure of GD using retroviral, lentiviral, and AAV vectors packaging the glucocerebrosidase gene. Using a GD mouse model, preclinical studies have shown promising and relatively long (20 weeks) *in vivo* gene expression which results in no detectable of Gaucher cells in spleen and liver (103, 143).

Gene Therapy for Genetic Disorder: Cystic Fibrosis

Cystic Fibrosis (CF) is an autosomal recessive disorder of secretory glands mainly in the lungs (248). This inherited disorder is caused by mutations in the gene coding for the Cystic Fibrosis Transmembrane conductance Regulator (CFTR) protein (located on q31.2 locus of chromosome 7) which is important for the balance of sodium and chloride ions across epithelial membranes. In most CF patients, the mutated *CFTR* gene expresses a mis-folded CFTR which results in an imbalance of electrical potential inside and outside the cell and blockage of ion channels that cause remodeling and infection in the lung.

Early clinical studies were attempted to deliver the normal *CFTR* gene using Ad vectors to the epidermal lung cells (121, 122). It was shown that first administration gave low or limited gene expression. Hence, second and additional attempts were aimed at increasing the amount and duration of gene expression. However, due to pre-

existing immune responses the therapeutic effects became very limited. The majority of CF patients also have pre-existing neutralizing antibodies against AAV making them also ineffective as delivery vectors (131). Recently, repeat administration of lentiviral vectors had been shown to potentially evade host immune rejection and exhibit long term gene expression (121).

Gene Therapy for Genetic Disorder: Leber's Congenital Amaurosis type (LCA) 2

Leber's Congenital Amaurosis type 2 (LCA2) is an inherited eye disease characterized by vision loss, retinitis pigmentosa, and severe retinal dysfunction. Visual loss in LCA2 is caused by the mutation in the *RPE65* gene (located on chromosome 1 locus p31) which results in the combination of a biochemical blockade of the retinoid cycle and degeneration of retinal photoreceptors (200). In the normal photo-transduction process of retinal epithelium cells, the Retinal Pigment Epithelium 65kDa protein (RPE65) functions in a multistep process (visual cycle). This process converts retinols between *trans* and *cis* conformations which is important for electric signal transmission and visual pigment regeneration in photoreceptor (rods and cones) cells (55).

RPE65 gene therapy using AAV2 vector has yield significant visual improvement among three tested patients in 2008. Visual performances were analyzed 90 days post-treatment and demonstrated an increase of 50-fold for cones and up to 63,000-fold for rods photoreceptor cell regenerations (72, 138, 196).

Gene Therapy for Genetic Disorder: Hemophilia B

Hemophilia B is an X-linked blood clotting disorder caused by mutation at gene coding for Factor IX (35, 90). Factor IX deficiency leads to an increased propensity for hemorrhage. After getting injured, hemophilia patients will bleed for a longer time than healthy patients. Factor IX deficiency may also lead to internal bleeding, in which,

otherwise treated, will lead to organ damage. Recently, it was reported that AAV gene therapy has treated six hemophilia B patients who produce less than 1% than normal levels of Factor IX. Studies resulted in spontaneous blood clotting and sustained expression of Factor IX in four out of six patients (240). While high doses of vector administration resulted in elevated levels of transaminase and liver enzymes, consumption of steroids has been shown to ameliorate the side effect of high dose vector application. These striking results suggest the potential for the use of a similar approach for the treatment of hemophilia A (deficiency in Factor VIII) (319).

Lessons and Future Perspectives in Viral Vector Gene Therapy

Gammaretroviral vectors accounted for about 20% of the trials in the 1990s. However, due to its capability to only infect dividing cells and its cellular toxicity caused by insertional mutagenesis, the use of these viral vectors is now less widespread. The PIC of these virus, including viral cDNA and a number of viral and host proteins, as well as viral integrase enzyme cannot get access to the nucleus except when the nuclear membrane breaks down during mitosis (210). In our body, most neurons, skeletal muscle cells, cardiomyocytes, endothelial cells, and peripheral blood lymphocytes are classified as non-dividing cells. Hence, the use of gammaretroviral vectors is limited to *ex vivo* delivery to cells that are actively dividing. In the case of insertional mutagenesis into the human chromosome, mounting evidence has demonstrated that these viruses preferentially target the promoter region of actively transcribed genes in human genome (60, 80). In 2002, two children treated with gammaretroviral vector for X-linked SCID developed acute lymphoblastic leukemia (T-ALL) (128, 167). This mutation has been shown to be due to the insertion of the retroviral vector into the LMO2 (LIM domain 2) proto-oncogene (129, 205). This attracted the attention and concern of the scientific

community and medical world to analyze gammaretroviral insertional mutagenesis properties. Subsequently, two other children from the same group in Paris and London also developed T-ALL. In all these patients, the gene coding for LMO2 protein was mutated due to the insertion of retroviral vector (127). Since then, insertion mutagenesis was reported in other disease models such as Wiskott–Aldrich Syndrome (WAS) and X-linked chronic granulomatous disease, as well as gene transfer in various animal models (43, 59, 82). However, despite the issue of insertional mutagenesis, the most successful hematopoietic gene transfer comes from gammaretroviral vector for ADA-SCID patients (10).

Lentiviral vectors began to be used as gene therapy vectors in 2003 especially suiting the need for transducing non-dividing cells, both *in vivo* and *ex vivo*. The first lentiviral related clinical trial was approved for HIV-1 infection (195). And ever since, 40 more clinical trials using lentiviral vectors have been approved or are in the process of approval. These trials include studies for monogenic disorders (X-linked SCID, sickle cell anemia, Fanconi anemia, X-linked cerebral adrenoleukodystrophy, β-thalassemia and mucopolysaccharidosis), cancers (metastatic melanoma, non-Hodgkin lymphoma and leukemia), and neurodegenerative diseases (Parkinson disease) (182). There are three generations of lentiviral vectors already developed (mentioned above). The first two generations raised safety concerns which have been addressed in the third generation of lentiviral vectors by limiting the viral protein production. However, whether the insertion of viral DNA in to the host genome would activate oncogenic genes is still under debate. *Ex vivo* transduction studies have showed that these vectors resemble wild-type HIV-1 in genome integration efficiency in the transduced cells. However,

lentiviruses integrate their viral genome into the entire gene transcription unit, whereas retroviruses preferentially integrate into the transcription started site, such as the promoter and first intron (61, 80). In a recent clinical study for adrenoleukodystrophy (ALD), the efficacy and safety of lentiviral gene transfer were verified in hematopoeitic stem progenitor cells. Several common insertion sites (CIS) have been identified in the patients' cells, suggesting a selective advantage associated with lentiviral integration (34, 58). Accounting for about 25% of gene therapy clinical trials, the first and second generations of Ad vectors have raised safety concerns due to immune and inflammatory responses (87, 220), which was responsible for the death of an 18-year old patient in a gene therapy trial for the hereditary deficit of ornithine transcarbamylase (OTC), at the University of Pennsylvania, Philadelphia in 1999 (25, 178). These vectors activated a series of inflammatory cytokines, which recruit macrophages, neutrophils, and NK cells to eliminate transduced cells. In liver, 80-90% of vectors are eliminated by inflammatory responses within 24 hours after administration. Subsequently, after 4-7 days of post-administration, antibody production was activated. This response was due to the presence of Ad vectors themselves, not against the gene expressed from the virus. Learning from such an unexpected experience, a gutless adenoviral vector was then introduced into the field of gene therapy. While less immune response was detected against transduced cells with this new vector, a transient inflammatory response and liver abnormalities, resulting from contamination of replication competent helper virus during vector preparation, was observed (70). Notably, growing interests have been focused on the development of ONYX-15 vector (mentioned above) (36). This viral vector has been approved for phase I and II clinical trials for the treatment of recurrent

squamous cell carcinoma of the head and neck (SCCHN) (112, 224). Administration using this viral vector in combination with chemotherapy had also been shown to be safe and efficient (161).

To date, AAV vectors represent the most promising delivery tool for *in vivo* gene therapy and the clinical trial number has been increasing substantially over recent years (Table 1-1). Their success is attributed to the biological characteristics of AAV vectors; simple genome organization (prevent contamination of wild-type viral protein with the vector which can lead to inflammation), limited genome integration (prevent the possibility of proto-oncogene caused by non-specific locus integration), they can infect both dividing and non-dividing cells, and serotypes-derived differential tissue specificities (52). Over 80 clinical trials have been conducted over past few years and are underway for phase I, II and III (116, 213) (www.clinicaltrial.org). Two examples of current examples of AAV vector gene delivery success are the treatments of LCA2 and Hemophilia B. Following studies from Hauswirth and Cicdeyan, visual assessment was performed for another group of 12 patients (8-44 age year old) who received RPE65 gene therapy. Results have shown this intervention can increase visual light response by at least 20 times and works even better in children (196).

Introduction to Parvoviruses

The *Parvoviridae* family consists of small (~26nm) non-enveloped icosahedral viruses that package a linear ssDNA genome of ~5kb (31). Based on the host range, these viruses are divided into two subfamilies: *Parvovirinae* and *Densovirinae* (29). The Parvovirinae, which infect vertebrates, is further subdivided (based on genome architecture) into five genera: Amdovirus, Bocavirus, Dependovirus, Erythrovirus, and Parvovirus. Members of the *Densovirinae* (subdivided into four genera: Iteravirus,

Brevidensovirus, Densovirus, Pefudensovirus) infect only insects and arthropods. This study will focus on the members of *Parvovirinae*, and especially the members in Dependovirus genus.

The type species of each of the *Parvovirinae* genera are; amdovirus: Aleutian mink Disease Virus (ADV); bocavirus: Bovine Parvovirus (BPV); erythrovirus: Human Parvovirus B19V (B19V); parvovirus: Minute Virus of Mice (MVM) and dependovirus: Adeno-Associated Virus serotype 2 (AAV2). While the first four genera contain pathogenic viruses that can replicate independently of helper virus function and are thus referred to as autonomous parvoviruses (45, 236), members of the dependovirus genus rely on co-infection with a complex helper virus (such as Ad or HSV) for a successful lytic life cycle (42).

Viral Genome and Capsid: Architectures and Functions

The common genomic structure of parvoviruses consists of two open reading frames (ORFs) flanked by two inverted terminal repeats (ITRs). The 5' end ORF (*rep* or *ns*) encodes non-structural proteins (referred to Rep in the dependoviruses and NS in the autonomous parvoviruses) which are important for genome replication and packaging, the 3' ORF (*cap*) encodes structural viral proteins (VP) which assemble the capsid (77) (Figure 1-1). Members of the bocavirus genus have a third ORF between *rep* and *cap* that codes for a non-structural protein, NP-1, required for genome replication (65, 276). The ITRs are palindromic sequences (120 to ~550 nucleotides (NT) in length) at the 5' and 3' ends of the genome that folds into hairpin structures and are essential for replication.

The parvovirus VP is a multifunctional protein capable of performing a wide variety of structural and biological functions during the viral life cycle, including host cell surface

receptor recognition, intracellular trafficking, nuclear entry, capsid self-assembly, genome encapsulation, maturation to produce infections virus progeny, nuclear exit, and host immune response detection and evasion (5, 6). The relatively small parvoviral genome has allowed the use of genetic manipulation to identify functional domains/regions of the VPs/capsid. These studies show that the parvoviruses have evolved to utilize the VP1u for a phospholipase A2 (PLA2) function required for endosomal escape and nuclear entry during infection (320), regions of VP2 for nuclear entry (in dependoviruses) and for nuclear exit (in some autonomous viruses), and amino acid stretches within the VP3 common region for receptor attachment, tropism and host range determination, capsid assembly, DNA packaging, and host antibody recognition (5, 6).

The number of VPs encoded by the *cap* gene and used to assemble the capsid differs between members of the Parvovirinae. The dependoviruses (Adeno-associated virus (AAV)) contain VP1, VP2, and VP3 formed by alternative mRNA splicing of the transcript and alternative translation initiation codon usage, whereas the autonomous parvoviruses are assembled from VP1 and VP2 translated from alternatively spliced mRNAs. For the parvovirus genus, a VP3 is generated by post translational cleavage of ~20 amino acids from the N-terminus of VP2 following genome packaging (77). Thus, ADV, B19V, and BPV contain only VP1 and VP2, while AAV2 and MVM virions contain VP1, VP2, and VP3. The amino acid sequences of the VPs are overlapping, with the entire sequence of VP3 (when present) contained within VP2 which is in turn contained within VP1. Sixty copies of these VPs, in a predicted ratio of 1:1:10 for VP1:VP2:VP3 (when present) or 1:10 for VP1:VP2, assemble the capsid with T=1 icosahedral

symmetry (62). VP1, containing a unique N-terminal region (VP1u), is always the minor component in all virus capsids while the smallest VP is always the major component.

The capsid, with its packaged ssDNA genome, has to traverse two cellular barriers during infection, the plasma and nuclear membranes, for replication in the cell nucleus (Figure 1-2). Like most other viruses, attachment to a cell surface receptor is an essential first step of parvovirus infection (23, 75). Extensive biochemical and molecular characterizations have led to the proposal that following initial attachment the parvovirus capsid is internalized through clathrin coated pits (95, 234) and trafficked through the endocytic pathway to the nucleus for genome replication and subsequent transcription of the genome and translation of the message for production of the Rep / NS and VP proteins required for the formation of progeny virus. *In vitro* and biochemical studies using lysosomotropic drugs (bafilomycin A1 and chloroquine) is shown to interfere with endosomal pH and block parvovirus infection, suggesting that endosomal acidification is essential for the viral infection (23, 24). For the dependoviruses, there is evidence that some AAV serotypes are trafficked through the Golgi and endoplasmic reticulum (ER) enroute to the nucleus, and for both dependovirus and autonomous members, cellular components, such as actin and dynein as well as microtubules, are proposed to be involved in cellular trafficking (94, 133, 135, 234, 252, 289).

Parvovirus Capsid Structure

Towards correlating the capsid structure with its various functions during cellular infection the three-dimensional structures for several *Parvovirinae* members have been determined using X-ray crystallography and/or cryo-electron microscopy and image reconstruction (cryo-reconstruction) (7, 8, 92, 119, 126, 157, 158, 171, 172, 180, 191, 207, 223, 225, 232, 266, 284, 291, 304, 312, 313). In all these structures only ~520

residues of the common VP2 or VP3 C-terminal region (depending on viruses) are resolved leaving the N-terminal extensions of the larger VP(s), which are proposed to be disordered, un-observed. Low copy numbers of the minor capsid proteins or differential conformations adopted by the N-termini, which is inconsistent with the 60-fold icosahedral averaging applied during structural determination, could result in the lack of N-terminal VP ordering (5, 6, 62). Cryo-reconstruction studies of AAV capsids in which medium resolution structures for capsids assembled with or without VP1 in addition to those containing only VP3 suggest that the VP1u is located in the interior of the capsid underneath the icosahedral twofold axis (171). For B19V, cryo-EM reconstruction of wild-type virions and empty particles showed VP2 exposed on the capsid surface (157).

The VP structure (the ordered ~520 residues) is highly conserved, even for members that are only ~20% identical at the amino acid sequence level, such as AAV2 and B19V. The core consists of a conserved eight-stranded (βB to βI, named from N to the C-terminus) antiparallel β-barrel motif and an α-helix (αA) (Figure 1-3). An additional β-strand, βA, involved in antiparallel interactions with βB, is also present in all the Parvovirinae structures. The remaining VP structure consists of loops inserted between the β-strands that contribute to the capsid surface topology. These loops also contain small stretches of β-strand structure. The loops are named after the strands between which they are inserted, for example, the DE loop is inserted between β-strands βD and βE and the HI loop is inserted between βH and βI. The top of these loops are structurally varied between members in the same and different genera, and dictate host-specific tropism, antigenic response, and transduction efficiency in viral vectors. The

BIDG β-sheet forms the interior surface of the capsid while the inserted loops form characteristic features at and around the icosahedral two-, three-, and five-fold symmetry axes (Figure 1-4). There is (I) a depression at each two-fold axis, (II) a single protrusion at the three-fold axis of members of the parvovirus genus (e.g. MVM, Canine Parvovirus (CPV), Feline Panleukopenia Virus (FPV), Porcine Parvovirus (PPV)) or three separate protrusions surrounding the three-fold axis (which thus appears as a "depression" in members of the amdovirus (e.g. ADV), bocavirus (HBoV), dependovirus (AAVs), and erythrovirus (B19V) genera, (III) a cylindrical channel at each five-fold axis, (IV) a depression surrounding the cylindrical channel, and (V) a "wall" between the two- and five-fold depressions (5, 62). The protrusions are more pronounced in ADV and the AAVs compared to B19V and HBoV. B19V and HBoV appear to share characteristics of members of the parvovirus and dependovirus genera and have flatter protrusions. The two-fold axis (in all the virus structures) is created by the loop after βI from two twofold symmetry related VP monomers; the single three-fold protrusion in members of the parvovirus genus are created from six loops (within the GH loop), two from each three-fold symmetry related VP monomer; each of the three separate protrusions in the other Parvovirinae members are created by three loop regions (also within the GH loop) from two VP monomers; the five-fold channel is created by five symmetry related DE loops and the surface of the depression surrounding this axis is lined by the HI loop.

Dependovirus: Overview of Adeno-associated viruses (AAVs)

These viruses are non-pathogenic and able to package foreign DNA, resulting in intense efforts to develop several members for therapeutic gene delivery applications. Currently, clinical trials are underway with AAV vectors packaging therapeutic genes for the treatment of several diseases, including alpha1-antitrypsin deficiency, Leber's

congenital amaurosis, muscular dystrophy, hemophilia B, cystic fibrosis, Alzheimer's disease, arthritis, lipoprotein lipase deficiency, Parkinson's disease and HIV infection (57, 217) (Table 1-1). Challenges for these clinical studies include the need to (I) improve viral-tissue specificity and (II) decrease the detrimental effects of the host immune response against the vector (especially for treatments that may require vector re-administration) (41, 209). Efforts to overcome these issues have included the isolation and characterization of novel AAV serotypes and/or variants to exploit their tissue tropisms, transgene expression efficiencies, and hopefully lack of human immune system recognition. Amino-acid sequence (VP1) comparison between the twelve serotypes (mentioned in previous section) shows ~60-99% identity, with AAV4 and AAV5 being the most different (113). In addition, AAV sequences have been isolated from several other mammalian hosts, including caprine, mouse, bovine, snake, lizard, avian tissues (17, 147, 156, 192, 245), which share different levels of sequence similarity with the isolates from the human and non-human primate sources.

AAV Capsid Structure and Capsid – Cell Surface Receptor Interactions

Currently, atomic structures of nine serotype members, AAV1-9, serving as the representative members of the AAV antigenic clades and clonal isolates (113), have been determined using X-ray crystallography and/or cryo-reconstruction (92, 180, 223, 225, 232, 291, 311, 312). For these viruses the conserved core regions (βB-βI and αA) are superimposable while the tops of the loops between these conserved regions are varied in sequence and structure and defined as variable regions (VRs) I-IX (119). Mutagenesis, biochemical, and structural studies have demonstrated that residues in these VRs are crucial in viral life infection, including viral-receptor binding (6).

Biochemical studies have identified primary receptors and co-receptors utilized for initial cellular recognition and internalization, respectively, during infection by the AAVs (Table 1) (12, 18, 28, 37, 88, 89, 91, 153, 155, 183, 188, 228, 244, 263, 264, 274, 275, 292, 298, 307). With respect to primary recognition several glycans are utilized by the AAVs. Heparan sulfate (HS) proteoglycan serves as the cell surface receptor for AAV2 and AAV3b (closely related to AAV2), terminal N-acetyl neuraminic acid (sialic acid (SA)) for AAV1, AAV4, AAV5, and galactose for AAV9 (Table 1) (6, 91, 228, 263, 264, 275, 292, 306, 307). AAV6 is able to utilize HS or SA depending on the cell type being infected (Table 1) (306, 307). The primary receptor for the other human and non-human primate AAV serotypes, AAV7, AAV8, AAV10-AAV12, are yet to be determined. Bovine AAV utilize chitotriose, a trimer of β-1-4-linked N-acetyl glucosamine found on gp96, for cellular transcytosis(89). The residues involved in glycan interactions have been characterized for AAV2, AAV5, and AAV6 as discussed below.

Mutagenesis of AAV2 followed by structure determination of AAV2-HS complexes mapped VP residues involve in the AAV2-HS interaction to several structurally adjacent basic residues R484, R487, K532, R585, and R588 (AAV2, VP1 numbering) (Figure 4), consistent with the highly acidic nature of HS molecules (160, 183, 228, 230). These AAV2 residues are located at the inner wall of the protrusions surrounding threefold axis (Figure 2B and 4). They are located in three VRs, VRV, VRVI, and VRVIII. Residues in VRV from one AAV VP interacts with VRIV and VRVIII from another three-fold symmetry related VP to assemble the top of the protrusions surrounding the three-fold axis while VRVI forms the base of the protrusions facing the two-fold axis (183, 228). Thus the binding site is only present on assembled capsids. The structure of AAV2

complexed with a HS oligosaccharide (183, 228) showed the location of the bound HS molecules adjacent to the residues mapped by mutagenesis. Levy *et al*. (183) also reported structural rearrangements of the HI loop on the canyon floor surrounding the five-fold channel which they proposed could be related to the opening of the channel to prime the capsid for (I) externalization of the VPIu for endosomal escape or (II) genome release following nuclear entry.

The capsid amino acids involved in glycan recognition have been reported for AAV5. AAV5 utilizes α2-3 N-linked SA for infection (153, 292). A single residue mutation, A581T (AAV5, VP1 numbering), affects airway cellular transduction shown to require SA binding (105). This residue, structurally equivalent to AAV2 A591, is also located on the inner wall of the threefold protrusion in the AAV5 capsid structure. AAV6 and the closely related AAV1 recognize α2-3 and α2-6 N-linked SA for cellular infection, with AAV6 also able to utilize HS as a cellular receptor (306, 307). Mutagenesis studies, in which the six amino acids (129, 418, 531, 584, 598, 642, AAV1/6 VP1 numbering) that distinguish the two viruses were reciprocally changed, identified K531 in AAV6 as playing an important role its HS recognition with a change to the E531 present in AAV1 abolishing this interaction (306). This residue, structurally equivalent to E530 in AAV2, is located on the AAV6 capsid surface at the base of the threefold protrusion within the vicinity of the AAV2 HS residues, but is on the wall facing the twofold depression not the threefold depression (225). Recently, a second mutagenesis study identified another AAV1/6 residue, K459, as being important for AAV6 HSPG recognition (312). This residue is structurally equivalent to AAV2 S458 located at the plateau close to the top of the threefold protrusion and is not adjacent to K531. The AAV2-HS mutagenesis and

structure data combined with the mutagenesis data for AAV5 and AAV6 suggests that the AAVs commonly utilize amino acids in the three-fold region for recognition of different carbohydrate moieties.

Although the galactose binding site of AAV9 capsid surface is not yet structurally characterized, several mutagenesis and transduction studies have shown the roles of residues on AAV9 variable regions corresponding with cardiac, liver, and muscle cellular transductions (170, 185, 243). Pulicherla *et al*. have shown mutations on residues Trp 503 and Pro 504 on AAV9 VRV is important for liver cellular transductions (243). Using capsid genome shuffling, a new chimera virus was generated from combination of AAV1, AAV2, AAV8 and AAV9 which has improved cardiac transduction. Regions of AAV9 that contributes to this chimera virus are VRIV (456-479) and VRVII (550-568) (185). Another region which is identified to be important for delayed blood clearance in cardiac transduction using AAV9 is 699-735, located in VRIX (170). Altogether, these results suggest that VRIV, VRV, VRVII and VRIX are the potential determinant for AAV9 superior liver, cardiac and muscle cellular transduction.

Following the recognition of a cell surface receptor by the AAVs, an interaction with cell membrane proteins, which serve as co-receptors, are required for capsid internalization. For AAV2, several internalization co-receptors have been identified, including integrin αVβ5, integrin α5β1, fibroblast growth factor receptor 1 (FGFR1), hepatocyte growth factor receptor (HGFR), and 37/67 kDa laminin receptor (LamR) (12, 244, 274, 298). LamR was actually identified as a co-receptor for AAV8 that could also serve a similar function for other AAVs, including AAV2, AAV3b and AAV9 (12), and similar to AAV2, AAV3b also utilizes LamR, HGFR and FGFR1 as its co-receptors (12,

37, 188). The interaction between AAV3 and HGFR appears to be specific for human cell derived HGFR (hHGFR), while AAV2 is also able to bind the murine derived receptor, mHGFR. Sequence differences between the murine and human receptors are suggested as a source of the differential AAV3 and AAV2 recognition (188). Other proteins required for internalization of other AAV serotypes include platelet derived growth factor receptor (PDGFR) and epidermal growth factor receptor (EGFR), for AAV5 and AAV6, respectively (88, 298).

For the AAV co-receptors, the VP residues important for α5β1 and LamR binding have been identified (12, 18), the binding site for the other co-receptors are unknown. An 511-NGR-513 motif (AAV2 VP1 numbering), was reported to play a role its binding to α5β1 (18). These residues are located close to the base of the three-fold protrusion (two/fivefold wall) proximal to the HS binding residues with G512 exposed on the capsid surface. The NGR sequence is conserved in most of the AAV serotypes, with the exception of AAV4, AAV5, and AAV11. This motif is partially conserved in B19V that utilizes α5β1 as a receptor. Due to the close proximity of this region to the HS binding site in AAV2, it has been postulated that the primary HS receptor binding might promote this AAV2 capsid-co-receptor interaction or serve as a pre-requisite. The binding site for LamR on the AAV8 capsid was mapped to two large peptide regions containing residues 491-547 and 593-623 (AAV8, VP1 numbering) (12). These residues are located on the inner surface of the AAV8 three-fold protrusions facing the three-fold axis (223) and include GH loop amino acids in VRV and VRVI in the first stretch of amino acids and residues in a structurally conserved VP region past VRVIII and before the βH strand in the second stretch. The report that this receptor is utilized by several AAVs

would thus suggest that second stretch of residues, 593-623, conserved in sequence and structure (223), may be more important for this recognition. These residues, structurally equivalent to residues 590-620 in AAV2, are close to those reported to bind HS in AAV2 and SA in AAV5, with surface amino acids clustered around the three-fold axis. The proximity to AAV primary glycan recognition regions, as for the α5β1 motif, again suggests the possibility that the initial cell surface recognition leads to a subsequent engagement of LamR for internalization.

AAV Capsid Internalization and Post-Entry Events

The interaction of the AAV capsid with internalization receptors results in host cell surface rearrangement which is a prerequisite for endocytosis, a clathrin mediated process (285). Several immunofluorescence microscopy and chemical inhibition studies showed AAV capsids co-localized with dynamin and microtubules as well as markers from early, late, and recycling endosomes, and lysosomes (135). In addition, endosomal processing is reported to be the rate limiting step in viral transduction in several cell lines (6, 96). Biochemical experiments confirmed that the AAV VP1u (amino acids 1-137, VP1 numbering) is exposed during endosomal trafficking (39, 272). Once exposed, the VP1u PLA2 activity hydrolyzes membrane phospholipids to cause the endosomal membrane rearrangement required to facilitate viral capsid release (320). During the transition from early to late endosomes, acidification induced capsid structural changes, including the externalization of the VP1u, is reported to be essential for viral trafficking, uncoating, and genome release in nucleus. However, pH alone is not sufficient to mediate VP1u externalization for the AAVs, suggesting a requirement for yet to be identified cellular factors in this capsid transition (171). Artificial heat treatment (65^0 C) alone can mimic the endosomal conditions required for VP1u externalization in the

presence of viral genome (171). Higher temperatures (75º C) are required to release the VP1u in capsids that are devoid (empty) of DNA (171). As discussed above, the structure of VP1u inside the capsid or in its externalized state has not been structurally observed, but is predicted to be α-helical in nature as reported for other PLA2 domains. Mutagenesis and biochemical studies suggest that the fivefold channel might play a role in its extrusion (39). Confocal microscopy studies have shown that in addition to the trafficking through the endocytic pathway, AAV2 can localize to the secretory pathway enroute to the nucleus (149) while electron and immunofluorescence microscopy have observed AAV5 in the Golgi compartment (21, 22). Further studies are required to characterize the role of these alternative trafficking routes and the role of capsid interactions in facilitating them.

The AAV8 capsid structure is the best characterized serotype with respect to the effect of the pHs encountered in the endocytic pathway. Structures determined by X-ray crystallography to 2.7Å resolution for capsids incubated at pH7.5, pH6.0, pH5.5, and pH4.0 identified two regions affected by pH that are conserved among the AAVs (222). The first region, designated as the “pH quartet”, involves residues R392, H529, E566, and Y707 (AAV8, VP1 numbering), and is located close to the icosahedral two-fold axis, with residue Y707 (equivalent to AAV2 Y704) visible on the capsid surface viewed down the axis. The amino acid side-chain transitions occurring as pH decreases result in a reduction in the number of interactions between two-fold related VP monomers and “weaken” this interface (222). It was thus proposed that amino acids at the two-fold interface may be involved capsid destabilization events that enable AAV VP1u externalization without capsid disassembly. The second region is located on capsid

interior surface under the three-fold axis and involves residues F631 and H632 (AAV8 VP1 numbering). Previous structural studies have assigned this region as the nucleic acid binding pocket for AAVs (119, 180, 223, 225) and implied a role in AAV genome stabilization. A low pH induced H632 side-chain conformational change disrupts the interaction of the VP with the ordered nucleic acid density observed in crystal structures. The loss of this density was suggested to be a priming of the capsid for genomic uncoating. Thus similar to other viruses (229, 251), this study suggests that the AAV viral genome undergoes rearrangement inside the capsid prior to its release and that altered capsid-genome interactions, triggered by pH, are important aspects of cytoplasmic pre-processing prior to nuclear entry for genomic uncoating.

Several cellular host protein machineries have been reported to interact with the AAV capsid during trafficking to the nucleus that is detrimental to infection. As an example, targeting of AAV2 capsids to the proteasome in the cytoplasm is reported to limit viral transduction efficiency (323, 324). Phosphorylation of capsid surface exposed tyrosines followed by ubiquitination is reported to be the signal for recognition by proteasome and subsequent capsid degradation. Mutation of the seven AAV2 capsid surface exposed tyrosine residues, Y252, Y272, Y444, Y500, Y700, Y704, and Y730 (AAV2 VP1 numbering) to phenylalanine resulted in significant (up to ~700-fold) increase in transduction efficiency dependent on cell lines (324). Significantly, AAV8 Y707, equivalent to AAV2 Y704, clustered at the icosahedral twofold axis with Y700 and Y730, undergoes the pH mediated transition discussed above, consistent with a role in capsid – cellular interactions during trafficking.

The exact mechanism of AAV genome translocation into the host cell nucleus following escape from cytoplasmic compartments is poorly understood as are the determinants of capsid uncoating in the nucleus. The VP1/VP2 N-terminal regions contain nuclear localization signals (NLSs) which when mutated significantly reduce AAV infectivity (120, 150, 269, 305). These N-terminal VP regions can be detected by antibodies in the cytoplasm of infected cells indicating that they become externalized prior to nuclear entry (269). Capsid processing prior to cytoplasmic release and subsequence nuclear entry, as suggested by the pH mediated structural changes described above and the reported release of the VP1u N-terminus, is consistent with the observation that microinjection of virions into the cytoplasm does not confer a nuclear translocation phenotype, even if the N-terminal regions are pre-exposed by heating (269). While the size of the AAV capsid at ~260Å in diameter is small enough to be translocated through the nuclear pore complex (NPC), there are conflicting reports on the issue. Some reports say that it can while others say that this may not be the case (134, 310). The exact mechanism remains to be elucidated.

The majority of studies indicate that AAV genome uncoating occurs in the nucleus (150, 151, 256, 269, 310). However, there are reports that uncoating may occur before or during nuclear entry. Regardless of the uncoating site, the capsid transitions resulting in genome release following nuclear entry remains poorly understood and likely requires cytoplasmic pre-processing, some discussed above, prior to nuclear entry (150).

Following viral genome release into the nucleus, rolling hairpin replication (RCR) is proposed as the mechanism for parvovirus genome replication (76). However, there little is known about the role of the capsid protein in this process. Two elements of the

AAV genome shown to be indispensable for replication are the ITRs and p5 rep transcript. The two large replication proteins, Rep78 and 68 (Rep78/68), encoded by the rep ORF and translated from the p5 transcript, possess terminal resolution site (trs) endonuclease, DNA terminal repeat binding (RBS), and DNA 3'-5' helicase activities. Viruses with mutations in Rep78 and Rep68 are defective for viral DNA replication (268, 295). In vitro studies show that after successful genome replication, the viral ssDNA genome is packaged into pre-assembled empty capsids in the nucleus (97, 163).

Expression of the AAV VPs alone is sufficient for capsid assembly suggesting that genome packaging is not required for this process (e.g. (38)), although the observation of a nucleotide in most AAV capsid structures determined to date, including virus-like particles expressed in heterologous systems in the absence of viral genome, suggests otherwise. Recent studies identified a transiently expressed 23kDa protein, assembly activating protein (AAP), which is required for capsid assembly (270, 271). This protein, expressed from a newly identified 'ORF2' of the cap gene, targets VPs into the nucleolus where capsid assembly is proposed to occur. Interestingly, comparison of capsid assembly for AAV1, 2, and 5 showed that AAV5 requires its own AAP and cannot be complemented by the AAV2 AAP. AAV5 is one of the most sequence diverse serotypes AAV1-12 (113) and this observation suggests that AAP engages in specific interactions with the VP during assembly. The step in capsid assembly requiring AAP is yet to be determined. Site-directed mutagenesis studies have identified several AAV VP residues that are important for capsid assembly. These are mostly charged residues involved in symmetry interface interactions (6). Significantly, residues in the HI loop,

which forms the majority of the fivefold symmetry related interactions in assembled AAV capsids, plays a role in capsid assembly as well as genome packaging (93, 120).

The AAVs package both strands of their ssDNA genome with equal frequency into different capsids in a process that is highly dependent on the small replication proteins, Rep52 and Rep40, which are encoded by the rep ORF. A reduction in expression of these proteins results in a significant decrease in the packaging efficiency (63). Biochemical studies have shown that oligomeric Rep 52/40 has a 3'-5' helicase activity (73), which is believed to interact with the assembled empty capsid and unwind the replicative products of AAV genome for packaging into the capsid. The interactions between Rep 52/40 and the AAV capsid have been reported to be both DNA dependent and independent (199, 202-204, 231, 316, 318). Post capsid assembly and genome packaging, wild-type AAV virions must exit the nucleus and traffic to the cell surface for a second round of infection.

Significance

Variable residues on the capsid surface have been shown to dictate differential functional properties among the AAV serotypes e.g. receptor binding, transduction efficiency, and antigenicities. Recently, there has been a lot of interest in the use of AAV1 and AAV6 as gene delivery vectors to transduce cardiac, muscle, and lung cells compared to AAV2 because of their superior transduction properties in these tissues. These two serotypes only differ in 6 of 736 residues in VP1, with 5 of these located within the overlapping VP3 region which assembles the capsid shell and is responsible for essential capsid functions associated with infection, such as receptor attachment and internalization. Furthermore, this small number of amino acid differences between AAV1 and AAV6 has been reported to confer receptor attachment and transduction

differences. We hypothesized that the comparison of AAV1 and AAV6 and their receptor interactions will aid dissection of the contribution of specific capsid residues / regions to AAV receptor attachment and transduction phenotypes. In this study, we utilized structural, biochemical, and molecular approaches to characterize these properties for these two viruses.The data obtained will be applicable to the development of cell/tissue targeted AAV gene delivery vectors by enabling the engineering of surface residues for specific receptor recognition.

Table 1-1. Current Ongoing Clinical Trials using Adeno-associated Virus Vectors

Disease	AAV[A] Serotype	Transgene Product	Phase
α1 antitrypsin deficiency	1, 2	α1 antitrypsin	I/ II
Batten's disease	2, rh10[B]	CLN2[C]	I
Canavan's disease	2	Aspatoacylase	I
Cystic Fibrosis	2	CFTR[D]	I/ II
Hemophilia B	2, 8	Factor IX	I/ II
Leber's Congenital Amaurosis	2	RPE65[E]	I/ II/ III
LPL[F] deficiency	1	LPL	I/ II/ III
Parkinson's disease	2	AADC[G], GAD[H], Neurotrophin	I/ II
Pompe's disease	1	GAA[I]	I/ II
Muscular dystrophy	1, 2.5	Microdystrophin, α-sarcoglycan	I
Macular degeneration	2	sFLT01[J]	I
Severe heart failure	1, 6	SERCA2a[K]	I/ II
Rheumatoid arthritis	2	TNFR-Fc[L]	I

[A]AAV=Adeno-associated Virus; [B]rh10= rhesus macaque variant 10; [C]CLN2=ceroid-lipofuscinosis type 2; [D]CFTR=Cystic Fibrosis Transmembrane Regulatory Receptor; [E]RPE65=retinal pigmentosa epithelium 65kDa; [F]LPL=Lipoprotein lipase; [G]AADC=Aromatic L-amino acid decarboxylase; [H]GAD=Glutamic acid decarboxylase; [I]GAA=acid alpha-glucosidase; [J]sFLT01=platelet-derived growth factor receptor; [K]SERCA2a=sarcoplasmic reticulum Ca2+ ATPase; [L]TNFR-Fc=Tumor Necrosis Factor Receptor Fc. (Table modified from (213))

Table 1-2. Adeno-associated virus: Cellular Receptors, and Host Range

Virus	Receptors	Co-receptors	Host
AAV1	α2-3 and α2-6 N linked sialic acid		Human
AAV2	HSPG[a]	Integrin α5β1, αVβ5, FGFR1[b], HGFR[c], LamR[d]	Humans
AAV3	HSPG[a]	HGFR[c], LamR[d], FGFR1[b]	Humans
AAV4	α2-3 O-linked sialic acid		NHP[e]
AAV5	α2-3 and α2-6 N-linked sialic acid	PDGFR[f]	Humans
AAV6	α2-3 and α2-6 N-linked sialic acid, HSPG[a]	EGFR[g]	Humans
AAV8		LamR[d]	NHP[e]
AAV9	Galactose	LamR[d]	Humans
Bovine AAV	Gangliosides, Chitotriose		Bovine

[a]HSPG=heparin sulfate proteoglycan; [b]FGFR1=fibroblast growth factor receptor1; [c]HGFR=hepatocyte growth factor receptor; [d]LamR=37/67-kDa laminin receptor; [e]NHP=non-human primate; [f]PDGFR=platelet-derived growth factor receptor; [g]EGFR=epidermal growth factor receptor. (Table modified from (132))

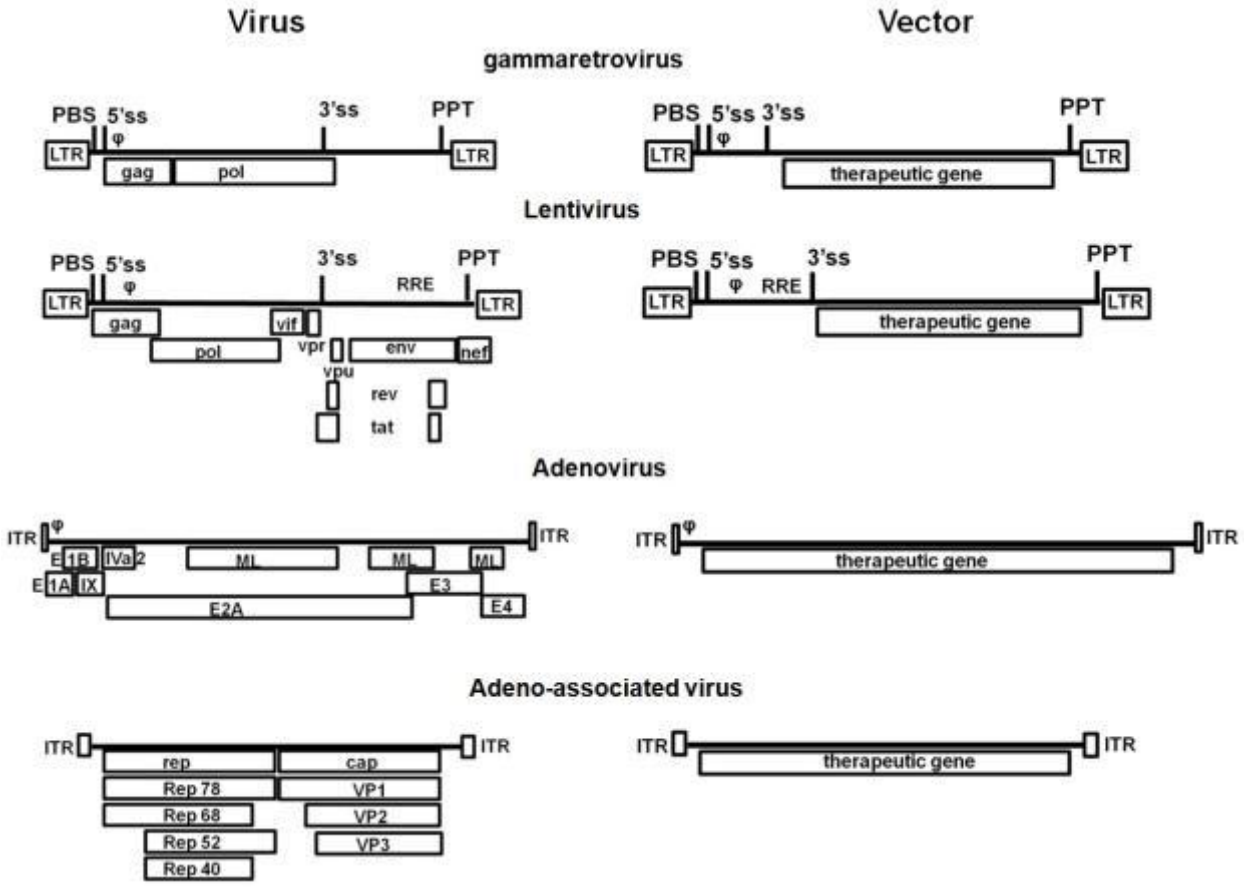

Figure 1-1. Genome architecture of (LEFT) gammaretrovirus (9-11kb), lentivirus (9-11kb), Adenovirus (36kb), and Adeno-associated virus (AAV) (5kb) and (RIGHT) the corresponding recombinant viral vectors for gene therapy. Genes coding for the protein for viral replication, viral capsid assembly, accessory proteins and toxic proteins are labeled (described in the text). LTR= Long Terminal Repeats, PBS= Primer Binding Site, PPT= PolyPurine Tract, ss=splice site, φ=packaging signal, gag=capsid, pol=polymerase (reverse transcriptase), env=envelope, ITR=Inverted Terminal repeats, E=Early transcript, ML=Major Late transcript, VP=Viral Protein (Figure modified from (117)).

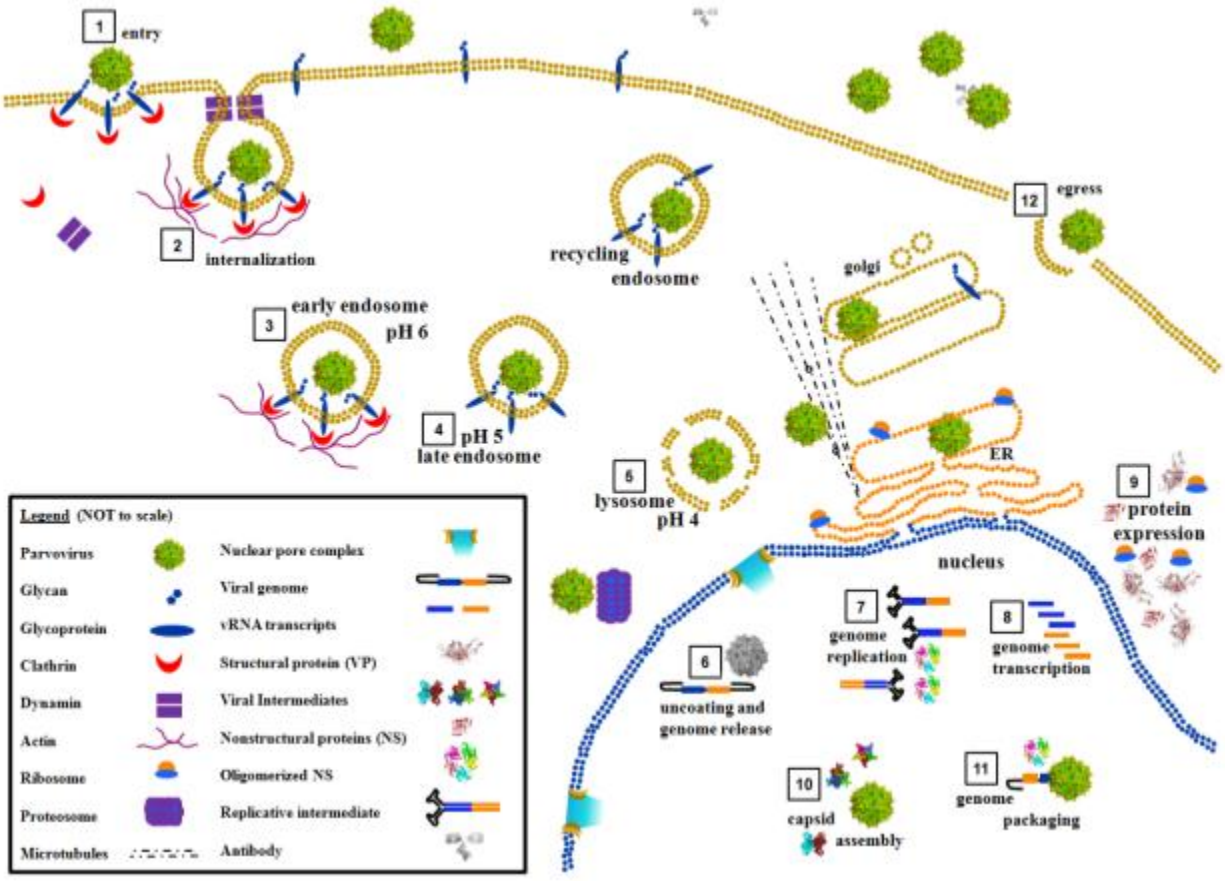

Figure 1-2. Schematic of the life cycle of Adeno-associated Viruses (figure modified from (132)).

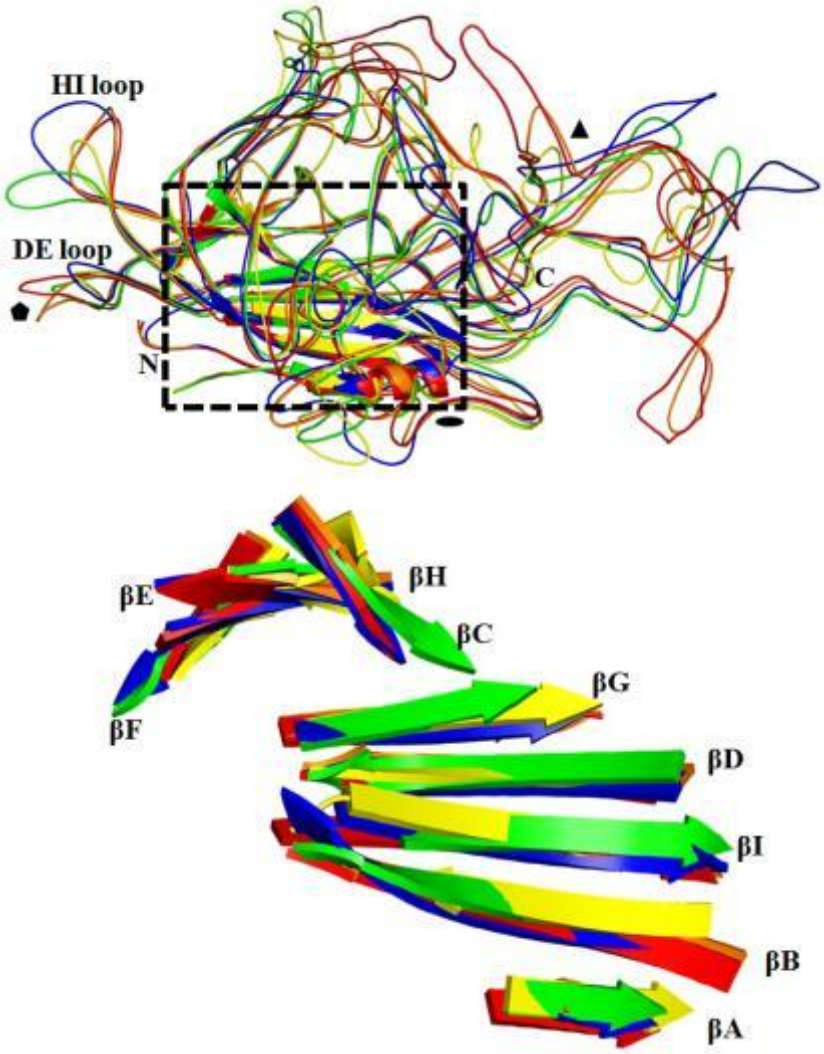

Figure 1-3. Conserved secondary structure superposition of VP for one member from every genus in *Parvovirinae* subfamily is shown: ADV (red),HBoV (yellow), AAV2 (blue), B19V (green) and MVMp (orange). Atomic coordinates for AAV2, MVMp, and B19V were obtained from RCSB protein database (PDB ID numbers 1lp3, 1z14, and 1s58, respectively). The ADV and HBoV images were generated from pseudo-atomic coordinates built into cryo-reconstructions (126, 207). The N-terminus (N), C-terminus (C), variable regions (VRI-IX, VR1-8), DE, and HI loops are labeled. The boxed region is shown below, depicting just the βA and β-barrel motif (βBIDG-βCHEF) conserved in all parvovirus VP structures determined to date (Figure adapted from (132)).

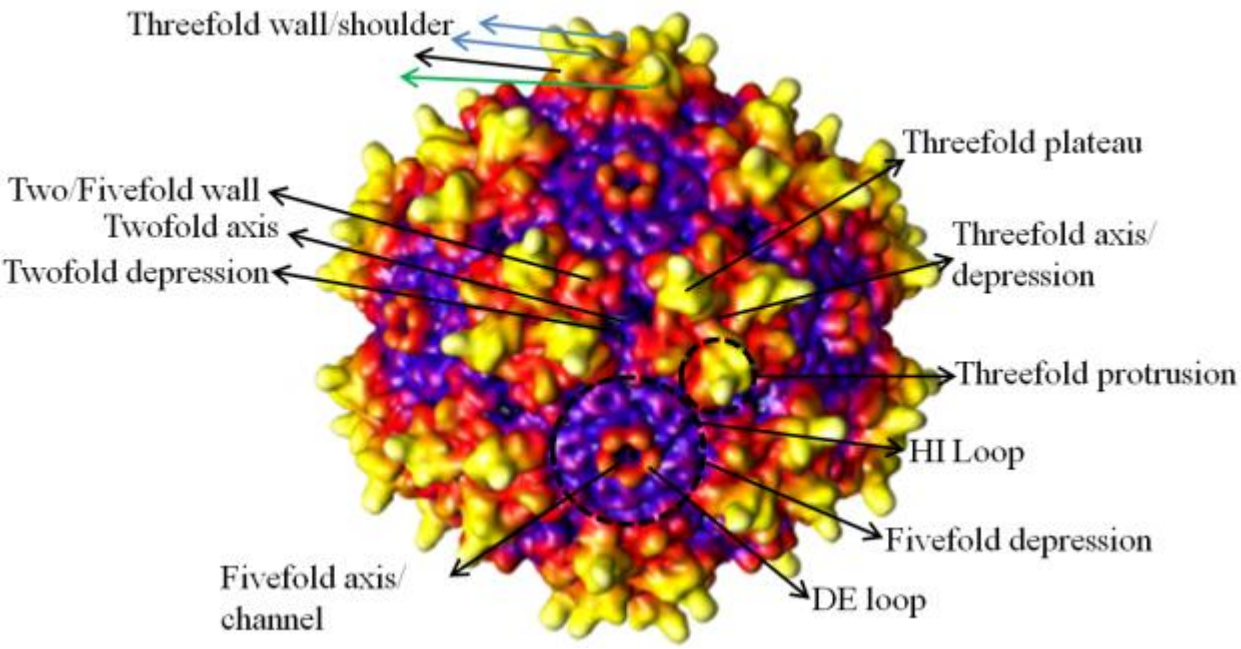

Figure 1-4. Surface representation of AAV2 used to illustrate the topological features of the parvovirus capsid surface as discussed in the text. The different colored arrows for the “Threefold wall/shoulder” label indicate the wall of the threefold protrusion facing the icosahedral twofold axis (black), icosahedral threefold axis (blue), and fivefold axis (green). The image is depth-cued (blue-red-yellow-white) to show regions at the shortest radial distance to capsid center in blue and those at the furthest radial distance in white (see Figure 3 for radial distances) (Figure adapted from (132)).

CHAPTER 2
MATERIAL AND METHODS

This chapter describes common experimental procedures and materials utilized throughout this thesis. The studies can be divided into two main sections: the first section involves the purification and structure determination of virus-like particles (VLPs) and the second section involves the purification (Figure 2-1) and biophysical characterization of mammalian expressed recombinant AAV virions (Figure 2-2).

Production and Purification of AAV Virus-Like Particles (VLPs)

A recombinant baculovirus encoding the AAV6 capsid proteins (VP2 and VP3 ORFs) or AAV1 capsid proteins (VP1, VP2 and VP3 ORFs) were provided by R. Jude Samulski (University of North Carolina, Chapel Hill (UNC)) and Sergei Zolotukhin (University of Florida (UF)), respectively. These constructs were generated using the Bac-to-Bac system (Gibco/Invitrogen Corporation). The DH10Bac-competent cells containing the baculovirus genome were transformed with pFastBac transfer plasmids containing the AAV component insert. Bacmid DNA purified from recombination-positive white colonies was transfected into Sf9 cells using the TransITInsecta reagent (Mirus). Three days post-transfection, media containing recombinant baculovirus with VLPs ORF inserted were harvested (P0) and plaque assays were conducted to prepare independent plaque isolates. Several individual plaques were propagated to passage one (P1) to evaluate the level of VP expression using Western blot against the anti-AAV B1 antibody (301). The clone with the highest level of protein expression was propagated to P2 and then P3 using Multiplicity of Infection (MOI) of 0.1 plaque forming units (pfu)/cell.

Sf9 insect cells cultured in Sf900 II SFM media (Gibco/Invitrogen Corporation) were infected with a titered P3 baculovirus stock, at an MOI of 5.0 pfu/cell. VLPs were expressed and purified from Sf9 cells as depicted in Figure 2-1. VLPs were released from infected cells by three freeze-thaw cycles in lysis buffer (50 mM Tris-HCl pH 8.0, 100 mM NaCl, 1 mM EDTA, 0.2% Triton X-100), with the addition of benzonase (Merck, Germany) after the second cycle. The sample was clarified by centrifugation at 12,100 x g at 4 ^{0}C for 15 minutes. Next, the cell lysate was pelleted through a 20% (w/v) sucrose cushion in TNET buffer (25 mM Tris-HCl pH 8.0, 100 mM NaCl, 1 mM EDTA, 0.06% Triton X-100) by ultracentrifugation at 149,000 x g at 4 ^{0}C for 3 h. The pellet from the sucrose cushion was resuspended in TNTM buffer (50 mM Tris-HCl pH 8.0, 100 mM NaCl, 0.06% Triton X-100, 30 mM MgCl2,) overnight at 4 ^{0}C. The sample was clarified by several rounds of centrifugation at 5,000 x g to remove insoluble material. The clarified sample was loaded onto a sucrose-step gradient (5-40% (w/v)) and spun at 151,000 x g at 4 ^{0}C for 3 h. A visible blue virus band was extracted from the 20/25% sucrose layer and dialyzed into 20 mM Tris-HCl pH 7.5, 2mM MgCl2, 350 mM NaCl at 4 ^{0}C. The approximate VLP concentration in mg/ml was calculated based on optical density measurements at 280 nm, assuming an extinction coefficient of 1.7. The purity and integrity of the VLPs were analyzed using Sodium Dodecyl Sulfate – Polyacrylamide Gel Electrophoresis (SDS-PAGE) and negative-stain electron microscopy (EM), respectively.

VLP and Vector Concentration

The VLP or vector was concentrated and buffer exchanged in a Biomax 100 K concentrator (Millipore, Bedford, MA). Three times the sample volume of desired buffer was added to wash the membrane on the retentate vial by centrifugation at ~1,933xg at

4^0C.In the last wash, sample was added into the retentate vial and centrifuged until the desired sample volume or concentration was reached. Buffer exchange was done by adding three times the final sample volume of the desired buffer onto the retentate vial and continued centrifugation at ~1,933xg at 4^0C.

Negative-Stain Electron Microscopy

Five microliters (µL) of purified samples was loaded onto carbon coated copper grids for two minutes and blotted dry using Whatman filter paper. The sample was then negatively stained twice with 5 µL of 2% Uranyl Acetate (UA) for 20 seconds and 7 seconds. The grids were air dried and then examined in a JOEL 1200 EX transmission electron microscope (TEM). The instrument was set to collect images at 50,000 x magnification and on film.

AAV6 VLP Structure Determination by Cryo-Reconstruction

Small (3.5 µl) aliquots of purified VLPs (~10 mg/ml) were vitrified via standard rapid freeze-plunging procedures (4, 98). Samples were applied to glow discharged (~15 s in an Emitech K350 glow-discharge unit) Quantifoil holey grids, blotted for ~5 s, plunged into liquid ethane, transferred to liquid nitrogen and then into a pre-cooled Gatan 626 cryo-specimen holder. Data was collected with an FEI Sphera microscope (200 kV, equipped with a LaB6 electron gun) under low dose conditions (24 e-/$Å^2$) at 50,000x nominal magnification and with a defocus range of 1.0 to 2.5 µm. Eighteen micrographs with minimal astigmatism and specimen drift were digitized at 7-µm intervals (representing 1.4-Å pixels) on a Zeiss SCAI scanner. A total of 1870 particles were extracted, pre-processed, and their defocus levels estimated using the RobEM program (http://cryoEM.ucsd.edu/programs.shtm) for reconstructing the structure of the AAV6 VLPs using the AUTO3DEM program (315). To compensate for the effects of

phase reversals in the contrast-transfer function of the images, phase corrections were performed but no amplitude corrections were applied. A Fourier Shell Correlation of 0.5 was used as the threshold for estimating the resolution of the reconstruction (288). The available coordinates for an AAV1 VP3 poly-alanine capsid model (aa218-736, VP1 numbering) extracted from X-ray crystal structure (PDB accession No. 3NG9) was docked into the AAV6 reconstructed density map using the Situs Package (colores; with angular degree of 30^0 and resolution of 9.7 Å) for pseudo-atomic model interpretation of the structure (303).

Structure Determination of AAV6 VLP using X-ray Crystallography

Crystals were grown from purified VLPs in 100 mM HEPES pH7.3 at a concentration of ~10.0 mg/ml using hanging drop vapor diffusion, with 60 mM MgCl2 and 100 mM NaCl as additives, 4% polyethylene glycol (PEG) 6000 as a precipitant, and 25% glycerol as the cryo-protectant. X-ray diffraction data were collected from a single crystal at the Cornell High Energy Synchrotron Source (CHESS) with a crystal-to-detector distance of 350 mm, oscillation angle of 0.30 per image, and exposure time of 50 seconds. The data were indexed, processed, scaled, and reduced using the HKL-2000 package (214). The crystal diffracted X-rays to 3.0 Å resolution and was in the rhombohedral crystal system, space group R32 with unit-cell parameters a = 262.6, c = 609.9 Å in the hexagonal setting.

The orientation of the AAV6 VLPs in the crystal unit cell were determined using the self-rotation function in the General Lock Rotation Function (GLRF) program with $\kappa = 180^o$, 120^o, and 72^o, searching for icosahedral 2-, 3-, and 5-fold symmetry axes with observed data in the 10.0 – 5.0 Å resolution range (282). The crystallographic 2- and 3-fold symmetry operators were observed to be coincident with icosahedral symmetry

operators, resulting in 10 VPs (non-crystallographic symmetry (NCS) operators) per crystallographic asymmetric unit of the R32 space group, similar to the structural determination of AAV1.

The diffraction data was phased using molecular replacement method in the AMoRe program (283). The orientation and position of the AAV6 10-mer in the crystal unit cell was determined by cross-rotation and translation searches using atomic coordinates for 10 AAV1 VP3 monomers (a 10-mer of residues 218 to 736, VP1 numbering) from AAV1 crystal structure (PDB accession No. 3NG9) with the amino acids that differ to AAV6, i.e. E418, E531, F584, A598, and N642, within VP3 mutated to alanine to eliminate phase bias. This VP3 10-mer model (generated with VIPER(56)) was oriented and positioned into the AAV6 crystal unit cell based on the output rotation angles and positioned at (0, 0, 0), based on space group packing considerations, to calculate initial phases. The phases were improved by refinement using the Crystallography and NMR System (CNS) package(48, 49), using simulated annealing, atomic position energy minimization, and atomic displacement parameter (ADP) refinement, with the application of strict 10mer NCS operators. A single cycle of electron density Fourier map ($2F_o$-F_c and F_o-F_c, in which F_o represents the observed structure factors and F_c the calculated from the model) averaging was carried in CNS, while maintaining strict NCS operators, using the experimentally measured amplitudes and the improved phases following each model refinement cycle. The refinement and averaging procedures were alternated with model building, using the Coot program, into averaged electron density maps(101, 102).

Following the building of VP3 common amino acids 218-736 into the averaged density maps, two regions of unassigned densities were observed in the Fourier F_o-F_c density map (at contour threshold of 3.0 σ) in the interior of the capsid into which a purine nucleotide (NT) and a pyrimidine base could be modeled. The identity of the purine and pyrimidine bases could not be unambiguously determined from the averaged densities at the 3.0 Å resolution of the map. However, there was no amino side-group density at the C2 position of the purine ring and no methyl group density at the C5 position of the pyrimidine ring, thus the base densities were interpreted as adenosine and cytosine, respectively. An occupancy of 0.5 was determined for each of the two bases by an empirical approach in which values (0.3 to 1.0) were applied to achieve temperature factors that were comparable with those of the average VP3 amino acid atoms. Finally, 12 solvent molecules were built into remaining positive Fo-Fc density. To improve the quality of the maps between refinement steps, density map modification was carried using the Density Modification (DM) subroutine in CCP4 (79, 300), which performed histogram matching, solvent flattening and NCS averaging. The refined structure has an R_{cryst} (where $R_{cryst} = \Sigma||F_{obs}|-|F_{calc}||/\Sigma|F_{obs}|x100$, in which F_o represents the observed structure factors and F_c the calculated from the model) and R_{free} (obtained from 5 % subsets of reflections that are not used in refinement) values of 27.5% and 28.8%, respectively, with final root mean square deviations (r.m.s.d.) of 0.009 Å for bond lengths and 1.48^o for bond angles. These values are within the range for structures reported at comparable resolution as calculated by the Polygon subroutine in the program PHENIX (Python-based Hierarchical Environment for Integrated Xtallography) (1-3, 286). The quality of the refined structure was analyzed using the

Coot program and MOLPROBITY (66, 83, 84). A Ramachandran plot showed 92.5% and 7.5% for residues in the most favorably and additionally allowed regions, respectively (144).

Structure Determination of AAV1 VLPs with Sialic Acid (SIA) using X-ray Crystallography

Crystals were grown from purified VLPs in 100 mM HEPES-NaOH pH7.3 at a concentration of 4.0 mg/ml using hanging drop vapor diffusion, with 50 mM $MgCl_2$, 7 % polyethylene glycol 6000 as a precipitant, and 25% glycerol as cryo-protectant. Forty eight hours prior to data collection, a crystal was soaked into cryo-protectant solution containing 25% glycerol and 10 fold excess molarity of 3'SLDN (Neu5Acα2-3GalNAcβ1-4GlcNAcβ). X-ray diffraction data were collected from a single crystal at Cornell High Energy Synchrotron Source (CHESS) with a crystal-to-detector distance of 300 mm, oscillation angle of 0.30 per image, and exposure time of 70 seconds. A total of 226 images were collected and used for data reduction. The data were indexed, processed, scaled, and reduced using the HKL-2000 package (214). The crystal diffracted X-rays to 3.0 Å resolution and was in the monoclinic crystal system, space group C2 with unit-cell parameters a = 455.46, b = 261.64, c = 450.93 Å, $\beta = 110^0$.

The orientation of the AAV1 VLPs in the crystal unit cell were determined using the self-rotation function in the GLRF program with $\kappa = 180^o$, 120^o, and 72^o, searching for icosahedral 2-, 3-, and 5-fold symmetry axes with observed data in the 10.0 – 5.0 Á resolution range (282). The diffraction data was phased using the molecular replacement method in the AMoRe program (283). The orientation and position of two AAV1 30-mers in the crystal unit cell was determined by cross-rotation and translation searches using the atomic coordinates for 30 AAV1 VP3 monomers (a 30-mer of

residues 218 to 736, VP1 numbering) from AAV1 alone crystal structure (PDB accession No.3NG9). This VP3 30-mer model (generated with VIPER(56)) was oriented and positioned into the AAV1 crystal unit cell based on the output rotation angles and positioned at (0, 0, 0), based on space group packing considerations, to calculate initial phases. The phases were improved by refinement using Refmac v5.5 in CCP4 package (79, 300), using simulated annealing, atomic position energy minimization, and atomic displacement parameter (ADP) refinement, with the application of restrained by 60 NCS operators. A single cycle of electron density Fourier map (defined as above) averaging was carried in Refmac v5.5, with NCS restraints, using the experimentally measured amplitudes and the improved phases, following each model refinement cycle. The refinement and averaging procedures were alternated with model building, using the Coot program (85, 101, 102), into averaged electron density maps.

Following the building of VP3 common amino acids 218-736 into the averaged density maps, an unassigned positive region of density was observed in the Fourier F_o-F_c density map (at contour threshold of 2.5 σ) on the exterior of the capsid into which an N-acetyl neuraminic acid (sialic acid / SIA) molecule could be modeled. This SIA molecule was generated suing PRODRG (262, 287) (Figure 2.3A). Currently, the refined structure has an R_{cryst} (where $R_{cryst} = \Sigma||F_{obs}|-|F_{calc}||/\Sigma|F_{obs}|x100$, where F_{obs} and F_{calc} are the amplitudes for the observed and calculated reflections, respectively) and R_{free} values of 26.3% and 27.0%, respectively, with root mean square deviations (r.m.s.d.) of 0.01 Å for bond lengths and 1.55^o for bond angles.

Site-directed Mutagenesis of AAV1 and AAV6

A series of single mutations for the six residues that differ between AAV1 and AAV6 (in the pXR1 and pXR6backgrounds, respectively) as well as the wild-type

plasmids were provided by R. Jude Samulski (UNC) (306). Plasmids expressing these mutants were extracted and purified using the QIAGEN DNA Mini Prep kit. Purified plasmids were then subjected to OD_{260} spectrophotometry to analyze the quantity of the plasmids. The samples were loaded onto 0.8% agarose gels with 1x Syber Safe stain and analyzed using Gel Doc (Biorad). A total of 7 primers were designed using Vector NTI and polymerase chain reaction (PCR) sequencing were performed to validate the AAV capsid sequences for the plasmids (Table2-1).

In order to confirm structurally mapped SIA binding site on the AAV1 capsid, mutagenesis was performed on the AAV1 ORF. Structural comparison between the AAVs was done using the SSM subroutinein the Coot package (85, 101, 102). Based on the transduction phenotype studies, we decided to mutate the SIA interacting residues to AAV2 corresponding residues, except Trp 503. However, recent mutagenesis study had showed this residue (W503A) plays a role in AAV9-Gal interaction. The residues selected for mutagenesis were N447S, S472R, V473D, N500E, T502S and W503A (AAV1 VP numbering). Due to 100% a.a. identity between AAV1 and AAV6 at these residues positions, a similar series of mutations were also generated for AAV6. Side-directed mutagenesis was performed using the Quick-Change XLII mutagenesis kit (Strategene). Ten nanograms (ng) of purified wild-type plasmids were used as the template for each mutagenesis with 125ng each of the forward and reverse primers and a total PCR reaction volume of 51 µL. The following cycling conditions were used: one cycle of 95^0C for 1 min, 18 cycles of 95^0C for 50 seconds, 60^0C for 50 seconds, 68^0C for 8 minutes, one cycle of 68^0C for 7 minutes, and product was kept at 4^0C. Following the PCR reaction, 10 U of *Dpn*I enzymes was added to each product and incubated at

37^0C for 1 hour. The DpnI-treated product was then analyzed using 0.8% agarose gel electrophoresis and subjected to plasmid transformation into DH5α *E.Coli* competent cells.

Transformation of DH5α *E.Coli* competent cells

Two µL of PCR product (for each wild-type and mutant virus) was added to 50 µL of DH5α competent cells in a-pre chilled 1.5 milliliter (mL) microcentrifuge tube, the cells were gently mixed and then incubated on ice for 30 minutes. The cells and DNA mixture were heat shocked for 45 seconds at 45^0C then immediately transferred into ice and chilled for 2 minutes. Five hundred µL of Luria broth (LB) medium was added to the newly transformed cells. The tube containing the transformants was shaken at 225 rotations per minute (rpm) for 1 hour at 37^0C. The transformation mix was then plated on the LB agar containing 100µg/mL of ampicillin and incubated at 37^0C overnight.

Cesium Chloride Plasmid Purification

For large scale purification of supercoiled plasmid DNA, cesium chloride sedimentation was performed. At least 30 hours prior to purification, an *E.coli* colony containing plasmid of interest was inoculated into 5 mL LB containing 100 µg/mL ampicillin and incubated at 37^0C with 225 rpm shaking for at least 8 hours. Log phase growing bacteria was added into 1L LB containing 100 µg/mL ampicillin and continue grow overnight at 37^0C. The bacteria were harvested by centrifugation at 4,450 xg for 20 minutes at 4^0C and resuspended with 20 mL resuspension buffer (25mM Tris-Cl pH 8.0, 10 mM EDTA, 15 % sucrose, and 100 µg/mL RNaseA). After the pellet was entirely resuspended, 50 mg of lysozyme was added to the resuspension. Forty eight mL of freshly made lysis buffer (1% SDS, 0.2N NaOH) was added to the mixture, gently mixed and incubated on ice for 10 minutes. To precipitate high molecular weight DNA and

proteins, 36 mL of 3M NaOAc pH 5.2, followed by 200 µL chloroform were added into the lysed cells. The slurry is then incubated on ice for 20 minutes and centrifuged at 14,300 xg for 20 minutes at 4^0C. To remove any cellular debris, the supernatant was filtered using cheese cloth and collected into a clean 500 mL bottle. The plasmid DNA was precipitated using an equal volume of isopropanol on ice for 30 minutes and centrifuged at 14,300 xg for 20 minutes at 4^0C. The DNA pellet was gently resuspended with 8 mL of sterile H_2O. Eight point four gram of cesium chloride (CsCl) was added into DNA solution and dissolved completely at 4^0C, followed by addition of 125 µL 10 mg/mL ethidium bromide. DNA sample was then subjected to ultracentrifugation at 361,800 xg at 12^0C overnight. Following sedimentation, a pink colored band was observed which contains supercoiled DNA. To remove ethidium bromide, the sample was diluted and washed several times with equal volumes of isoamyl alcohol until the DNA sample no longer looked pink. The aqueous fraction was transferred into a new centrifuge tube in each extraction. After final extraction, the CsCl DNA mixture was diluted with 2.5X the volume of sterile H_2O, followed by 2X the volume of 95% ethanol (EtOH) to precipitate DNA. The DNA precipitant was centrifuged at 14,300 xg for 15 minutes at 4^0C. The pellet was then washed with 1 mL sterile H_2O and extracted twice with equal volume of 25:24:1 phenol/chloroform/isoamyl alcohol. Final precipitation was performed by addition of 10% (v/v) 3M NaOAc pH 5.2, followed by 2.5 times volume of 95% EtOH. The DNA precipitant was pelleted twice using a bench-top centrifuge at maximum speed (11,000 xg) for 5 minutes, with a single 75% EtOH wash in between. The DNA pellet was then air dried and resuspended overnight at 4^0C with 1 mL sterile H_2O. The concentration of purified DNA was analyzed using optical density readings at OD_{260}.

Production of Mammalian Expressed Recombinant Virions

To produce recombinant AAV (rAAV) with wild-type or the mutated *cap* ORFs, transformed human embryonic kidney (HEK) 293 cells were triple transfected with 18µg pXR plasmid which contains AAV *rep* and *cap* ORFs, 18µg of pTRUF11which contains the green fluorescence protein (GFP) gene driven by Cytomegalovirus (CMV) promoter, chicken β actin enhancer, and AAV inverted terminal repeats (ITR) required for packaging, and 54µg of pXX6 which contains adenovirus helper genes. Transfection was performed using 190 µL of 1mg/ml polyethylenemine (PEI) at pH4.0 onto 75% confluent cells, incubated for 48 hours at 37^0C with 5% CO_2 and the transfection efficiency was analyzed using a UV microscope. The cells were then harvested by centrifugation at 1,140x g for 20 minutes and resuspended in 1 mL lysis buffer (50 mM Tris-HCl pH 8.0, 100 mM NaCl, 1 mM EDTA, 0.2% Triton X-100). The recombinant viruses were released by three freeze-thaw cycles. The lysate were clarified by centrifugation at 3,700 xg for 20 minutes and the rAAV virions were purified using 20% sucrose cushion in TNET buffer and ion exchange chromatography.

Purification of rAAV using Ion Exchange Chromatography

For ion exchange purification of the mammalian cell expressed rAAV1 and rAAV6 vectors, a 5-ml HiTrap Q column (Pharmacia) is washed with 25mL of distilled deionized H_2O and equilibrated at 5 ml/min with 25 ml of binding buffer (20 mM Tris-Cl pH 8.5, 15 mM NaCl), then 25 ml elution buffer (20 mM Tris-Cl pH 8.5, 500 mM NaCl), followed by 25 ml of binding buffer using a GE ATKA FPLC system. Ten mL samples of viruses resuspended in TNET (from the sucrose cushion pellet) were diluted 5 times with binding buffer (containing 5 µL phenol red) and applied to the column at a flow rate of 2 mL/min. After the sample is loaded, the column was washed with 50 mL of binding

buffer. The vector was eluted with a gradient concentration (100% in 30 minutes) of the elution buffer and fractions were collected into 1.5mL microcentrifuge tubes. Eluted fractions were then subjected to 10% SDS-PAGE to verify the quality of the sample.

Biochemical Characterization of Recombinant Virions

Total capsid titer was determined by an ADK1a enzyme-linked immunosorbent assay (ELISA) according to manufacturer's instruction (American Research Product, # PRAAV1). The clarified cell lysate were serially diluted (1:100, 1:500 and 1:1000) and 100 µL was added to the 96 kit well. The readings that were within the range of detection limit compared to the standards were used to calculate the numbers of capsids.

Total packaged genome or copy number was determined by real time or quantitative PCR (qPCR). Ten µL of crude lysate was treated with benzonase for 1 hour at 37^0C (in 50 mM Tris-Cl pH7.5, 10 mM $MgCl_2$) to degrade non-encapsidated nucleic acids. Each benzonase treated samples was digested with proteinase K (Roche #1373196) in 10 mM Tris-Cl pH8.0, 10 mM EDTA, 1% SDS) and incubated in 37^0C for 1 hour. The mixture was then treated twice with equal volume of 25:24:1 phenol:chloroform:isoamyl alcohol, and the upper aqueous solution were transferred into a new 1.5mL microcentrifuge tube after each extraction. The aqueous solution was washed with equal volume of chloroform and transferred into a new 1.5mL microcentrifuge tube. The DNA fraction was precipitated overnight with 10% (v/v) of 3M NaOAc and twice the volume of EtOH and incubated at -20^0C overnight. The sample was then pelleted for 20 minutes at 13,050 xg, air dried for 5 minutes and resuspended with 10 µL water. One µL of extracted viral DNA, 5 µM of primers (forward and reverse) of UF11, 12.5 µL of iQ SYBR Green supermix which contains Taq DNA polymerase and

fluoresein (Biorad #170-8882) was combined to a total volume of 25 µL with water. The sample was run on the Bio-Rad MyiQ v2.0.

In vitro GFP Infectivity Assay

The infectivity phenotype was determined using a GFP expression assay and measured by FACS Calibur (BD Biosciences). Approximately $1x10^4$ HEK293 cells were seeded with complete Dulbecco Modified Eagle's Medium (DMEM) on each well of a 96-well plates overnight in 5% CO2 at 37ºC. Approximately $5.8x10^9$ of purified r AAV vectors (wild-type and mutant) containing UF11 were mixed with $2x10^4$ infectious units (i.u.) of Ad5 (MOI of 1) in DMEM w/o fetal bovine serum (FBS), then used to infect HEK293 cells. Forty eight hours post infection, cells well harvested, washed, and resuspended with 300µL phosphate buffer saline (PBS). Percentage of cells that expressed GFP was analyzed using a FACS Calibur(BD Biosciences), implying the relative transduction efficiency of rAAVs-UF11. The number of cells analyzed was ~$4x10^3$. Mock infections, Ad infected HEK293 cells without rAAVs-UF11 were also analyzed.

In silico modeling and calculation of ligand binding to the AAV capsid

Molecular docking of the interaction between a heparan sulfate (HS) molecule and AAV1 (PDB accession No. 3NG9), AAV2 (PDB accession No. 1LP3), AAV5 (PDB accession No.3NTT), and AAV6 (PDB accession No. 3AOH) capsid was performed using the DOCK6 package v6.1 as described in program tutorial (175). The orientation and position of the VP monomers were moved to the Viper (56)standard orientation using SSM program, and an icosahedral trimer symmetric molecule was generated for AAV1, AAV2, AAV5 and AAV6 using Viper-oligomer generator (56). A HS dissacharide (consisting of 2-sulfamido-glucopyranosyl-6-O-sulfate and 2-O-sulfo-iduronic acid) PDB

coordinate was obtained and modified from the crystal structure of the C1 complement protein complexed with heparan sulfate determined to 2.3Å resolution (PDB accession No. 2WNU) (114). The atomic position of HS was translated closed to the adjacent region of AAV 3-fold wall surface. Hydrogen atoms were added to AAV VPand HS molecule coordinates using Dock Prep (in Chimera). The solvent accessible molecular sphere for all atoms was calculated and generated using thedmsprogram (implemented in Chimera v1.3 or later) with a water probe radius of 1.4 Å. A radius range of 15 Å from the initial HS molecule coordinate was used to filter and select the calculated spheres. An extra margin of 10 Å box was generated to enclose the calculated solvent accessible spheres. Scoring grid energy was calculated using the default parameter values including an attractive exponential of 6, a repulsive exponential of 12, and a dielectric factor of 4. In addition, a default 0.4 Å bump overlap filter was included in the calculation. Based on a series of energy scores calculated, rigid body fitting was performed on the solution with the lowest grid score for the HS molecule docked onto AAV VP trimer.

Structural Comparison among AAV Serotype Structures

The VP crystal structure was compared between AAV1 (PDB accession No. 3NG9), AAV2 (PDB accession No. 1LP3), AAV3b (PDB accession No. 3KIC), AAV4 (PDB accession No. 2G8G), AAV5 (PDB accession No. 3NTT), AAV6 (PDB accession No. 3OAH) AAV8 (PDB accession No. 2QA0), and AAV9 (PDB accession No. 3UX1), by structural alignment with the secondary structure matching (SSM) subroutine in the Coot program (85, 101, 102). The program superimposes Cα positions and provides information on residues that are structurally equivalent, inserts gaps when the atoms are too far apart to superimpose, and provides the distances (in Å) between the Cα

positions. Variable regions (VRs) between the AAV structures were identified as previously defined (119), stretches of more than two amino acids with Cα positions that are >1.0 Å apart between two serotypes.

Table 2-1.Nucleotide sequence of primers used in this study.

Primer Sequence	VP a.a.
5’CTCCAGCTGGCATGCGGGTTCAGCCCAAAAACTG3’	S472R
5’CAGTTTTTGGGCTGAACCCGCATGCCAGCTGGAG3’	S472R
5’CAGCTGGCATGCGTGTTCAGCCC3’	S472R
5’GGGCTGAACACGCATGCCAGCTG3’	S472R
5’GCTGGCATGTCTGACCAGCCCAAAAACTGGC3’	V473D
5’GCCAGTTTTTGGGCTGGTCAGACATGCCAGC3’	V473D
5’CTGGCATGTCTGATCAGCCCAAAAACTG3’	V473D
5’CAGTTTTTGGGCTGATCAGACATGCCAG3’	V473D
5’CAGACAACAACAACAGCGAATTTACCTGGACTGGTGCTTC3’	N500E
5’GAAGCACCAGTCCAGGTAAATTCGCTGTTGTTGTTGTCTG3’	N500E
5’CAACAACAACAGCGAATTTACCTGGACTGGTGC3’	N500E
5’GCACCAGTCCAGGTAAATTCGCTGTTGTTGTTG3’	N500E
5’CAACAACAGCAATTTTTCGTGGACTGGTGCTTC3’	T502S
5’GAAGCACCAGTCCACGAAAAATTGCTGTTGTTG3’	T502S
5’CAACAACAACAGCAATTTTTCGTGGACTGGTGCTTCAAAA3’	T502S
5’TTTTGAAGCACCAGTCCACGAAAAATTGCTGTTGTTGTTG3’	T502S
5’CCAATACCTGTATTACCTGAGCAGAACTCAAAATCAG3’	N447S
5’CTGATTTTGAGTTCTGCTCAGGTAATACAGGTATTGG3’	N447S
5’CAACAGCAATTTTACCGCTACTGGTGCTTCAAAATATAACC3’	W503A
5’GGTTATATTTTGAAGCACCAGTAGCGGTAAAATTGCTGTTG3’	W503A
• 5’GCCTGCGATCTGGTCAA3’	129
• 5’CGAGAACCCGCTTCTTGGCCTGG3’	129
• 5’CTGCGGTATAACCACGCCGAC3’	418
• 5’CCGGCCCAAGAGACTCAACTTC3’	418
• 5’CCGAGTCCGAGAAGACTTGAACC3’	531, 584, 598
• 5’CAACCCTGGCACTGCTATGGCC3’	531, 584, 598
• 5’CCAATGCAGTGTTTGAAGCTCCGGC3’	642
• 5’TAGAGACGTGTACCTGCAGGGTC3’	642

- Primers used for screening AAV1 and AAV6 reciprocal mutants

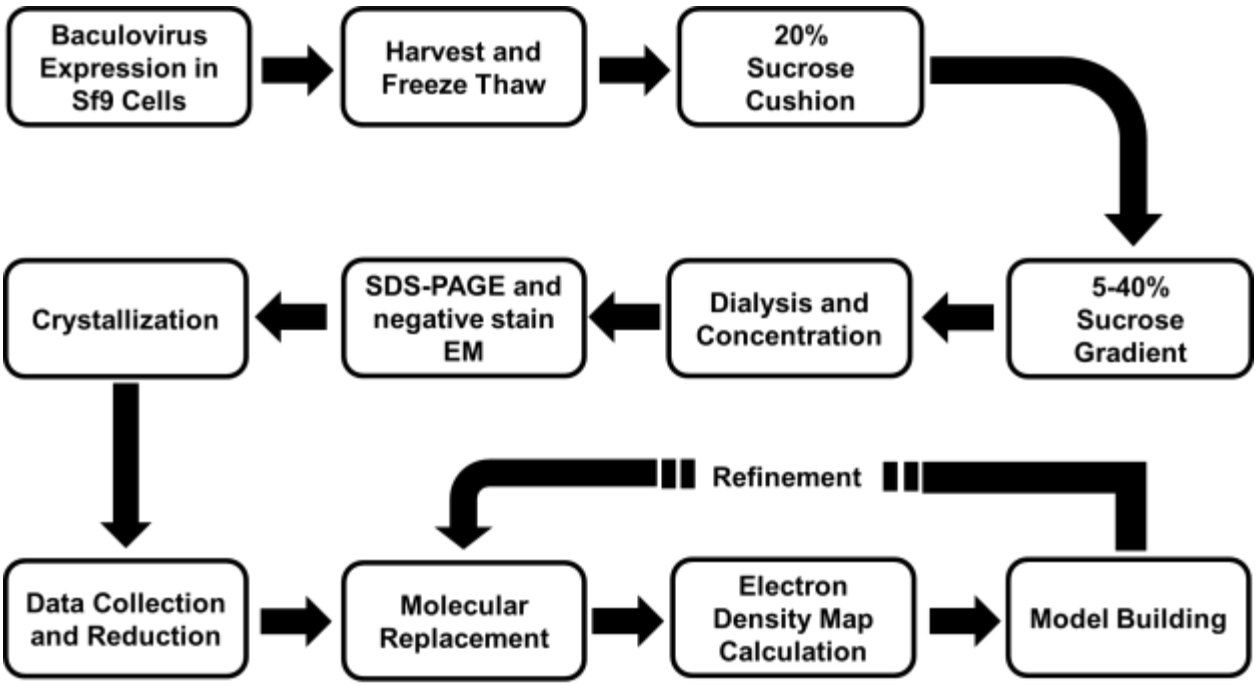

Figure 2-1.Schematic flow chart of AAV1 and AAV6 VLP expressions, purifications and structural determination.

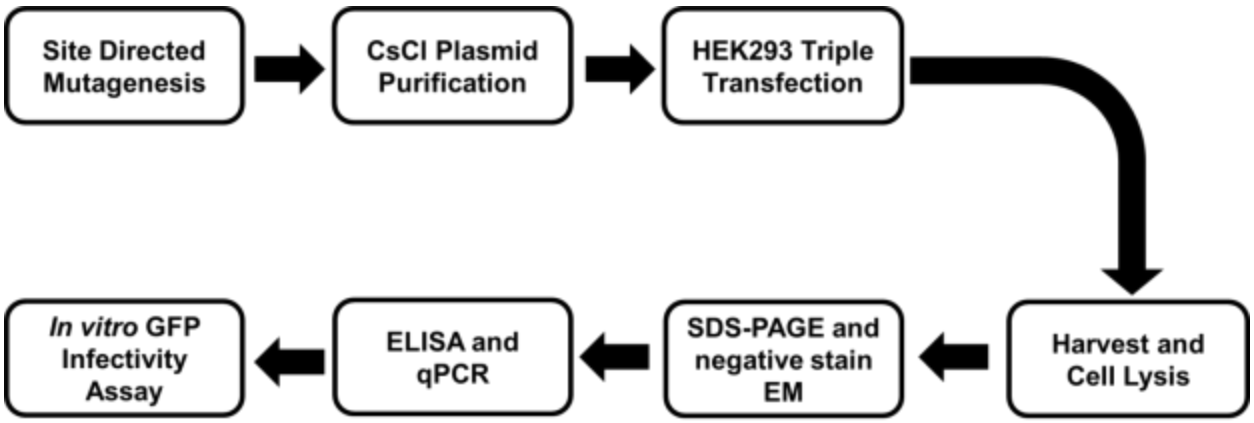

Figure 2-2. Schematic flow chart of mutagenesis and transduction phenotype studies of AAV1 and AAV6 SIA interaction residues mutants.

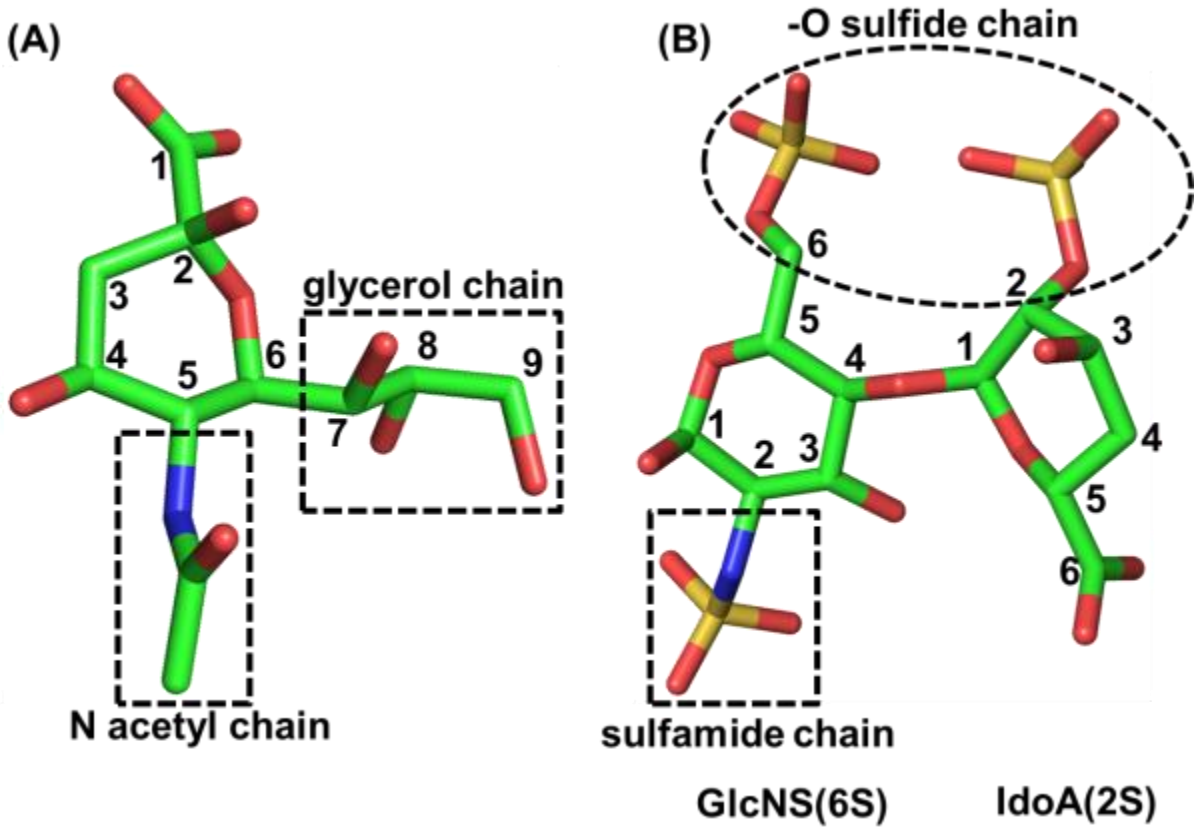

Figure 2-3. Stick representations of (A) a sialic acid (SIA) and (B) a heparan sulfate (HS) building block; GlcNS(6S)-IdoA(2S) molecule. Molecules are colored based on the elements; green for carbon (C), red for oxygen (O), blue for nitrogen (N), and orange for sulfur (S). The numberings on the carbon atom of the neuraminic acid, iduronic acid and glucopyranosic acid molecules are labeled.

CHAPTER 3
STRUCTURE DETERMINATION OF ADENO-ASSOCIATED VIRUS SEROTYPE 6

Introduction

AAVs have shown significant potential as clinical gene delivery vectors (discussed in chapter 1). To date, more than 100 AAV isolates have been identified (113). Among the human and nonhuman primate AAVs isolated, 12 serotypes (AAV serotype 1 (AAV1) to AAV12) have been described and are classified into six phylogenetic clades on the basis of their VP sequences and antigenic reactivities, with AAV4 and AAV5 considered to be clonal isolates (113). AAV1 and AAV6, which represent clade A, differ by only 6 out of 736 VP1 amino acids (5 amino acids within VP3) and are antigenically cross-reactive. Other clade representatives include AAV2 (clade B), AAV2-AAV3 hybrid (clade C), AAV7 (clade D), AAV8 (clade E), and AAV9 (clade F) (113). The AAVs are under development as clinical gene delivery vectors (e.g., (57, 71, 78, 123, 124, 240)), with AAV2, the prototype member of the genus, being the most extensively studied serotype for this application. Though AAV2 has been used to treat several disorders (213), it has the disadvantage of broad *in vitro* tissue tropism and its naturally acquired neutralizing antibodies makes this vector less effective for re-administration compared to other serotypes (69). Therefore, other serotypes have been studied and utilized to transduce specific tissues. Efforts have thus focused on characterizing the capsid-associated tissue tropism and transduction properties conferred by the capsid of representative serotypes of other clades (113). Outcomes of these studies include the observation that AAV1 and AAV6, for example, transduce cardiac, muscle, and airway epithelial cells more efficiently (e.g., up to 200-fold) than AAV2 (130, 137, 148). In addition, the six residues (Table 3-1) that differ between the VPs of AAV1 and AAV6 (a

natural recombinant of AAV1 and AAV2 (255)) confer functional disparity between these two viruses. For example, AAV6 shows ~3 fold higher lung cell epithelium transduction than AAV1 (130), and AAV1 and AAV6 bind terminally sialylated proteoglycans as their primary receptor, whereas AAV6 additionally binds to heparan sulfate (HS) proteoglycans with moderate affinity (306, 307). Therefore, a comparison of the AAV1 and AAV6 serotypes and, in particular, their capsid structures can help pinpoint the capsid regions that confer differences in cellular recognition and tissue transduction.

The structures of AAV1 - AAV5 and AAV7-AAV9 have been determined by X-ray crystallography and/or cryo-electron microscopy and image reconstruction (cryo-EM) ((92, 119, 172, 180, 223, 232, 291, 311) and unpublished data). The capsid VP structures contain a conserved eight-stranded (βB to βI) β-barrel core and large loop regions between the strands that form the capsid surface. The capsid surface is characterized by depressions at the icosahedral two-fold axes of symmetry, finger-like projections surrounding the three-fold axes, and canyon-like depressions surrounding the five-fold axes. A total of nine variable regions (VRs; VRI to VRIX) were defined when the two most disparate structures, AAV2 and AAV4, were compared (119). The VRs contain amino acids that contribute to slight differences in surface topologies and distinct functional phenotypes, such as in receptor binding, transduction efficiency, and antigenic reactivity (5, 62). The structure of AAV6 was determined to complete the structural library for the representative members of the AAV clade and clonal isolates and was used to further annotation the differential properties of the AAVs when correlated with the available functional data.

Results and Discussions

Structure of AAV6 VLP

The structure of the AAV6 VLP was determined to 9.7-Å resolution by cryo-EM and X-ray crystallography to 3.0 Å resolution. The capsid surface of the cryo-reconstructed AAV6 structure exhibits the previously defined characteristic features of AAV capsids, with a depression at each 2-fold axis, protrusions surrounding each 3-fold axis, and a canyon-like depression surrounding the channel at each 5-fold axis (Figure 3-1 A and B). Consistent with the high degree of structural similarity between AAV1 and AAV6, a correlation coefficient of 0.94 was calculated for the fit between the cryo-reconstructed density map and a map generated from structure factors calculated from the docked AAV1 crystal structure (PDB accession No. 3NG9) based on a polyalanine model generated using the Mapman program (152). The docked model provided information on the Cα positions of five of the six amino acids (418, 531, 584, 598, and 642) that differ between AAV1 and AAV6 in the C-terminal regions of VP3 (Figure 3-1 C and D). The side chain orientations and potential interactions of these residues could not be determined from the cryo-reconstructed structure but were obtained from the X-ray crystal structure.

The AAV6 crystal structure was determined to 3.0-Å resolution (Table 3-2). The refinement and molecular geometry statistics are consistent with those reported for other members of the Parvoviridae as well as structures determined for other virus families at comparable resolution, as reported on the VIPERdb website (http://viperdb.scripps.edu/). As has been previously reported for other AAV capsid structures, the N-terminal region of VP2 and the first 15 amino acids of VP3 were

unresolved in both the cryo-EM and X-ray structures ((92, 119, 172, 180, 223, 232, 291, 311)). In all of these AAV structures, only the overlapping C-terminal VP (~520 a.a.) region common to the VP1, VP2, and VP3 sequence is unambiguously resolved. The lack of ordered density for the VP N termini in the AAV6 VLPs used in this study likely results from the low copy number of VP2 (~5 copies) and the fact that the VP3 N-terminus likely adopts different conformations, two factors which are incompatible with the icosahedral symmetry imposed during the structure determination procedures. The C-terminal 519 a.a. (residues 218 to 736, VP1 numbering) common to VP2 and VP3 (hereafter referred to as VP3) were unambiguously assigned in the averaged AAV6 electron-density map (Figure3-2 A and B). This same stretch of amino acids was fitted into the cryo-reconstructed density map (Figure 3-1 B to D). The structural topology of the AAV6 VP3 is similar to that previously reported for other parvoviruses, with a conserved eight-stranded β-barrel (βBIDG-βCHEF sheets) core that forms the contiguous capsid and an α helix (αA, residues 290 to 302, VP1 numbering) located on the wall of the depression surrounding the icosahedral 2-fold axes ((92, 119, 172, 180, 223, 232, 291, 311)) (Figure 3-2 C). A tubular density feature consistent with helix αA was also observed in the cryo-reconstructed density map (data not shown). The capsid surface is formed by loop structures inserted between the β strands (Figure 3-2 C). These loops also contain small stretches of β structure (Figure 3-2 C). Comparisons of the previously determined AAV crystal structures identified regions of variable conformation (VRI to VRIX) in these loops (119). The VRs are spread throughout the VP3 structure but are clustered on the capsid surface. These regions also differ between AAV6 and the other AAVs, in particular, AAV4 (Figure 3 A; see Table 3-3).

These VRs contribute to phenotypic differences, such as receptor attachment, transduction efficiency, and antigenic reactivity, between the AAVs (5, 62). The conserved DE and HI loops (Figure 3-2 C and 3 A), between the βDE and βHI strands, respectively, play essential structural and functional roles in the life cycle of the AAVs and other parvoviruses. The DE loops in five (symmetry-related) monomers interact and form the channel at the 5-fold axis through which genomic ssDNA is postulated to be packaged (171). This is also where a phospholipase A2 (PLA2) domain, located within the VP1 unique N termini, is proposed to be externalized during cellular trafficking (171). Structural variation is observed at the top of the DE loop (Figure3-3 A, VRII), consistent with dynamics which might be required for genome packaging or the PLA2 externalization (168, 171). The HI loop lines the floor of the depression around the icosahedral 5-fold axes and is implicated in capsid assembly as well as capsid dynamics associated with receptor attachment (93, 183).

In addition to the VP3 structure and solvent molecules, densities consistent with a purine NT and a pyrimidine base were observed in the AAV6 VLP capsid structure, despite the fact that these particles should be empty (devoid of DNA). The purine base, assigned as an adenine due to the lack of a C-2 amino group density, is located in a conserved DNA binding region and occupies the same position as the bases previously reported in the crystal structures of AAV3, AAV4, and AAV8 (119, 180, 223) (Figure 3-4; the structure of AAV8 is not shown). The conserved binding region contains amino acids E417, V419, P420, D609, H630, P631, and S632, which are capable of forming polar and hydrophobic interactions with the NT and sandwich the bases between the two prolines (Figure 3-4; residue D609 is not shown). However, in AAV6, the orientation

of the base as modeled into the F_o-F_c map is rotated 180° about the plane of the base relative to the bases built into the other AAV structures due to the position of the density interpreted as the deoxyribose sugar (Figure 3-4). In the $2F_o$-F_c Fourier map (calculated before initial NT model building), a dual position of the density interpretable as the deoxyribose was observed, whereas the densities interpretable as the base and phosphate groups overlap with positions observed for the other AAV NTs (Figure 3-4). The dual orientation of the sugar portion of this ordered NT suggests that both orientations can occur with equal probability. The overlapping position of the base within the conserved binding pocket suggests that its interactions with the surrounding amino acids dictate the ordering of this nucleotide. The observation of a single sugar conformation in the F_o-F_c Fourier density map (Figure 3-4) suggests a higher propensity for the orientation modeled inside the AAV6 VLPs.

Five angstroms from the purine base, a second base, cytosine (assigned on the basis of the absence of methyl group density at the C-5 position of the pyrimidine ring), is ordered in a position proximal to the 3-fold axis (Figure 3-4). No sugar or phosphate groups were observed for this base, which interacts with the main chain of H630. This Histidine is conserved in representative clade members of the AAVs (Figure 3-4), but despite this conservation, the density for this base was not reported in the AAV3 crystal structure (180), nor was it observed in our structures of AAV4 and AAV8 (119, 223). There is no indication that this cytosine base and the purine NT are components of a single DNA chain. Significantly, like the AAV6 structure, that of AAV8 was also determined from baculovirus/Sf9-expressed VLPs produced in the absence of the *rep* ORF. These observations support a proposal that the AAVs are able to package

fragments of host cellular DNA in the absence of Rep proteins (183). A similar packaging of cellular genomic material is commonly observed for RNA viruses expressed in a heterologous system, most likely due to a requirement for interaction with nucleic acid for capsid assembly (106). For bacteriophage ΦX174, a small ssDNA virus that packages a genome similar in size to those of parvoviruses, in virions, subgenomic pieces of DNA are also observed in empty capsids and are also likely required to facilitate capsid assembly (208). DNA packaging is not required for the assembly of autonomous parvovirus VLPs, as reported for minute virus of mice (141, 168), but the AAV observations suggest that it may play a role for the dependoviruses, though this remains to be verified.

The lower occupancy (0.5) of the AAV6 bases, relative to the surrounding protein (as was reported for AAV8 (223)), is consistent with the expected lack of icosahedral symmetry for NTs ordered within VLPs. Indeed, only a single copy of the ssDNA genome is packaged into wild-type virions, and thus, the same NT/base cannot be ordered in all 60 sites within the capsid, unless it is part of a conserved DNA sequence repeated 60 times and forming specific interactions with the capsid. Such a conserved DNA sequence has not been reported for the AAVs. Given occupancy of less than one, the strict NCS utilized for electron-density averaging during the structure determination would be expected to result in reduced sigma for NT/base density at each averaging cycle and eventual loss of signal. Thus, the unexpected observation of ordered DNA density inside AAV6 and other AAVs suggests the presence of a common DNA recognition motif inside the capsid directly under the 3-fold axes (Figure 3-2 C). The fact that the recognition site amino acids are conserved in most AAV sequences and all the

structures determined to date suggests an important function for this DNA interaction in the life cycle of the viruses, such as a role in capsid stabilization or assembly.

Comparison of AAV6 Structure to Those of Other AAVs Pinpoints Capsid Regions That Control Differential Tissue Transduction Property

Superposition of the AAV6 structure with those available for AAV1 to AAV5, AAV8 and AAV9 using the SSM application in the Coot program (101, 102) shows differences (stretches of two or more amino acids with Cα positions that are >1.0 Å apart between two serotypes (119)) with (i) AAV2 at VRI, VRII, VRIV, VRV, and VRVII; (ii) AAV3 at VRI, VRII, VRIV, VRVI, VRVII, and VRIX; (iii) AAV4 at VRI to VRIX; and (iv) AAV8 at VRI, VRII, VRIV, VRV, and VRVII (Figure 3-3). Variable regions I and IV were commonly divergent in conformation between AAV6 and these four AAVs (Table 3-3; Figure 3-3 B and C). The amino acids that form these two surface loops are also highly divergent between the representative members of the AAV clades. AAV1 and AAV6 are 99% identical and superimpose with an RMSD of 0.33 Å, and they exhibit the lowest difference between the Cα positions of residues in their VRIV regions (Table 3-3; Figure 3-3). AAV4 is the most structurally diverse from AAV6, with which it shares the lowest degree of sequence homology (59% compared to 80 to 99% with the other AAVs; Table 3-3). For example, the Cα positions of amino acids in VRIV differ from 1.0 to 14.6 Å, though the structures superimpose with an overall RMSD of 0.94 Å. AAV6 and AAV2 (83% identical) superimpose with an RMSD of 0.67 Å, and the Cα positions in VRIV differ between 1.3 and 4.9 Å (Table 3-3). The AAV VRs cluster on the capsid surface in the raised regions between the icosahedral 2- and 5-fold axes (VRs I, III, and IX) and on the wall (VRs VI and VII) and top (VRs IV, V, and VIII) of the protrusions surrounding the icosahedral 3-fold axes (5, 62). Significantly, VRI and VRIV (Figure 3-3 B and C)

have been shown to play a role in AAV tissue transduction and antigenic recognition (192, 265). These reports suggest that structural heterogeneity, in addition to sequence variation, confers these capsid-associated functions. The observation that VRIV adopts slightly different conformations in AAV1 and AAV6 may be related to this loop being the least-ordered VP3 common region in the AAV6 structure. Atoms in the amino acids at the top of the loop exhibit high-temperature factors, consistent with high thermal motion and minor conformation variation compared to those for AAV1.

To obtain a more detailed analysis of the structural determinants that dictate differences in receptor attachment and tissue transduction in the highly homologous AAV1 and AAV6, we superimposed the AAV1 crystal structure (PDB accession No.3NG9) onto the refined AAV6 structure in the electron-density map. This enabled the visualization of the positions of five of six amino acids (AAV1 and AAV6 amino acids E418D, E531K, F584L, A598V, and N642H) that differ between the AAV1 and AAV6 VPs (F584L and N642H are shown in Figure 3-2 A and B, respectively). Amino acid 129 (VP1 numbering) in the VP1 unique region was not present in the VP2/VP3 VLP construct used for this structure determination. Three of the ordered residues (531, 584, and 598) are located on the capsid surface, at (V598) or close to (K531 and L584) the icosahedral 3-fold-symmetry axes (Figure 3-5), whereas D418 and H642 are located on the interior surface of the capsid, below the same capsid region (Figure 3-5). Residues D418 and H642 are located in structurally conserved VP regions, whereas surface residue 531 is located in VRVI, residue 584 is located in VRVIII, and residue 598 is close to VRVIII. The localization of these five amino acids at or surrounding the icosahedral 3-fold axes, with K531 being near the icosahedral 2-fold axes in VRVI,

highlights the importance of these capsid regions in AAV biology with respect to receptor attachment and transduction efficiency. The surface exposed amino acid differences indicate potential sites for conferring the differential receptor recognition and transduction properties of AAV1 and AAV6 that are associated with entry or pre-uncoating interactions. The residues on the inside, with 418 in the vicinity of the DNA binding region (Figure 3-5) are unlikely to play a role in receptor attachment but could be involved in post-entry / uncoating events that affect transduction efficiency.

With respect to receptor attachment, residue K531 in AAV6 (E531 in AAV1) has been reported to be important for its HS binding properties, and an E531K mutant of AAV1 shows strong affinity for HS and also confers liver cell transduction (305), identifying a position at the base of the protrusions and close to the depression at the icosahedral 2-fold axes (Figure 3-5) that confers this phenotype. None of the mutations in AAV1 converting the remaining five amino acids which differ from those in AAV6 to the type found in the latter virus conferred an HS binding phenotype (306). A novel primate AAV variant, AAV(VR-942), which also uses HS as a primary receptor, contains a K528 residue that is predicted to be structurally equivalent to the AAV6 K531 residue (258) (Table 3-5). AAV2 also binds HS (275) but lacks this basic residue and, instead, utilizes two critical residues, R585 and R588, along with R484, R487, K527, and K532 (minor contributors) (AAV2 VP1 numbering) (Table 3-4) for this interaction (160, 183, 228, 230). Except for R487, these residues form a basic footprint on the surface (Figure 3-6 B) of the AAV2 capsid on the inner face of the protrusions surrounding the 3-fold axes. Interestingly, AAV1 and AAV6 contain basic residues R485, R488, K528, and K533 (equivalent to R484, R487, K527, and K532, respectively, in AAV2) in the

equivalent region of the mapped AAV2 HS binding site, plus R576 and H597 (Figure 3-6 A, B, and D). A basic region is created on the AAV1 and AAV6 capsid surface by residues R485, R576, and H597 close to the 3-fold axis and is missing in AAV2, which contains R484, Q575, and N596 at the structurally equivalent positions (Figure 3-6 A, B, and D). However, a role in HS binding has not been reported for R576 and H597. On the other hand, in AAV6, K531 is located adjacent to R488 (equivalent to AAV2 R487, but is now surface exposed), K528, and K533, which creates a second continuous basic patch on the capsid surface, whereas in AAV1, E531 creates a gap in this patch (Figure 5A and D). Hence, this continuous, basic region is likely sufficient for and the determinant of HS binding by AAV6. AAV5, which binds sialic acid, is missing all these basic residues, except for R471, which is equivalent to AAV6 R485 (Table 3-4). In addition to these basic residues, the juxtaposition of acidic residues on the capsid surface and their interactions with amino acids in the vicinity of the mapped basic HS binding residues appears to be important for the binding of this glycan by AAV serotypes. Mutation of an acidic residue, D532 to N532, adjacent to K533 on the AAV6 capsid surface (Figure 3-4 D and 3-7), in an AAV variant derived by directed evolution from AAV libraries, shH10, was reported to confer HS binding dependence and sialic acid binding independence (Table 3-1) for cellular transduction by the variant (165).

Though wild-type AAV6 binds HS, it can transduce cells in the absence of HS but not in the absence of sialic acid (33, 58, 70). Residue D532 is predicted to stabilize the surface loop containing K531by means of electrostatic interactions with H527 and D562 (Figure 6A), which are likely to be disrupted if the acid group at position 532 is lost. This loop also contains K528 and K533, which flank K531 on the capsid surface, as

discussed above (Figure 5D and 6A). The D532N mutation reduces the negative charge on the capsid and likely disrupts the D532-H527-D562 interaction; consequently, it could alter the conformation of this loop and thus the cellular interactions of constituent residues. The predicted loop-stabilizing interaction is conserved in HS binding AAV2 through the interactions of E531-H526-D561 and also E563 (Figure 3-7); thus, the stabilization is expected to be tighter in this virus. The side chain of AAV6 residue E564, with a Cα position equivalent to AAV2 E563, adopts a different orientation and does not participate in the stabilizing interactions (Figure 3-7). The shH10 mutant has improved HS binding compared to that of wild-type AAV6 and exhibits an improved transduction phenotype. AAV6, on the other hand, binds HS more weakly than AAV2 but also exhibits better transduction properties. Thus, binding affinity alone does not control transduction efficiency (165). Also, improved HS binding of the AAV6 D532N mutant nullified the virus's need for sialic acid, although it still transduced cells that contain sialic acid. These observations highlight the complex nature of cellular interactions that control cellular transduction mechanisms.

Further support for the role of acidic residues in HS binding was reported by Wu *et al*., who found that alanine scanning mutagenesis of acidic AAV2 residues 561-DEEE-564 to 561- AAAA-564 resulted in a noninfectious HS-negative (HS-) mutant (305). AAV6 residue D562 is not on the capsid surface but is structurally equivalent to AAV2 D561, which along with E563 and E531 participates in interactions which stabilize the basic residues involved in AAV HS binding (Figure 3-7), as discussed above. A disruption of the D561 and E563 interactions with neighboring residues, which is predicted to occur when these acidic residues are mutated to alanine in AAV2, is likely

involved in the HS- phenotype of the 561-AAAA-564 mutant. Interestingly, AAV2 E531, D561, and E563 are contained in two highly conserved acidic stretches of amino acids in the representative AAV clade members, with the exception of clonal isolates AAV4 and AAV5. The above observations suggest that their interactions are important for stabilizing the configuration of HS binding regions on the AAV2 capsid as well as the AAV6 capsid. The region of the AAV capsid required for interaction with sialic acid has not been structurally mapped, but mutagenesis studies with AAV5 suggest the involvement of A581 at the icosahedral 3-fold axes (105) (Figure 3-6 C). An alanine is conserved at the equivalent positions in AAV1, AAV2, and AAV6 (A592, A591, and A592, respectively) (Table 3-4; Figure 3-6). Of note, the region at or immediately adjacent to the icosahedral 3-fold axis is hydrophobic in AAV1, AAV5, and AAV6, which bind sialic acid, and polar in AAV2, which does not (Figure 3-6). Thus, if this is a conserved, sialic acid recognition site among the AAVs, the V598A difference between AAV6 and AAV1, which, along with V582 and A592, forms a continuous hydrophobic surface at the 3-fold axes (Figure 3-6 A and D), may be involved in the sialic acid binding interaction of both viruses. Both viruses are reported to have common sialic acid linkage recognition (307), and thus, if residue 598 exhibits a serotype specific phenotype in transduction, it is unlikely to be due to this interaction. Efforts to engineer AAV variants with improved/tissue-specific transduction properties have led to chimeric AAV1 and AAV6 vectors that show differential lung epithelial cell transduction efficiency dependent on which residues in the two serotypes are located at VP1 unique position 129 and within the common VP3 sequence (186, 187). The AAV6 F129L mutation (AAV6.2 in Table 3-1) confers 2-fold better transduction in airway epithelium compared

to the parental serotype and AAV6 K531E (AAV6.1 in Table 3-1), which eliminates HS binding, confers an AAV1 transduction phenotype that is reduced compared to that of the parental AAV6 (187). This observation suggests that amino acids at both the 129 and 531 positions affect cellular transduction. Residue 129, located in the VP1 unique region, is part of a PLA2 domain in the parvoviruses that is predicted to be located inside the assembled capsid but that later becomes externalized through the 5-fold channel during capsid trafficking through the endocytic pathway. This is purported to aid endosomal escape for nuclear localization and subsequent genome replication (171). Residue 531, as discussed above, facilitates HS binding in AAV6. Thus, residues 129 and 531 are likely involved in post-entry events and receptor recognition, respectively. Consistent with this suggestion, a mutant containing F129L and K531E (Table 3-1, AAV6R2) had the reduced transduction phenotype of the virus with the single K531E mutation (187), indicating that the K531E mutation functions early in infection, prior to the step affected by amino acid F129L. Li *et al*. used directed evolution from an AAV library to identify chimeric human airway epithelia (HAE) transducing vectors, HAE-1 and HAE-2 (Table 3-1), which contain mostly AAV1 and AAV6 sequences and which have improved transduction efficiency relative to that of the parental serotypes (186). HAE-1 contains AAV1 residues 1 to 583/641 to 736 and AAV6 residues 584 to 640, and HAE-2 contains AAV9 residues 1 to 30/104 to 193, AAV1/AAV6 residues 31 to 103, AAV6 residues 194 to 641, and AAV1 residues 642 to 736. The reported transduction efficiencies for these viruses compared to those of the parental serotypes were in the order AAV1/AAV9 < AAV6 < HAE-1 < HAE-2, with HAE-1 and HAE-2 showing ~3- to 4-fold and ~2-fold improved transduction compared to that of AAV1 and AAV6,

respectively. HAE-1 contains AAV1 residue L129 (not observed in the crystal structures), capsid surface residue E531, and interior residues E418 and N642, with AAV6 contributing surface residues L584 and V598 (Table 3-5). Thus, L584 and V598 confer the ~3-fold improvement in HAE-1 transduction compared to that of AAV1. The improvement in transduction relative to that in AAV6 could be due to the L129 from AAV1, as discussed above. HAE-2 contains the equivalent of AAV1 L129 (contributed from AAV9) and interior residue N642 from AAV1 and AAV6 capsid surface residues, K531, L584, and V598, as well as interior residue D418 from AAV6 (Table 3-1). For this vector, the AAV6 K531 residue likely combines with the L129, L584, and V598 residues of HAE-1 to achieve the further improvement in transduction compared to that of the parental viruses and HAE-1. Both chimeras were observed to bind equally to the apical surface of HAE, suggesting that their difference in transduction was post-entry, consistent with an intracellular step in the viral life cycle at which L129 is critical. A functional role for the interior residues, 418 and 642, is yet to be defined.

In summary, this comparative analysis of AAV1 and AAV6 highlights key AAV residues that control host interactions, including receptor recognition and attachment as well as post-entry events, which enable successful infection and improved cellular transduction. These results should facilitate further molecular characterization and manipulation of AAV vectors for improved tissue-specific targeting.

Table 3-1. Amino acid differences between AAV1 and AAV6 and their reported mutants

AAV	129	418	531	532	584	598	642	Glycan Target
AAV1	L	E	E	D	F	A	N	S
AAV1 E/K	L	E	K	D	F	A	N	HS^+ (and S)[c]
AAV6	F	D	K	D	L	V	H	HS and S
AAV6.1	F	D	E	D	L	V	H	HS^-(and S)[c]
AAV6.2	L	D	K	D	L	V	H	HS (and S)[c]
AAV6R2	L	D	E	D	L	V	H	HS (and S)[c]
HAE1	L	E	E	D	L	V	N	(HS^- and S)[d]
HAE2	L	D	K	D	L	V	N	(HS^- and S)[d]
shH10	F	D	K	N	L	V	N	HS (and S-ind)[e]

[a] = Mutant residues in bold face have an AAV6 parental original; those underlined have an AAV1 parental origin; [b] = S: sialic acid; HS: heparan sulfate; HS^+: HS positive; HS^-: HS negative; [c] = The sialic acid binding phenotypes of these mutants were not discussed in the respective publications but are assumed to be still present; [d] = The glycan targets for these mutants were not discussed in this publication; thus, the phenotypes indicated are assumed; [e] = This mutant is sialic acid independent (S-ind) for cellular transduction. Table was adapted from (225).

Table 3-2. Data Collection, Reduction and Refinement Statistics a

Data Collection	CHESS F1
Wavelength (λ , Å)	0.917
Space group	R32:H
Unit cell parameters (Å)	a = 262.6, c = 609.9
Resolution	40.0 – 3.0 (3.1 - 3.0)
No. of unique reflections	119,617 (8,285)
Completeness (%)	72.3 (50.5)
Average I/sigma	6.5 (2.5)
Rmerge (%)	15.4 (44.3)
Refinement	CNS v1.2
No. of atoms (protein/solvent/DNA)	4,117/ 12 /25
Average B factors ($Å^2$)	61.87
Rcryst / Rfree (%)	27.5 / 28.8
RMSD bonds (Å) and angles (^{0})	0.009 / 1.48
Ramachandran plot	
Most favorable allowed (%)	92.5
Additionally allowed (%)	7.5

[a] Values in the parenthesis are for the highest resolution shell; [b] CNS = Crystallography and NMR System; [c] Rmerge = $(\Sigma|\boldsymbol{I}_{hkl}-<\boldsymbol{I}_{hkl}>| / \Sigma|\boldsymbol{I}_{hkl}|) \times 100$, where $\boldsymbol{I}_{hkl}$ is the intensity of an individual hkl reflection and $<\boldsymbol{I}_{hkl}>$ is the mean intensity for all measured values of this reflection; [d] Rcryst = $(\Sigma||F_{obs}|-|F_{calc}|| / \Sigma|F_{obs}|) \times 100$, F_{obs} and F_{calc} are the amplitudes for the observed and calculated reflections, respectively; Rfree was calculated with the 5% of reflections excluded from the data set during refinement. Table was adapted from (225).

Table 3-3. RMSD in Cα position between AAV6 and the available AAV serotype crystal structures overall and for VRI and VRIV

AAV Serotype	a.a. % identity	VR Cα distance ranges (Å)		
		Overall	VRI	VRIV
AAV1	99	0.33		1.3 – 1.8
AAV2	83	0.67	1.2 – 5.7	1.3 – 4.9
AAV3	86	0.57	1.7 – 5.8	1.3 – 6.4
AAV4	59	0.94	0.9 – 6.8	1.0 – 14.6
AAV8	80	0.57	1.3 – 7.4	1.4 – 2.4
AAV9	80			

(The table was adapted from (225)).

Table 3-4. Comparison of residues reported to be involved in heparan sulfate and sialic acid binding for AAV6, AAV1, AAV2, AAV5, andAAV-VR942 and the amino acids at equivalent positions in each virus

	Amino acid at residue(AAV6 VP numbering)							
AAV	485	488	528	531	533	586	589	592
6	R	R	K	K	K	S	T	A
1	R(485)	R(488)	K(528)	E(531)	K(533)	S(586)	T(589)	A(592)
2	R(484)	R(487)	K(527)	E(530)	K(532)	R(585)	R(588)	A(591)
5	R(471)	G(474)	L(515)	S(518)	N(519)	S(575)	T(578)	A(581)
VR942	R(482)	R(485)	K(525)	K(528)	K(530)	N(583)	A(586)	T(589)

*; Numbers in parentheses are based on VP1 numbering for the respective serotypes.Table was adapted from (225).

Figure 3-1.AAV6 structure. (A) Surface representation of the AAV6 cryo-reconstructed image at 9.7Å resolution. The capsid surface density is shown as a radially colored, depth-cued image (low to high radii, pink to gray). Selected icosahedral 2-fold (2f), 3-fold (3f), and 5-fold (5f) axes of the capsid are indicated by arrows. (B) Cross-sectioned slab from the cryo-EM density map (gray isosurface) with the docked Cα backbone of the polyalanine model (residues 218 to 736, pink) derived from the AAV1 crystal structure (PDB accession No. 3NG9). Dashed arrows indicate the approximate locations of icosahedral axes of symmetry. (C) Coil representation of an AAV6 VP backbone trace (pink) showing the locations of the five amino acids (pink spheres) within VP3 that differ between AAV1 and AAV6. The first and last letters in each residue label refer to AAV6 and AAV1, respectively. (D) A trimer of AAV6 VPs (pink, green, and blue) showing the symmetry-related clustering of the differing residues (spheres) shown in panel C and colored according to the monomer in which they reside. These residues cluster near the icosahedral 3-fold axes in both the interior (residues 418 and 642) and exterior (residues 531, 584, and 598) surfaces of the capsid. The view is approximately down the icosahedral 3-fold axis. Approximate positions of icosahedral 2-, 3-, and 5-fold-symmetry axes of the capsid are depicted as filled ovals, triangles, and pentagons, respectively, in panels C and D. Panels A and B were generated using the Chimera program (237), and panels C and D were generated using the PyMol program (86) and adapted from (225)

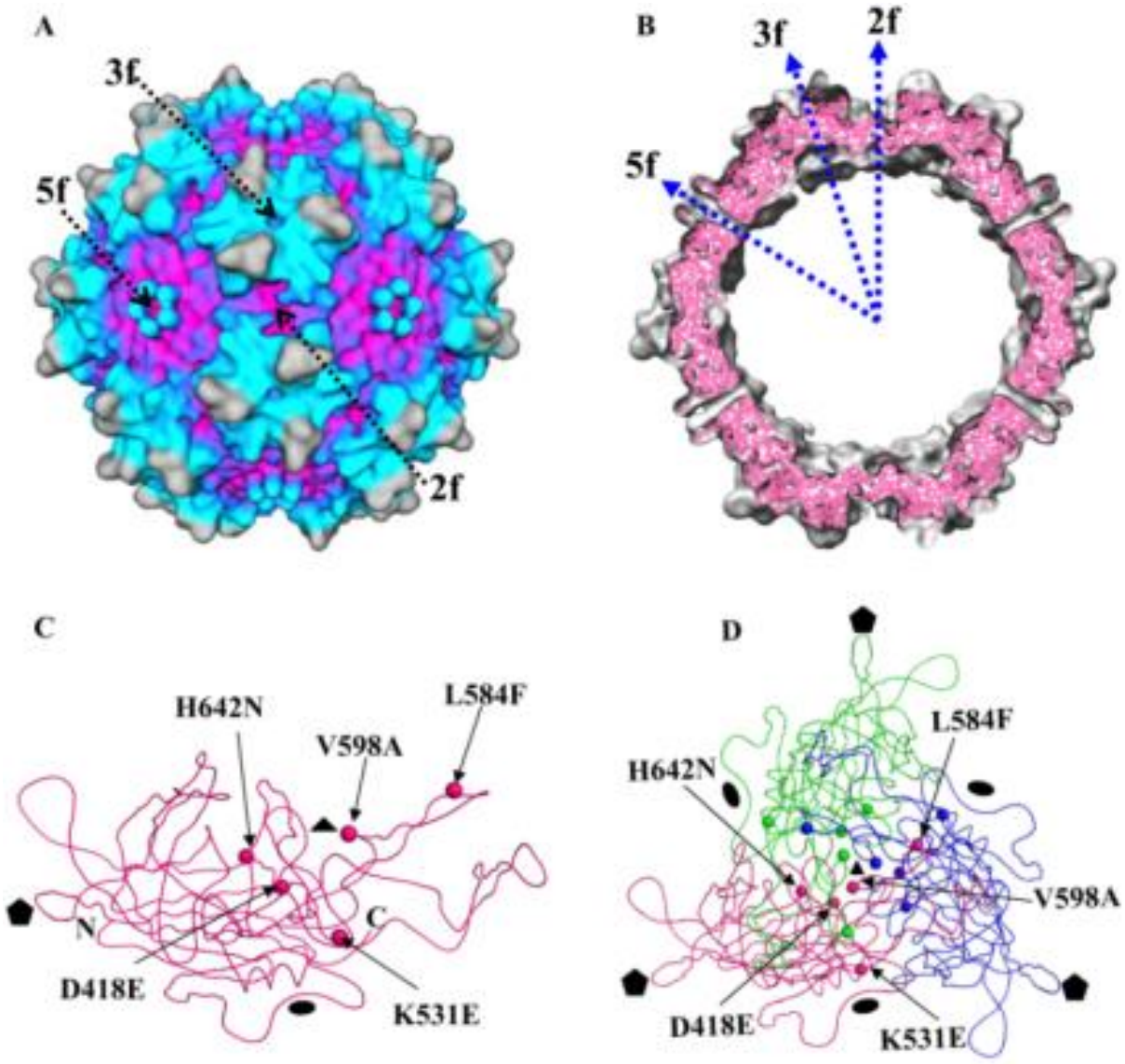
A
3f
5f
2f
B
3f
2f
5f
C
H642N
L584F
V598A
N
C
D418E
K531E
D
L584F
H642N
V598A
D418E
K531E

.

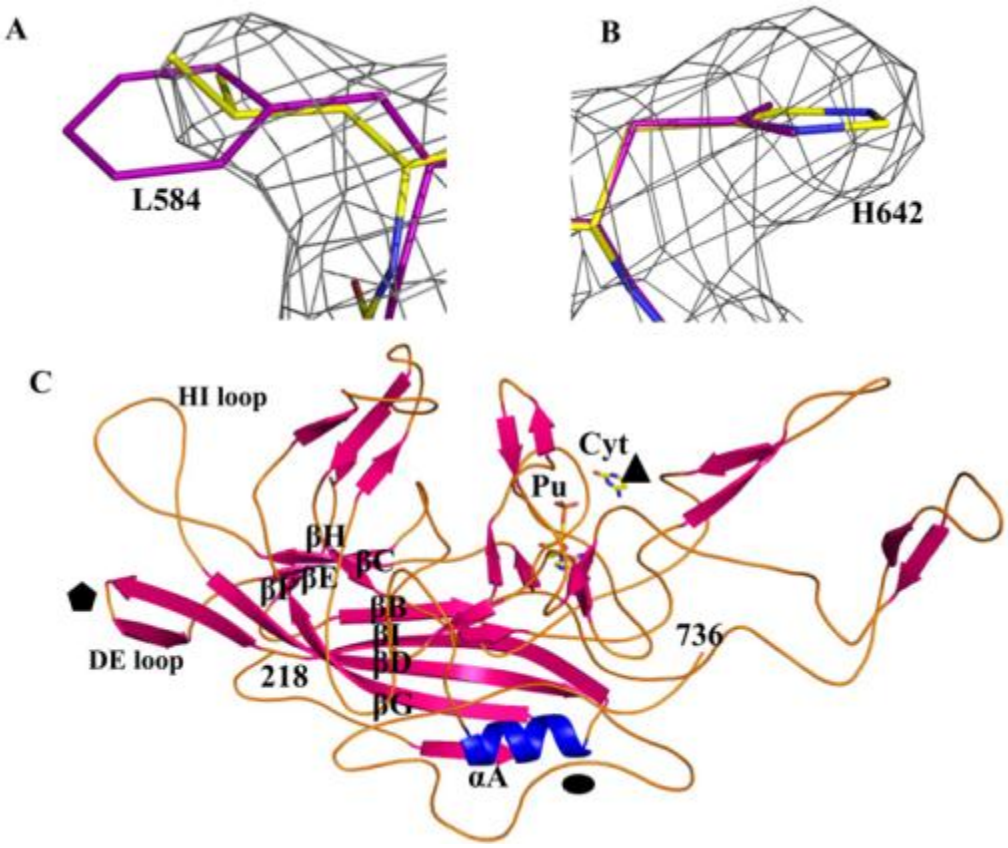

Figure 3-2.Crystal structure of AAV6. (A and B) Sections of the 2Fo-Fc electron-density map (gray mesh) of AAV6, contoured at 1.0σ, for two of the residues (residue 584 in panel A and residue 642 in panel B) that differ between AAV6 and AAV1. The AAV1 (purple) and AAV6 (atom type) coordinates are shown in stick form. (C) Ribbon diagram representation of AAV6 VP3 monomer (ordered residues 218 to 736), with labels highlighting the conserved β-barrel core motif (βBIDG-βCHEF, pink) and the αA helix (blue). Loop regions (orange) between the core βstrands. This figure was generated using Pymol program (86) and adapted from (225).

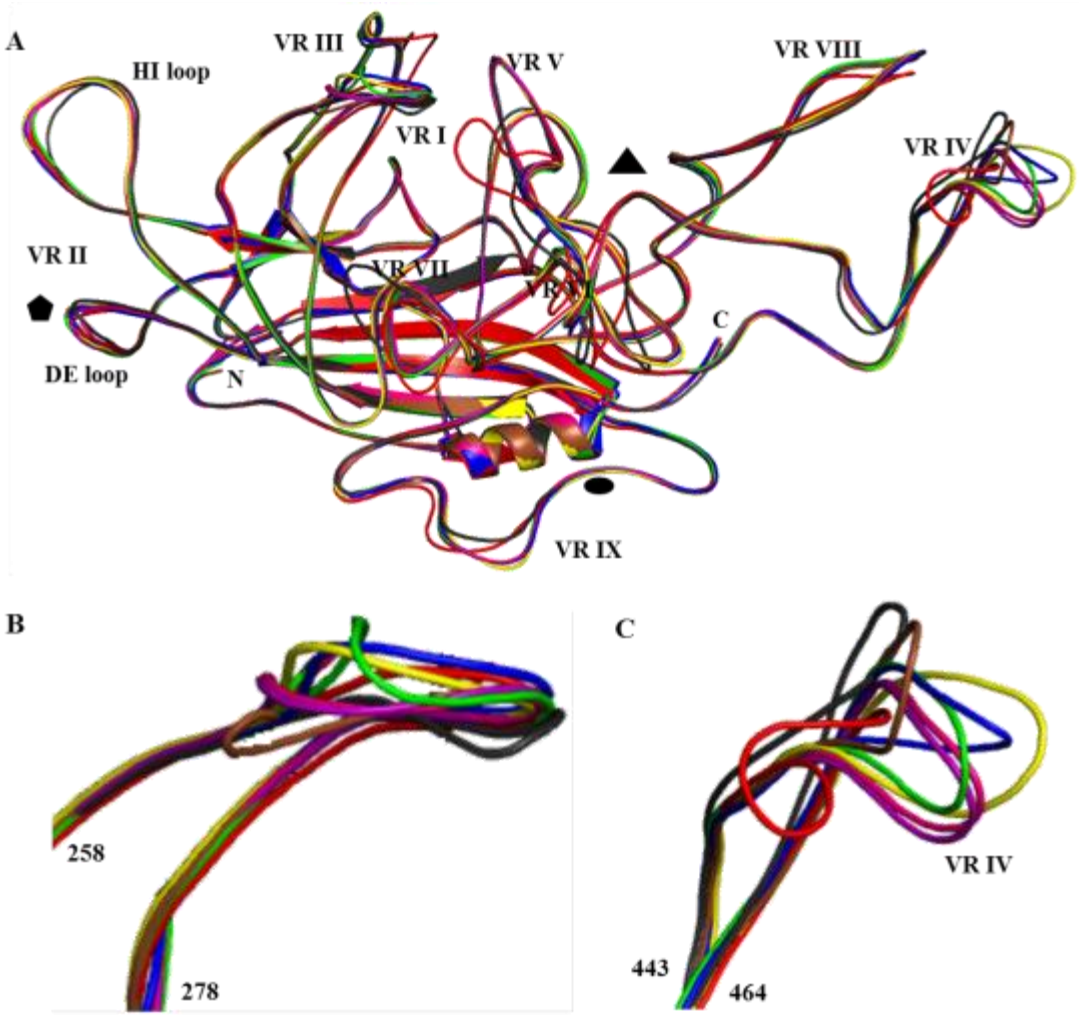

Figure 3-3.Comparison of available AAV crystal structures. (A) Superposition of the VP3 monomer structure of AAV1 (purple), AAV2 (blue), AAV3 (yellow), AAV4 (red), AAV5 (gray), AAV6 (pink), AAV8 (green), and AAV9 (brown). Common variable regions VRI to VRIX are labeled with roman numerals. The DE and HI loops are labeled. Approximate positions of the icosahedral 2-, 3-, 5-fold axes are depicted as described in the legend to Figure 1. (B and C) Close-up views of VRI and VRIV, respectively. This figure was generated using Pymol program (86) and adapted from (225).

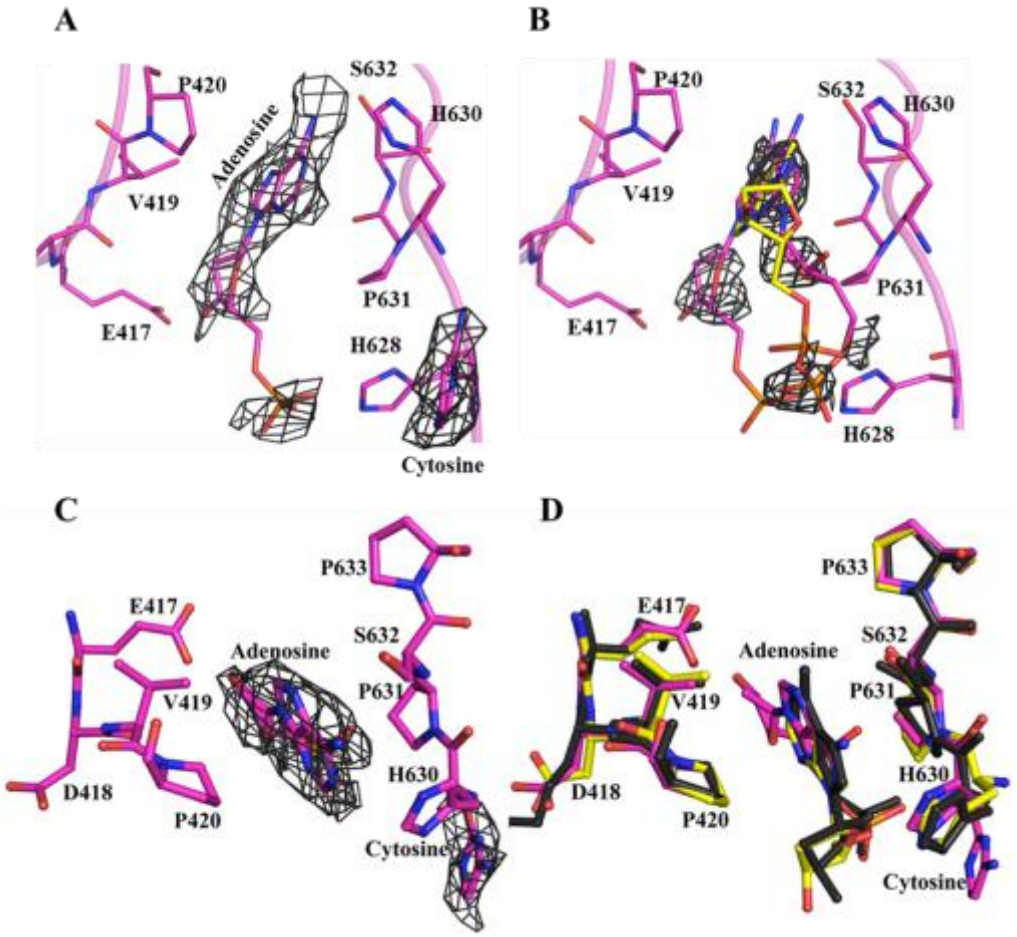

Figure 3-4. AAV6 DNA binding site. A. The conserved nucleotide binding pocket, showing the ordered Fo-Fc densities (grey mesh) contoured at 3.0 σ, interpreted as a deoxyadenylate and cytosine (labeled). This orientation shows position of the density interpreted as the deoxyribose sugar, which is rotated approximately 180º relative to the positions of the sugars in the NT models built for other available AAV structures. B. The dual conformation of the deoxyadenylate NT observed in the 2Fo-Fc density map. Refinement of two models (I and II) built into this density indicated that the model I conformation had the highest occupancy (based on temperature factor comparison), consistent with the orientation that was dominant in the Fo-Fc difference density map. (C) 900 rotation from panel (A); residue D609 has been omitted for clarity. (D) Comparison of nucleotide binding pocket in AAV3 (yellow), AAV4 (black), and AAV6 (pink) crystal structures. This region (structure and DNA) is also conserved in AAV8 (data not shown). AAV6 amino acid positions are labeled. This figure was generated using the PyMol program (86). AAV6 amino acids within 2.4 Å to 5.0 Å of the ordered density are shown and labeled. This figure was modified from (225).

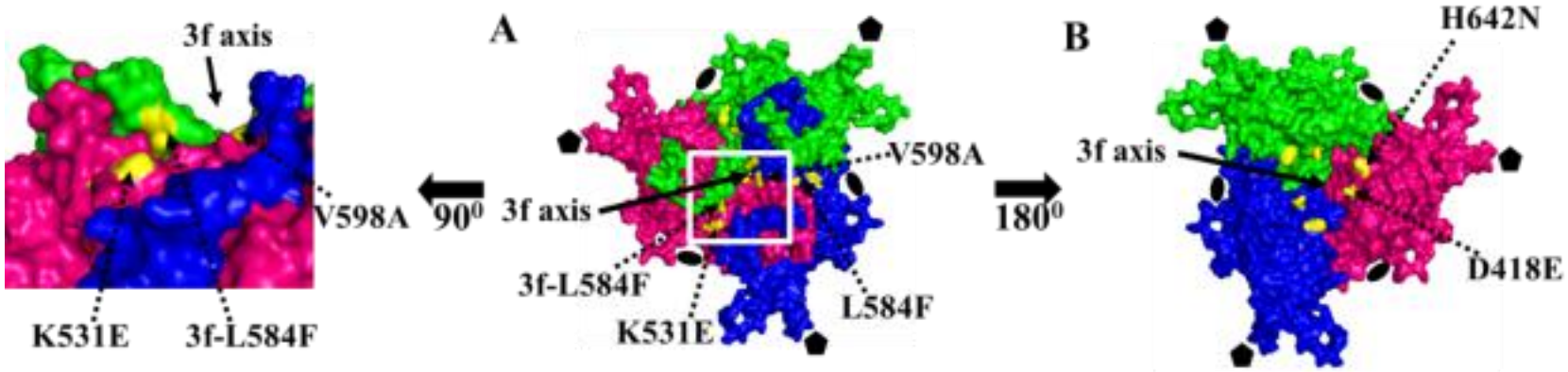

Figure 3-5. Locations of amino acid differences in AAV1 / AAV6 capsids. (A) Surface representation of an AAV6 trimer viewed from outside approximately along a 3-fold axis (middle) with the white boxed section rotated 900 (top). The monomers are colores pink (reference), green (3-fold) and blue (3-fold), with the differing AAV1/AAV6 amino acids colored in yellow. Residues K531E, L584F (3f-L584 is from a 3-fold related monomer) and V598A (first letter AAV6 and second letter, AAV1) are located on the capsid surface. The panel on the left shows the close proximity of residue 531 and 584 at the base of the 3 fold protrusions facing icosahedral 2-fold axis. (B) Same as panel A, but rotated 1800 to show the location of the residues D418E and H642N on the interior surface of the capsid. The approximate position of the 3-fold axis (3f axis) is indicated with a solid arrow in all three panels. Approximate positions of icosahedral and 2- and 5-fold symmetry axes on the capsid are depicted as in Figure 1. This figure was generated using Pymol program (86) and modified from (225).

Figure 3-6. Comparison of AAV surface residues. Schematic Roadmap projections (309) of surface residues in a portion of the icosahedral asymmetric unit for crystal structures of AAV1 (A), AAV2 (B), AAV5 (C), and AAV6 (D) are shown. The area occupied by each amino acid residue correlates to surface exposure when the capsid is viewed down an icosahedral 2-fold axis. The boundary for each residue is shown in black, and the colors correspond to acidic (red), basic (blue), polar (yellow), and hydrophobic (green) residues. Dashed outlines highlight regions proposed to play a role in glycan binding by the respective serotypes. Residues are labeled by type and number. The icosahedral 3-fold axis is depicted by the filled triangle. Figure is adapted from (225).

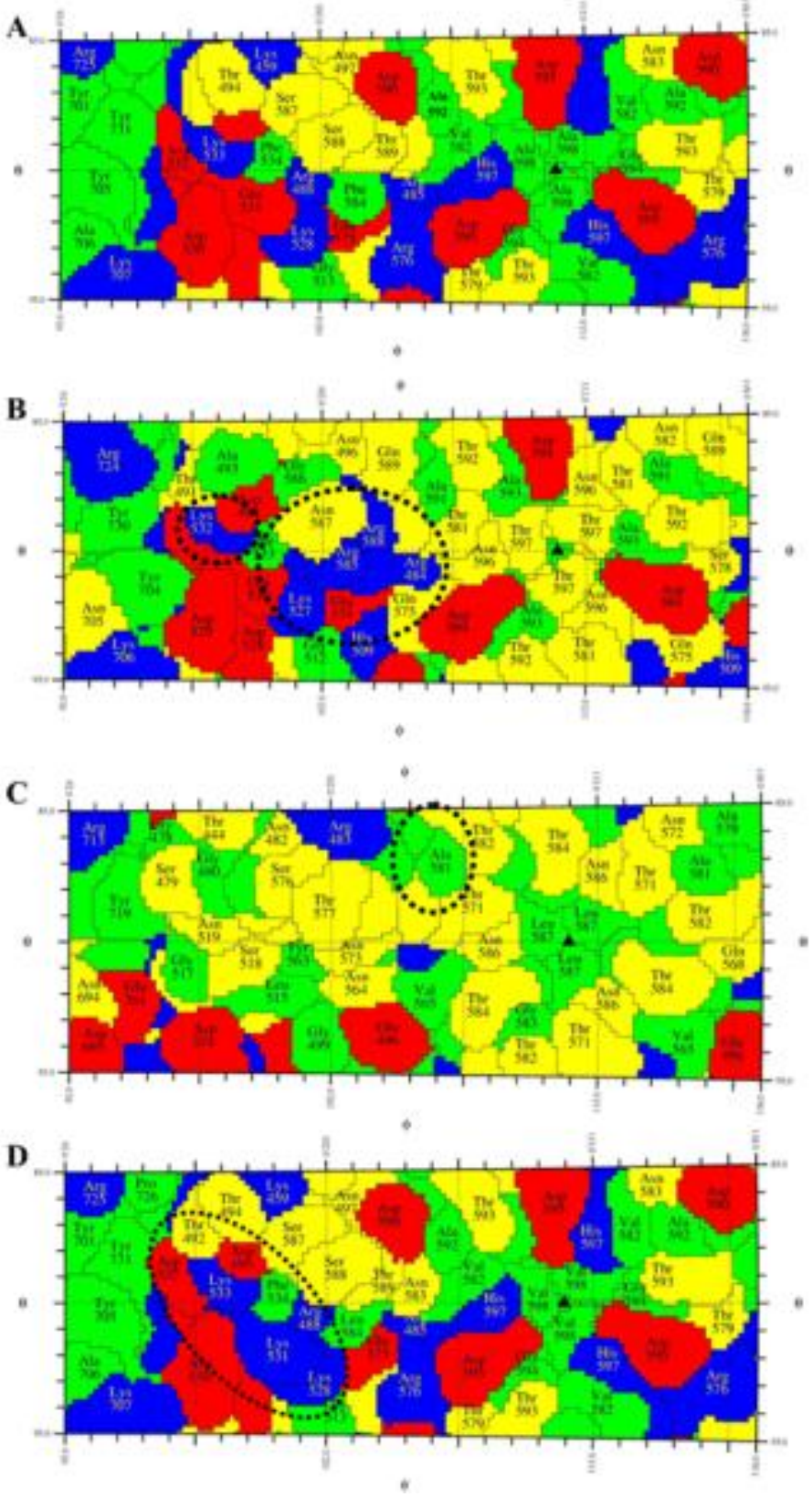
A
B
C
D

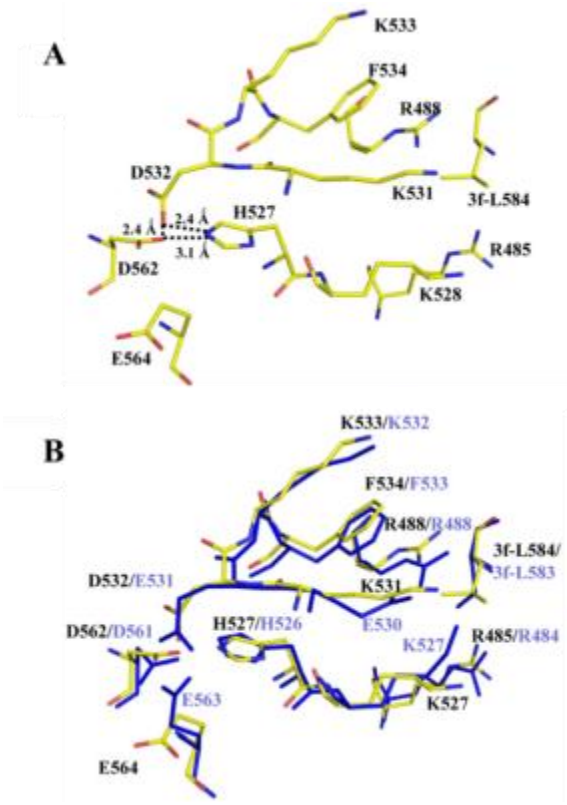

Figure 3-7. Stabilizing interactions for the K531 loop. (A) Residues D532, H527, and D562 that form electrostatic interactions at the base of the loop containing basic residues K528, K531, and K533 are shown along with neighboring residues R485 and R488, equivalent to R484 and R487, respectively, involved in HS binding by AAV2. 3f-L584 is contributed from a 3-fold (3f) related VP3 monomer. The residues (in stick form) are colored according to atom type: carbon, yellow; nitrogen, blue; and oxygen, red. Dashed lines indicate the distance between interacting residues. Disruption of the D532-H527-D562 interaction by a D532N mutation is predicted to alter the conformation of the basic loop and in turn could alter AAV6 HS binding properties. (B) AAV2 residues E531, H526, D561, and E563 that form electrostatic interactions which stabilize an equivalent surface loop in this serotype containing residues K527, E530, and K532 and the neighboring amino acids, R484 and R487, involved in HS binding. Mutation of D561 and E563 to alanine disrupts HS binding in AAV2. 3f-L583 is contributed from a 3f VP3 monomer. Residues are colored as in panel A.A superposition of the residues shown panel A with AAV2 (PDB accession No. 1LP3) using the AAV6 amino acids (labeled in black) shown according to atom type and those for AAV2 are colored blue (labeled in blue). This figure was generated using the PyMol program (86) and adapted from (225).

CHAPTER 4
STRUCTURALLY ANNOTATING AAV1 AND AAV6 GLYCAN BINDING INTERACTIONS

Introduction

One key feature of the viral capsid that determines cell type specificity or tissue tropism is its interaction with a specific host receptor (glycoproteins or glycolipids) (260). Several receptors have been identified to be involved in AAV infection and these receptors can function either as the primary receptor or the co-receptor (Table 1-2) (12, 37, 53, 88, 153, 155, 188, 244, 263, 264, 274, 275, 298, 306, 307). The primary receptor, also called the attachment receptor, is the first receptor recognized by the virus capsid and initiates the interaction of viral capsid surface with the cellular membrane. On the other hand, co-receptors are cell membrane associated molecules that are critical for viral internalization.

Several AAVs utilize sialic acid (SIA) as their primary receptor and, for these serotypes, neuraminidase treatment abolishes cellular transduction (153, 263, 307). AAV2 and AAV3 utilize heparan sulfate proteoglycan (HSPG) as the primary receptor for the liver cells (37, 275). AAV4 utilizes O-linked sialylated oligosaccharides and AAV5 utilizes N-linked sialylated oligosaccharides to infect cells (153). Glycan microarray screening (by the Consortium for Functional Glycomics (CFG)) and biochemical assays showed N-linked sialic acid as the primary receptor for AAV1 (307). AAV6, which belongs to the same phylogenetic clade as AAV1 and differs by only 6 of 736 residues on the VP1, can bind both SIA and HS molecules as the primary receptors (306). Recently, biochemical and *in vitro* has identified terminal galactose containing glycans as receptor for AAV9 (264). The cell surface glycans utilized by the other AAV

phylogenetic clade representatives, AAV7-AAV8 are currently unknown. Other than AAV2, AAV3, AAV5, and AAV9 (27, 91, 105, 160, 179, 183, 228, 230), the region on the remaining AAV capsid surfaces required for the binding of HS / SIA glycans are yet unknown. Regions on the 3-fold axis of capsid surface have been shown to be the critical for HS binding by AAV2 as well as SIA binding by AAV5. In order to improve the efficacy of AAV gene delivery with respect to cardiac, muscle and lung cellular targeting, we need to structurally and biochemically annotate the receptor binding sites of AAV1 and AAV6 capsids and characterize the difference role in receptor recognition and tissue specificity. This chapter will focus on the study to identify and pinpoint residues on the AAV1 and AAV6 capsids utilized for glycan recognition.

Results and Discussions

Crystal Structure of AAV1 – 3'SLDN Complex

To better understand the interaction between AAV1 and SIA, we soaked AAV1 VLP crystal in cryo-protectant solution containing 3' SLDN for 48 hours prior data collection. Diffraction data sets were obtained for the complex and processed to 3.0Å resolution in the monoclinic system with C2 space group and completeness of 60.5%. Data collection and refinement statistics are shown in Table 3-1. These statistical values and quality of the data sets was consistent with those used to solve the crystal structures of other parvoviruses (e.g.,(191, 212)). Using the method of molecular replacement with the AAV1 crystal structure (PDB accession No.3NG9) to solve the phase problem, we were able to assign 519 residues (218-736) of the VP3 common C-terminal region using averaged $2F_o$-F_c electron density map. To identify the glycan binding site on AAV1 capsid, an averaged F_o-F_c difference map was calculated and a

SIA molecule was modeled into a 2.5σ contoured level positive difference map in a shallow pocket on the outside wall of 3-fold protrusion facing the 5-fold cylindrical pore. Although longer sialylated glycan (Neu5Acα2-3GalNacβ1-4GlcNAc) was utilized for this structural study, all the carbohydrate components of 3'SLDN were not observed in the crystal structure which implies that only the terminal SIA moiety was structurally stabilized upon capsid interaction (Figure 4-1). The orientation of the SIA molecule was assigned into the density in which the extension of the GalNac and GlcNAc was not sterically clashing with VP coordinates. The modeled SIA molecule was refined with occupancy of 1.0 and resulted in the averaged B factor of ~20.3$Å^2$.

The crystal structure reveals a 1:1 stoichiometry of binding between AAV1 VP and SIA molecule and thus suggests a total of 60 SIA binding sites on AAV capsid. The glycan interacts (contact distance less than 4.0 Å) with residues S268, D270, N271, N447, S472, V473, N500, T502 and W503. This binding pocket is contributed by two interacting VP monomers. Variable regions involved in SIA interactions are VRI (268, 270 and 271), VRIV (447, 472 and 473), and VRV (500, 502, and 503). Other than N447, which interacts with SIA via a main chain atom (carboxyl oxygen to SIA C11) and ND with SIA O4, the other interactions involve hydrogen and hydrophobic bonding interactions between the VP a.a. side chains and SIA molecule. Glycerol group of the SIA interacts with side chains of residues S268, D270, N271, S472, V473 and W503. Side chain of residues N500 and T502 interact with SIA carboxylate group. These similar SIA interacting residues were also observed in the influenza virus hemaglutinin (HA) – 6'SLN complex structure (PDB accession No.1RVZ), which involves residues V135, T136, A137, W153, L194, and Q226 (111). Structural comparison between the

AAV1 (PDB accession No.3NG9) and AAV1-SIA crystal structures reveals no dramatic conformational changes in the Cα position of the VP monomer residues except for residues on the tip of VRIV. RMSD between the C alpha positions of this region (residue 453-456) between two structures were calculated to be in range of 0.6 – 1.1 Å. These residues are known to have the highest B factor range within VP (more than 2 fold of the averaged thermal factor for protein atoms) among all available AAV structures. This suggests that the variability might due to the inherent flexibility of VRIV within the VP monomers. In addition to VP amino acids assignment, averaged positive F_o-F_c difference density was also observed in the interior surface surrounding the center of 3-fold symmetry axis which was been modeled and proposed as density for nucleotide molecules in several available AAV crystal structures (discussed in Chapter 3).

Structural Comparison of AAV Serotypes at AAV1 SIA Interacting Residues

Superposition of the AAV1 crystal structure with those available for AAV2 to AAV6, AAV8, and AAV9 using the Coot program (101, 102)showed Cα variability within the AAV1 SIA interacting regions (AAV1 SIAIR = AAV1 SIA contact residues ± 2a.a) (Figure 4-3) (Table 4-2) ((5, 6, 62, 92, 119, 180, 223, 225, 232, 291, 311, 312) and unpublished data). Among the serotypes compared, AAV4 (PDB accession No. 2G8G) and AAV5 (PDB accession No. 3NTT), which have 61.8 and 60.0 % a.a. identity to AAV1 respectively, possess the most diverse conformations within these variable regions which create steric clashes into the SIA electron density map. Amino acid structural alignment of SIA interacting residues on VRI among AAVs shows 100% identity (except AAV4 and AAV5). This implies contact residues on VRI might not be the potential important residues for AAV1 SIA interaction.

Structural alignment and Cα superposition of AAV6 (PDB accession No.3AOH) to AAV1 (PDB accession No.3NG9) shows a 99.2% identity and small r.m.s.d. (0.05-0.78 Å) within these interacting regions suggesting that AAV6 might utilize this same capsid region for SIA interaction. On the other hand, structural alignment between AAV1 and AAV6 and most clinically studied serotype AAV2 (binds HSPG in different region) within this capsid region identified five different residues: N447S, S472R, V473D, N500E, and T502S (AAV1/6 to AAV2 a.a.) (Table 4-4). While a series of single mutations of AAV2 residues equivalent to AAV1 SIA binding site to alanine have no significant effect in capsid assembly and genome packaging properties, these single mutations significantly increase (3-4 fold) or knockdown (~20 fold) HeLa and HepG2 cellular transduction (compared to wild-type AAV2 at 100%).

In addition to the VRI SIA interacting region, W503 in the VRV interacting region is also conserved among AAVs. Recent biochemical, *in vitro* and *in vivo* studies showed that AAV9 utilizes the similar capsid region (D271, N272, Y446, N470 and W503 (AAV9 VP numbering)) for its interaction with terminal galactose (GAL) glycans (27, 264). Galactose differs from SIA molecule in that it does not possess the carboxylate and glycerol chain in SIA; instead four carbons (C1, C3-C5) are occupied by oxygen atoms. This implies that the AAV1 residues that interact with SIA glycerol and carboxylate chains and are different to AAV9, are the potential AAV1 and AAV9 residues that dictate receptor binding specificity. Using molecular docking with PatchDock(261), the potential interaction site between GAL molecule on AAV9 trimer molecule was calculated and modeled into the similar binding pocket (27). Superposition of the AAV1 and AAV9 glycan binding region highlighted differences in capsid residue side chains that might be

affecting their receptor binding properties. The side chain of AAV9 N470 (equivalent to G470 in AAV1) sterically clashes into the AAV1 SIA binding pocket. The O3 and O4 of GAL interact (2.6–3.3 Å) with side chain of N470 and the GAL binds deeper in the pocket and involves residues D271, N272, and W503. Although mutagenesis study had showed a mutation in Y446 is critical for AAV9-GAL binding (27), the molecular docking result indicates the distance between Y446 is more than 4.5Å away from the GAL molecule. Previous mutagenesis studies on the Y444F in AAV2 (equivalent to AAV9 Y446), which is proposed to avoid ubiquitin-mediated proteasome degradation, resulted in significant increase (~13x compared to wild-type AAV2) in hepatocyte transduction (323, 324).However, an AAV3 Y444F mutation does not show similar transduction properties, which implies diverged functional roles of tyrosine residue in this capsid region among different AAVs (67).

***In silico* Docking Model of AAV6 – Heparan Sulfate**

While efforts are ongoing to determine a crystal structure for AAV6 bound to HS, a molecular docking approach using Dock6 has been used to obtain a low and stable interaction energy for HS binding to the AAV6 capsid surface (175). In order to validate the quality of this computational approach, the AAV2 crystal structure (PDB accession No.1LP3) was used as a positive control. A HS molecule (obtained and modified from 2WNU PDB file) was initially modeled onto the AAV2 capsid surface adjacent to the previously characterized HS binding region: R484, R487, H509, K527, R585 and R588. Using the default parameters (as mentioned in chapter 2), DOCK6 was able to calculate the lowest interaction energy for the HS molecule in which the final orientation and location is shifted compared to the initial modeled position relative to the AAV2 capsid

surface (data not shown). The AAV2 capsid surface basic residues identified to be within interacting distance with HS are R484, R487, H509, K527, R585 and R588 (Figure 4 A-C); consistent with the previously identified binding residues using mutagenesis studies and cryo electron microscopy and image reconstruction (cryo-reconstruction) (160, 183, 228, 230). A similar approach was undertaken for analyzing a potential AAV6 – HS complex with DOCK6 which was able to calculate the lowest interaction energy between these molecules. The surface basic residues identified for the AAV6-HS interaction are R485, R488, K528, K531, and R576 (Figure 4 D-F). The position of this calculated model is consistent with previous mutagenesis studies in AAV1 and AAV6, in which a single mutation K531E was able to abolish AAV6 HS binding property (306). These residues are located on AAV6 VRV (R485 and R488), VRVI (K528 and K531), and VRVIII (R576). The HS model utilized in this study consists of two core carbohydrate domains; monosulfatediduronic acid (IdoA) and bisulfatedglucopyranosic acid (GlcNS). The sulfate group from IdoA is shown to interact with side chains of R485 and R576, and the sulfate group from GlcNS interacts with R488 and K531. In addition to the sulfate group interactions, the side chain of K528 is shown to bind the HS molecule via the carboxyl chain of IdoA. Another HS carboxyl chain is shown to interact with main chain atom from G513 (which is nota residue of any VR). Besides the hydrogen bonding interactions, L584 (F584 in AAV1) is shown to involve in van der Waal interaction with the HS. This predicted interacting region is assembled from two VP monomers and located on the shoulder of the protrusion facing the capsid 5-fold symmetry axis.

In silico modeling using AAV1 and AAV5 trimer molecules also localized the HS molecule in proximity with AAV2 and AAV6 HS interaction region (data not shown). Grid scores calculated from DOCK6 suggested relative AAV-HS interaction energies; AAV6= -64.4, AAV2= -54.6, AAV5= -50.1, and AAV1= -44.8.

Structural Comparison of AAV Serotypes at AAV6-HS Interacting Residues

Structure alignment and superposition of the AAV6 structure with those available for AAV1 to AAV5, AAV8, and AAV9 shows the degree of variability (r.m.s.d) within the AAV6 HS interacting VR among different serotypes ((5, 6, 62, 92, 119, 180, 223, 225, 232, 291, 311, 312) and unpublished data) and identifies five AAV2 / AAV6 HS interacting regions (HSIR) (483-490, 508-515, 526-535, 574-578,and 584-591) (Figure 4-5 and Table 4-3). Residues R585 and R588 (AAV2 VP numbering) are unique to AAV2 HS interaction and none of the compared serotypes have basic amino acids at this on position. The highest Cα deviation among AAV2/AAV6 HSIRs is identified to be present in residues 526-531 (VRVI) (Table 4-3). Except for AAV4 and AAV5 (which are shown to have the highest variability in these IRs), the r.m.s.d. among serotypes was calculated to be much smaller than for the SIA interacting regions. Sequence alignment within HS contact residues among different serotypes showed that AAV4 and AAV5 do not have similar basic amino acids at these positions (Table 4-4), except for AAV6 R485 (K479 and R471 in AAV4 and AAV5, respectively). In addition to R585 and R588, and H509 are unique for AAV2 HS interaction, and AAV6 utilizes an alternate residue R576 (equivalent to Q575 in AAV2). The calculated model of AAV6-HS interaction also involve residue G513 which is conserved among AAV serotypes and the HS interaction is shown to be contributed by main chain.

Besides the involvement of HSIR for AAV2 / AAV6-HS binding, several studies have identified this region as also being important for AAV serotype specific transduction phenotype. AAV9 is a unique serotype due to its capability to surpass blood brain barrier (BBB) and has been shown*in vivo* to transduce neurons in brain and spinal cord (197). Zhonget. al. has isolated a new AAV variant (CLvD8) from chimpanzee which differs by only four a.a. (I647T, Y445H, H527Y, and R533S (AAV9 to CLvD8)) in VP3 protein compared to wild-type AAV9, and has lost the potential to cross vascular barrier (325). Site-directed mutagenesis was performed within these four residues to generate four single mutant vectors carrying luciferase reporter gene. Comparisons of *in vivo* luciferase expression after intravenous, intramuscular and intranasal administrations showed that two single mutants (H527Y and R533S) were not able to perform similar transduction phenotype as wild-type AAV9. This data suggests the role of residues H527 and R533 in VRVI for surpassing vascular barrier during systemic delivery.

Previous studies had demonstrated that mutations of surface-exposed tyrosine residues (Y-F) on AAV capsid are able to protect AAV delivery vectors against ubiquitin-mediated proteasome degradation (323, 324). Ubiquitination is a post translation modification process in which the activated ubiquitin enzyme creates an amide bond via the lysine residue in the protein and targets it for proteasomal degradation. Gabriel et.al. had performed site-directed mutagenesis on surface exposed lysine residues on AAV capsid, and shown that AAV2 single K532R (equivalent to K533 in AAV6) mutation can increase HEK293 and HeLa cellular transductions by 9x and 18x, respectively (110).

This study suggests the important role of residue 533 in VRVI in AAV2 cellular transduction properties.

In summary, the crystal structure of AAV1-3'SLDN complex was determined to 3.0Å resolution and an *in silico* method was utilized to predict the HS binding site on the AAV6 capsid surface. Variable regions important for AAV1 / AAV6 SIA binding are VRI, VRIV, and VRV, and for AAV2 / AAV6 HS interaction are VRV, VRVI and VRVIII. Structural superposition of the receptor binding sites on AAV1 and AAV6 onto different AAV serotypes have provided useful information to identify and pinpoint specific regions on AAV1, AAV2, and AAV6 capsid surface required for glycan receptor binding. Results from these studies will be applicable for the modification of glycan contact residue to engineer recombinant vectors with specific receptor targeting properties which will be the first step towards increasing the transduction efficiency of AAV vector.

Table 4-1. Data Collection, Reduction and Refinement Statistics [a]

Data Collection	CHESS F2
Wavelength (λ , Å)	0.979
Space group	C2
Unit cell parameters (Å)	a = 450, b = 260, c = 450, β = 110
Resolution	50.0 – 3.0 (3.1 - 3.0)
No. of unique reflections	593,542 (45,233)
Completeness (%)	60.5 (46.3)
Average I/sigma	4.0 (1.6)
R_{merge} (%)	16.6 (45.3)
Refinement	Refmac
No. of atoms (protein/SIA/DNA)	4,117/ 21 /18
Average B factors ($Å^2$)	31.0
Rcryst / Rfree (%)	26.3 / 27.0
RMSD bonds (Å) and angles (^{0})	0.014 / 1.37
Ramachandran plot	
Most favorable allowed (%)	92.1
Additionally allowed (%)	6.0

[a] Values in the parenthesis are for the highest resolution shell; [b] CNS = Crystallography and NMR System; [c] R_{merge} = $(\Sigma|\boldsymbol{I}_{hkl}-<\boldsymbol{I}_{hkl}>| / \Sigma|\boldsymbol{I}_{hkl}|) \times 100$, where $\boldsymbol{I}_{hkl}$ is the intensity of an individual hkl reflection and $<\boldsymbol{I}_{hkl}>$ is the mean intensity for all measured values of this reflection; [d] $R_{cryst} = (\Sigma||F_{obs}|-|F_{calc}|| / \Sigma|F_{obs}|) \times 100$, F_{obs} and F_{calc} are the amplitudes for the observed and calculated reflections, respectively; Rfree was calculated with the 5% of reflections excluded from the data set during refinement.

Table 4-2. RMSD in Cα position between AAV1 and other AAV serotype crystal structures overall and for SIA interacting regions (SIAIR)

Sero-Type	a.a. % identity	VR Cα distance ranges (Å) (AAV1 VP numbering)				
		Overall	266-273	445-449	470-475	498-505
AAV2	83.7	0.63	0.28-3.19	0.44-0.86	0.48-1.02	0.18-1.18
AAV3	85.8	0.61	0.28-3.66	0.40-0.90	0.32-0.92	0.13-0.59
AAV4	61.8	0.92	0.45-3.25	0.46-1.39	0.25-1.05	1.15-3.11
AAV5	60.0	1.00	0.56-2.63	0.71-1.78	0.32-2.01	0.90-3.25
AAV6	99.2	0.33	0.09-0.77	0.05-0.32	0.05-0.42	0.20-0.79
AAV8	80.0	0.54	0.29-3.47	0.20-0.63	0.11-0.40	0.63-0.99
AAV9	79.8	0.50	0.18-3.20	0.76-0.99	0.16-0.33	0.40-0.78

R.m.s.d was calculated using SSM superposition in Coot program. SIAIR = SIA contact residues ± 2 a.a.

Table 4-3. RMSD in Cα position between AAV6 and other AAV serotype crystal structures overall and for HS interacting regions

Sero-Type	a.a. % identity	VR Cα distance ranges (Å) (AAV6 VP numbering)					
		Overall	483-490	510-515	526-535	574-578	584-591
AAV1	99.2	0.33	0.26-0.55	0.09-0.43	0.15-0.72	0.06-0.32	0.22-0.62
AAV2	83.7	0.67	0.26-0.91	0.35-0.90	0.21-0.84	0.26-0.80	0.35-0.84
AAV3	85.6	0.60	0.06-0.24	0.25-0.70	0.30-1.24	0.40-0.89	0.37-0.68
AAV4	62.0	0.94	0.30-1.44	0.23-1.02	1.21-3.99	0.13-1.21	1.36-2.94
AAV5	59.4	1.05	0.63-1.78	0.30-1.15	0.41-3.16	0.67-0.90	0.71-2.49
AAV8	80.0	0.54	0.16-0.51	0.36-0.64	0.19-0.52	0.12-0.52	0.34-0.98
AAV9	79.6	0.50	0.13-0.52	0.38-0.66	0.13-1.03	0.16-0.34	0.23-0.82

R.m.s.d was calculated using SSM superposition in Coot program.
SIAIR = SIA contact residues ± 2 a.a.

Table 4-4. Structure alignment of AAV residues involve in SIA and HS interaction.

Amino Acids[a]	AAV Serotypes								References
	AAV1	AAV2	AAV3	AAV4	AAV5	AAV6	AAV8	AAV9	
268	S	S267	S267	Q259	S258	S268	T270	S269	(193)
270	D	D269	D269	S260	A260	D270	D272	D271	(27, 193)
271	N	N270	N270	N261	N261	N271	N273	N272	(27, 193)
345	S	T344	T346	A335	T335	S345	T347	T346	(211)
444	Y	Y443	Y443	W437	Y436	Y444	Y446	Y445	(325)
445	Y	Y444	Y444	G438	R437	Y445	Y447	Y446	(27, 67, 323, 324)
447	N	S446	N446	Q440	V439	N447	S449	S448	(193)
470	G	D469	S470	N464	R456	G470	T472	N470	(27, 193)
472	S	R471	S472	S466	A458	S472	A474	A472	(193)
473	V	D472	L473	N467	N459	V473	N475	V473	(193)
485	R	R484	R485	K479	R471	R485	R487	R485	(160, 183, 193, 228, 230)
488	R	R487	R488	G482	G474	R488	R490	R488	(160, 183, 193, 228, 230)
500	N	E499	N500	I493	S487	N500	N502	E500	(193)
502	T	S501	P502	L501	A488	T502	A504	A502	(193)
503	W	W502	W503	I502	F489	W503	W505	W503	(193)
505	S	G504	A505	Y504	T491	S505	A506	G505	(211)
510	N	H509	H510	T509	E496	N510	H512	A510	(160, 183, 193, 228, 230)
513	G	G512	G513	G512	G499	G513	G515	G513	(18, 193)
527	H	H526	H527	A526	N514	H527	H529	H527	(193, 325)
528	K	K527	K528	G527	L515	K528	K530	K528	(193)
531	E	E530	E531	D530	S518	K531	E533	E531	(193, 306)
533	K	K532	K533	S531	N519	K533	R535	R533	(110, 193)
576	R	Q575	Q576	M574	V565	R576	E578	S576	(193)
586	S	R585	S586	S584	S575	S586	Q588	S586	(160, 183, 193, 228, 230)
589	T	R588	T589	N587	T578	T589	T591	A589	(160, 183, 193, 228, 230)
592	A	A591	T592	T590	A581	A592	Q594	Q592	(91, 105, 193)

[a] = AAV1 VP numbering

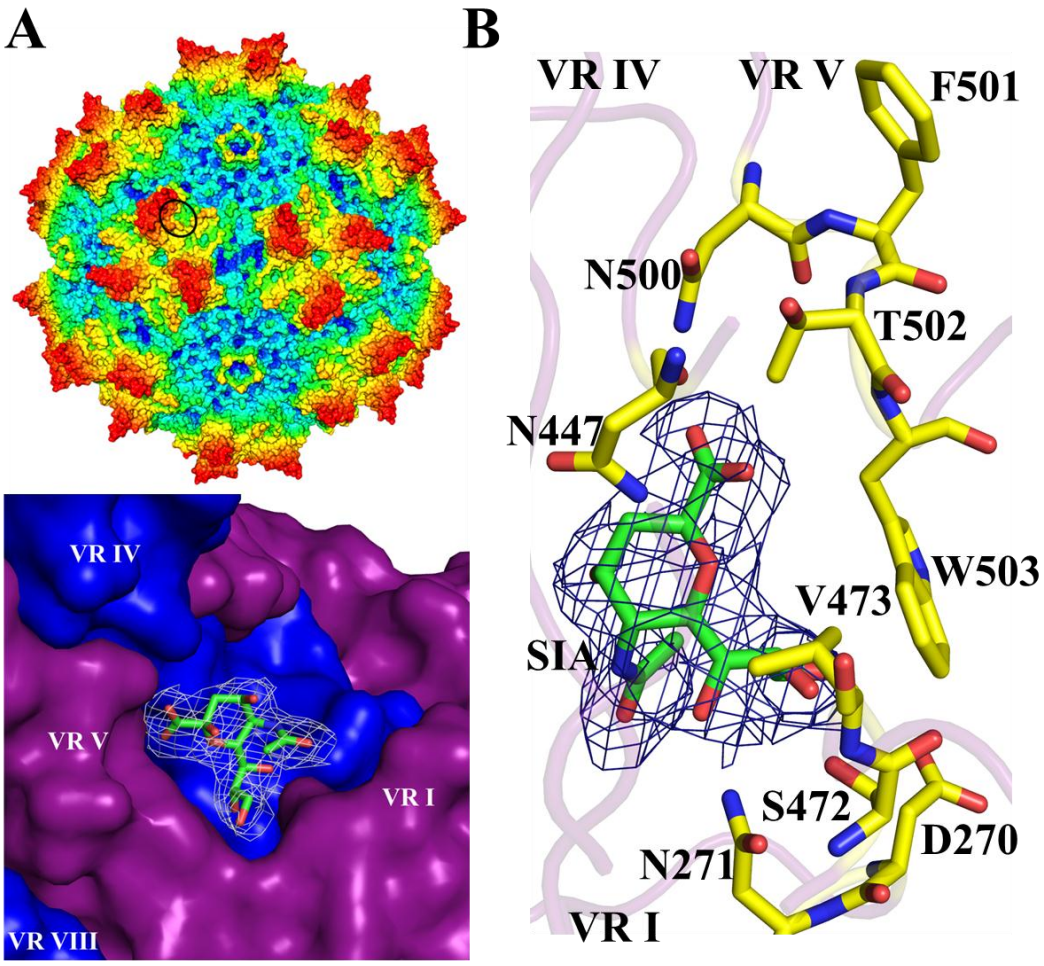

Figure 4-1.Crystal structure of AAV1-3'SLDN complex. (A) Surface representation of AAV1 colored in depth cue rendering (from blue (in) to red (out). The black open circle represents the location of AAV1 SIA interaction. Lower panel is the close up window of the AAV1 SIA interaction region. Different colors (purple and blue) represent different VP monomers The SIA molecule (shown as stick representation) was modeled onto the shoulder of the protrusion surrounding 3-fold symmetry axis. Variable regions involved in these intra-monomer interactions were labeled (VRI, VRIV, VRV and VRVIII). White mesh represents the averaged $2F_o$-F_c electron density map contoured at 1σ level. The SIA molecule is colored based on the atom types (green for carbon, red for oxygen, and blue for nitrogen). (B) Stick representation of AAV1 colored based on atom types (yellow for carbon) showing the potential SIA interacting residues (except F501) which are within a distance of 4.0 Å from the $2F_o$-F_c density shown in blue mesh. These SIA interacting residues are located on VRI, VRIV, and VRV. Figures were generated using the PyMol program (86).

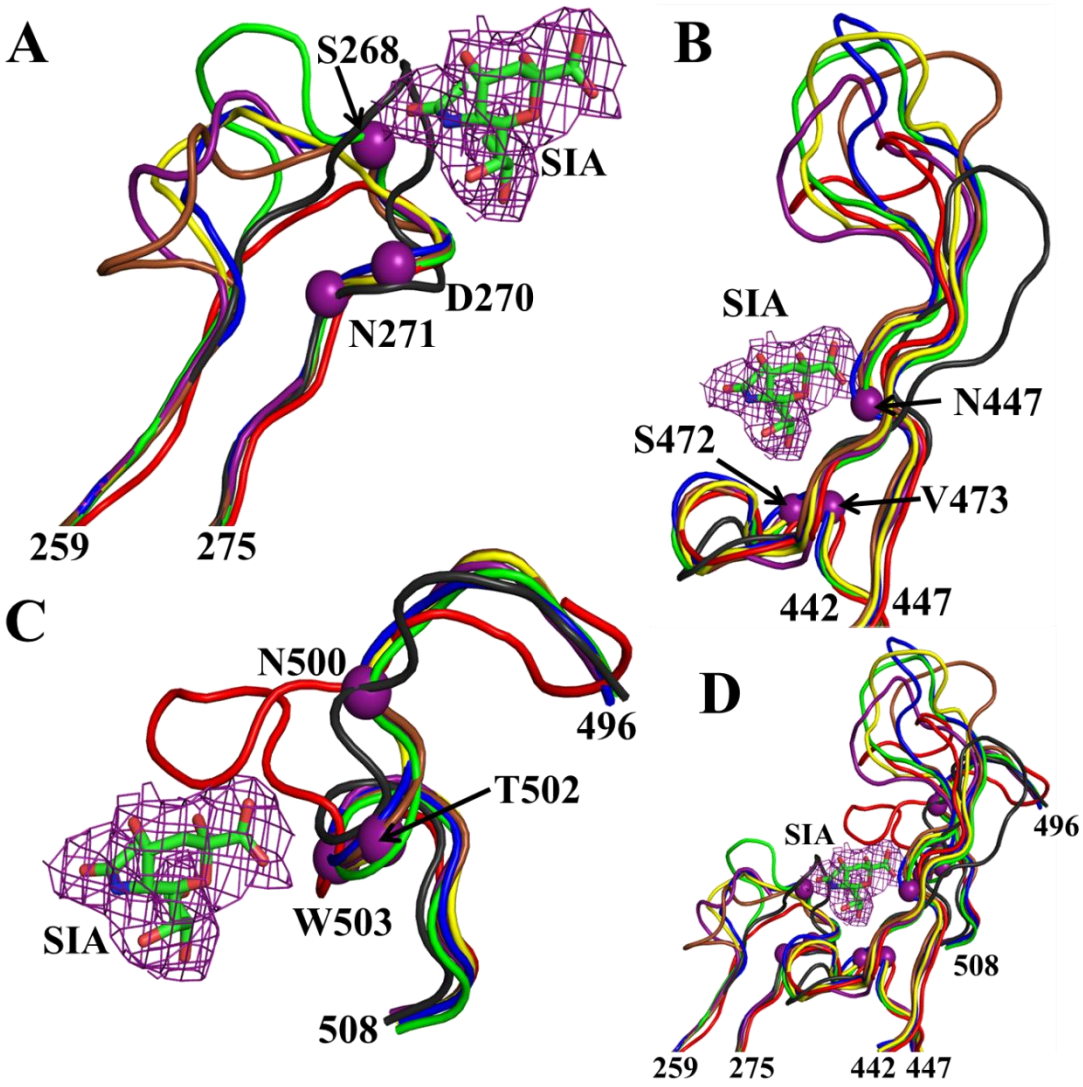

Figure 4-2. Superposition of AAV1-SIA crystal structure with other AAV structures in VRI: 259-275 (A), VRIV: 442-477 (B), and VRV: 496-508 (C). (A-C) AAV1 SIA interacting residues (Cα) are shown as purple spheres. (D) Overall superposition of panel A-C. Purple mesh represents the averaged $2F_o$-F_c electron density map contoured at 1σ level for SIA molecule. AAV structures are shown in coiled Cα representations and color-coded as purple: AAV1, blue: AAV2, yellow: AAV3, red: AAV4, grey: AAV5, pink: AAV6, green: AAV8 and brown: AAV9. Figures were generated using Pymol program (86).

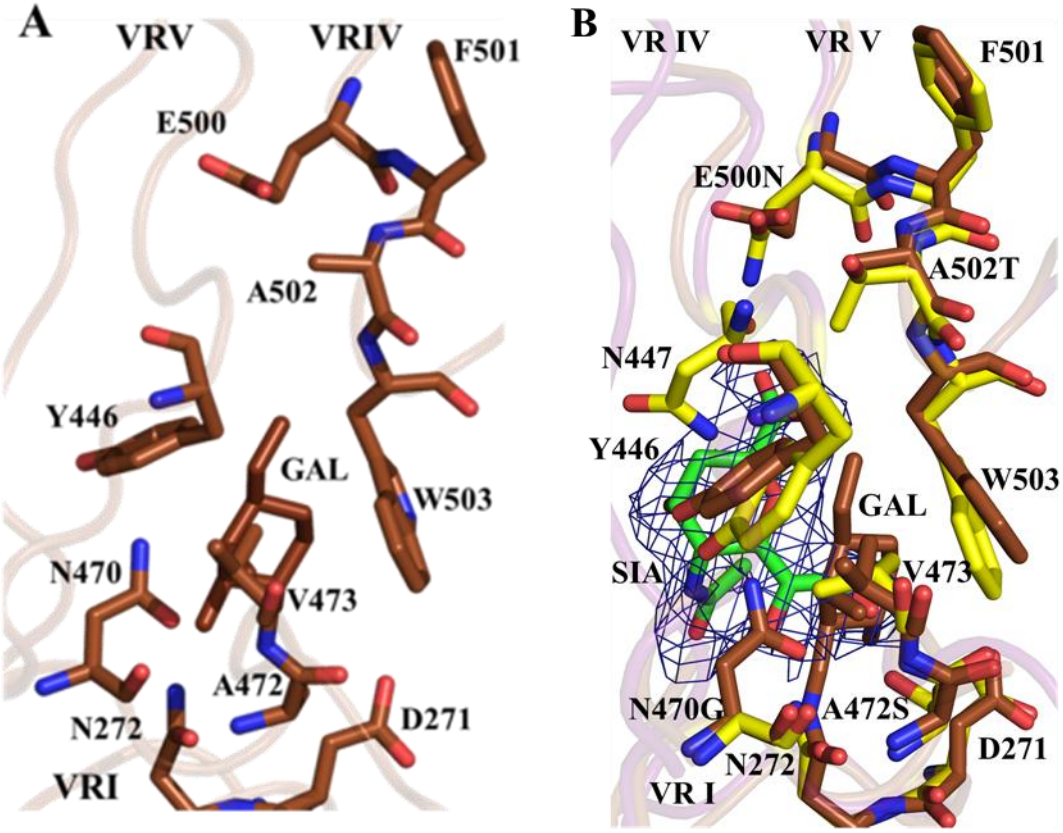

Figure 4-3.Molecular docking model of AAV9 crystal structure with GAL using patch-DOCK. (A) Stick representation of AAV9 crystal structure colored based on atom types (brown for carbon, red for oxygen and blue for nitrogen) (PDB accession No. 3UX1) showing the location and position of modeled GAL (brown) using patch-DOCK. Residues in the vicinity of the GAL are labeled and located on VRI, VRIV, and VRV. (B) Superposition of AAV1-SIA crystal structure (as shown in Figure 4-1B) onto AAV9-GAL model. Residues with similar amino acids are labeled as inpanel A. Figures were generated using Pymol program (86).

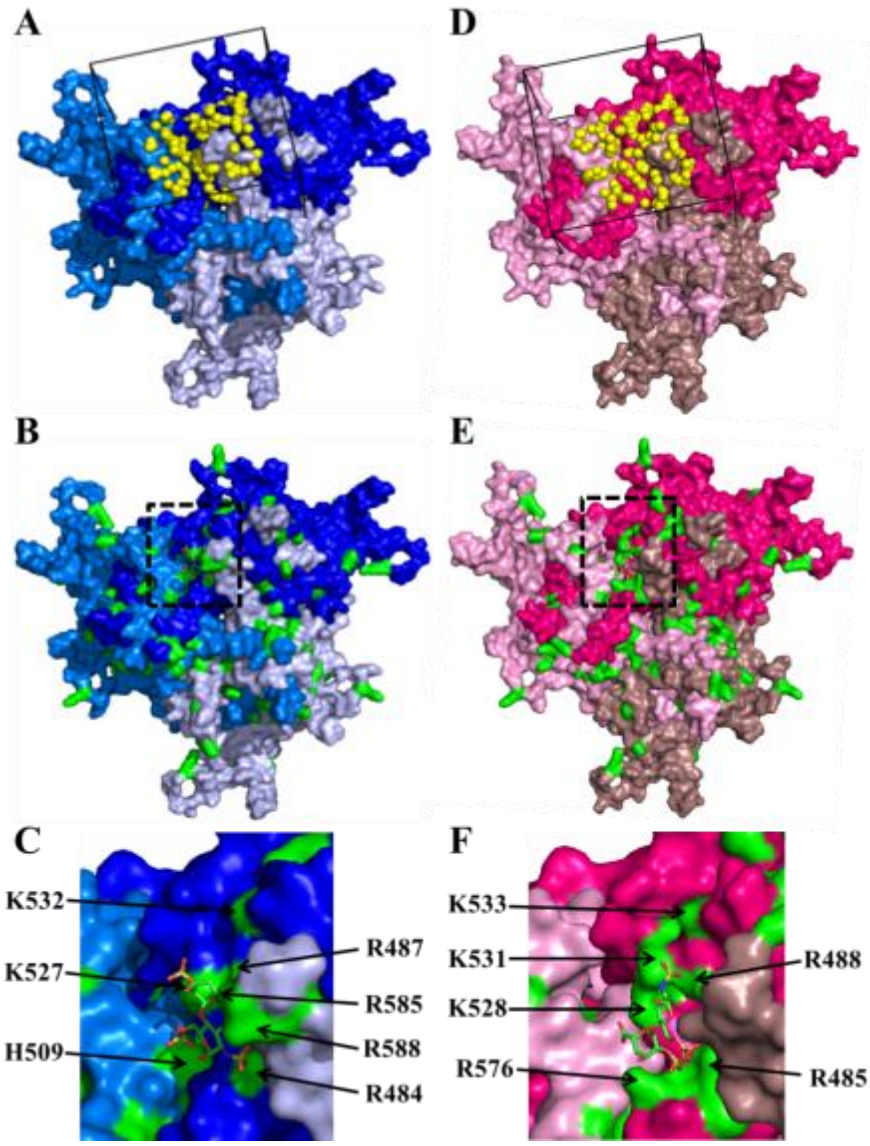

Figure 4-4. Surface trimer representation of AAV2 (A-C) and AAV6 (D-F) showing *in silico* calculation of HS interaction region on AAV2 and AAV6 trimer molecules using DOCK6. Different colors represent different VP monomers. (A and D) Surface trimer representation showing the solvent accessible surface area (yellow spheres) calculated and generated by INSPH in DOCK6 with the site box (10Å) shown in black line. (B and E) Surface trimer representation as panel A and D (for AAV2 and AAV6, respectively) showing the location of DOCK6-modeled HS molecules shown as stick representations. Basic residues on the AAV capsid surface are colored green. Dashed-line boxes show the close up window for panel C and F. Figures were generated using Pymol program (86).

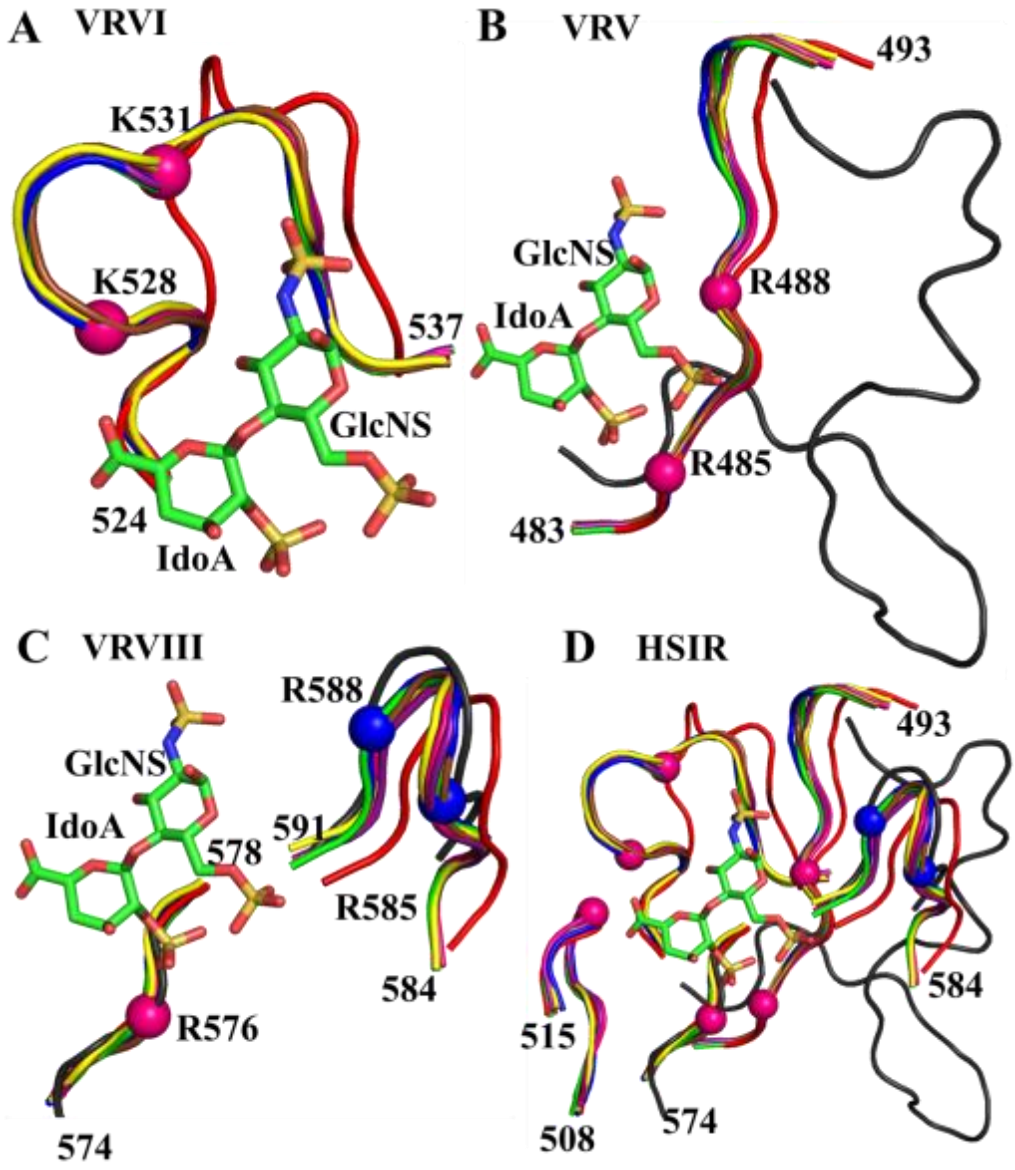

Figure 4-5. Superposition of AAV6 - HS *in silico* model with other AAV structures in VRVI: 524-537 (A), VRV: 483-493 (B), and VRVIII: 574-578 and 584-591from two different VP monomers (C). (A-C) AAV6 HS interacting residues (Cα) are shown as pink spheres, and AAV2 – HS unique residues (R585 and R588) are shown as blue spheres. (D) Overall superposition of panel A-C. HS molecule is shown in stick representation. IdoA =iduronic acid and GlcNS= Glucopyranosic acid. AAV structures are shown in coiled Cα representations and color-coded as purple: AAV1, blue: AAV2, yellow: AAV3, red: AAV4, grey: AAV5, pink: AAV6, green: AAV8 and brown: AAV9. Figures were generated using Pymol program (86).

CHAPTER 5
CHARACTERIZING THE TISSUE TRANSDUCTION DETERMINANTS IN AAV1 AND AAV6

Introduction

The crystal structures of AAV1 and AAV6, determined to 2.5Å and 3.0Å resolution (PDB accession No. 3NG9 and 3AOH), respectively, showed 5 of the 6 differing AAV1/AAV6 amino acids within the ordered VP structure (~218-736) localized proximate to the icosahedral 3-fold axis. This observation suggested that this capsid region plays an important role in dictating the differences in tissue transduction observed for these two closely related viruses (reviewed in (5, 6, 62, 132) and Chapter 1, 3, and 4). Two of the residues (418 and 642) were located in the interior surface of the capsid and three residues (531, 584 and 598) were located on the exterior capsid surface (225). Thus a series of reciprocal single residue mutations (AAV1 to AAV6 and AAV6 to AAV1) were generated to interrogate the role of the interior and exterior residues in dictating the AAV1 and AAV6 transduction efficiency (306). Data arising from these studies will provide clues on the role of these residues in initial cell surface recognition, post-entry transitions, capsid trafficking, and possibly capsid processing for efficient transduction.

Results and Discussion

To pinpoint critical residues dictating differential lung and muscle transductions between AAV1 and AAV6, series of single reciprocal mutants were generated (as described in (247, 306)) and expressed using human embryonic kidney (HEK) 293 cells. Polymerase chain reactions (PCR) were performed using sets of reverse and forward primers to confirm the mutated codons in the

*cap*ORF. Capsid titers (determined using a commercially available ADK1a ELISA) for recombinant AAV1s (rAAV1) and rAAV6 are in the range from 2.4 x 10^{13} to 6.6 x 10^{13} and 2.5 x 10^{12} to 5.9 x 10^{13} capsids/ml, respectively (Table 5-1).

With respect to genome packaging, for the rAAV1s and rAAV6s, despite the fact that rAAV1 and rAAV6 constructs carried *rep* ORFs from different serotypes (rAAV1 with AAV2-Rep and rAAV6s with AAV6-Rep), the viral genome titers were similar at approximately ~1x10^{11}vg/ml. This result is consistent with the previous studies which showed the complementary Rep function between AAV serotypes in genome replication and packaging (68, 142).

Recombinant AAV1 and rAAV6s were purified using ion exchange chromatography (327) and subjected to negative-stain electron microscopy (EM) (Figure 5-1 and 5-2). Intact rAAV capsids (~25nm) were observed in the EM (Figure 5-2). The preliminary transduction efficiencies among recombinant virions were assessed using the commonly used HEK293 cell (Figure 5-3). When the percentages of green cells were compared to the wild-type virions (normalized to 100%), no significant differences (n=3, P value < 0.05) were observed among the single site mutations (Figure 5-3B).

In summary, mutagenesis and biochemical characterization of the twelve reciprocal single mutations between AAV1 and AAV6 show no significant difference in the capsid assembly and genome packaging. A preliminary GFP infectivity assay showed no significant difference in the transduction phenotypes of the mutants in HEK293 cells.

Table 5-1. Biochemical characterization of AAV1 and AAV6 reciprocal mutants[a]

Recombinant AAV [b]	capsids/mL [c]	genome/mL [d]
AAV1wild-type	3.45×10^{13}	4.05×10^{11}
AAV1.L129F	2.40×10^{13}	5.40×10^{11}
AAV1.E418D	4.40×10^{13}	4.60×10^{11}
AAV1.E531K	2.55×10^{13}	3.83×10^{11}
AAV1.F584L	6.80×10^{13}	3.93×10^{11}
AAV1.A598V	3.45×10^{13}	4.74×10^{11}
AAV1.N642H	3.95×10^{13}	4.65×10^{11}
AAV6 wild-type	3.49×10^{12}	3.49×10^{11}
AAV6.F129L	3.58×10^{12}	3.58×10^{11}
AAV6.D418E	4.41×10^{13}	4.41×10^{11}
AAV6.K531E	4.37×10^{13}	4.37×10^{11}
AAV6.L584F	7.40×10^{12}	7.40×10^{11}
AAV6.V598A	2.52×10^{12}	2.52×10^{11}
AAV6.H642N	5.89×10^{13}	5.89×10^{10}

[a] Averaged from three independent repeats
[b]Recombinant virions were generated as previously described (306).
[c]Determined using ELISA (Progen # PRAAV1)
[d]Determined using BioRAD SYBR-Green against UF11

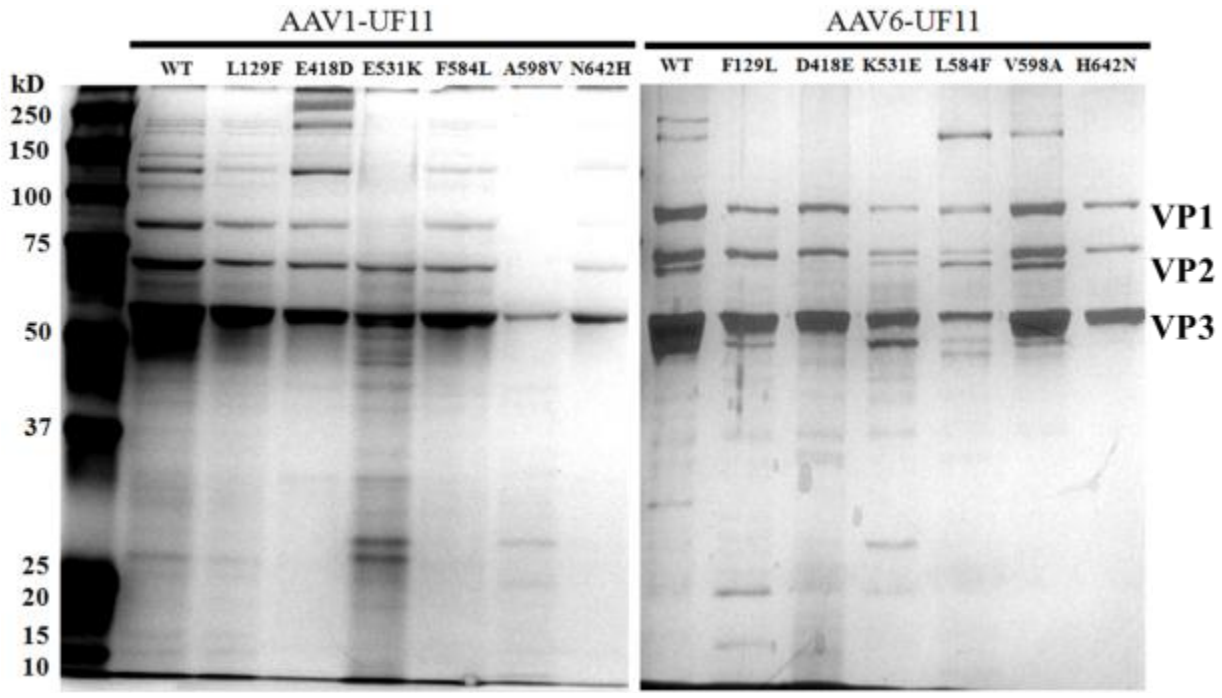

Figure 5-1. Silver stain SDS-PAGE of purified r AAV1 and rAAV6 reciprocal mutants showing the presence of VP1 (81kDa), VP2 (72kDa), and VP3 (63kDa).

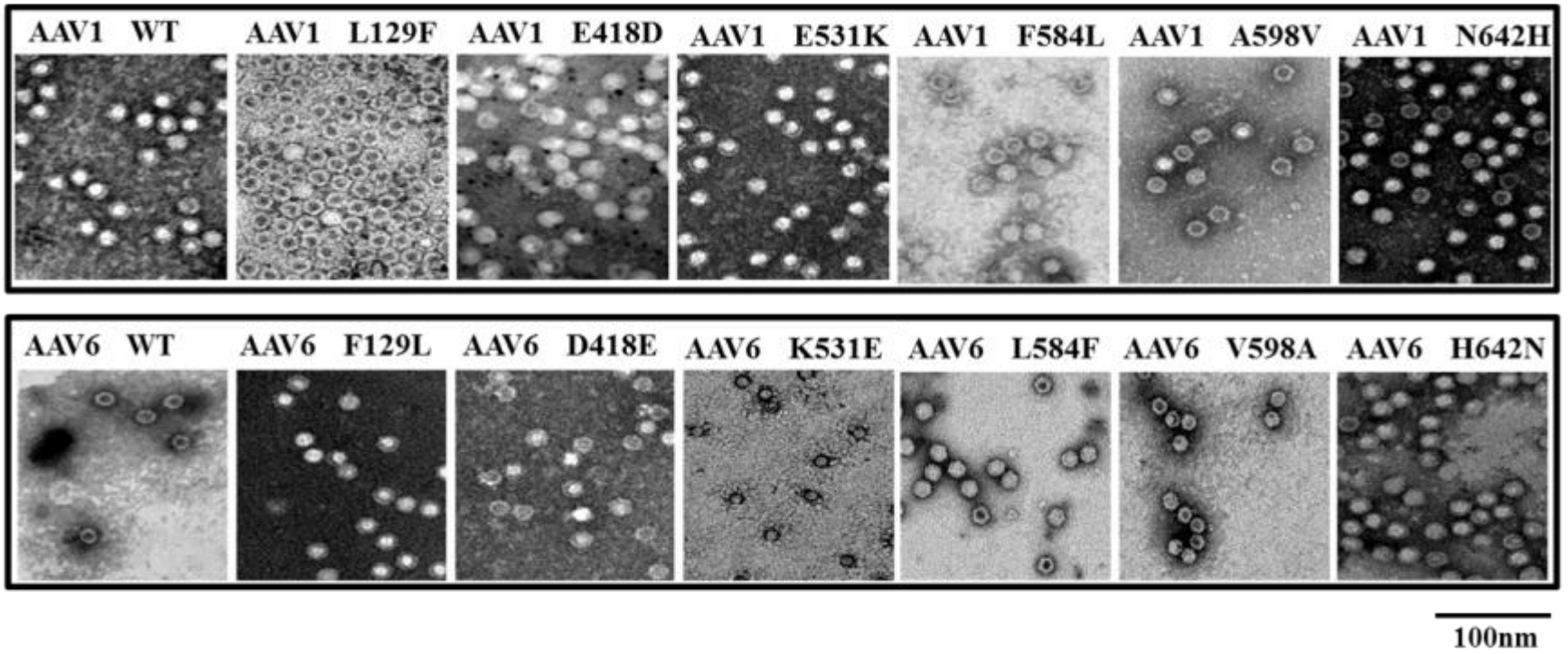

Figure 5-2.Negative-stain electron microscopy (EM) of purified rAAV1 and rAAV6 wild-types and reciprocal mutants. Figures were obtained from an FEI Spirit microscope.

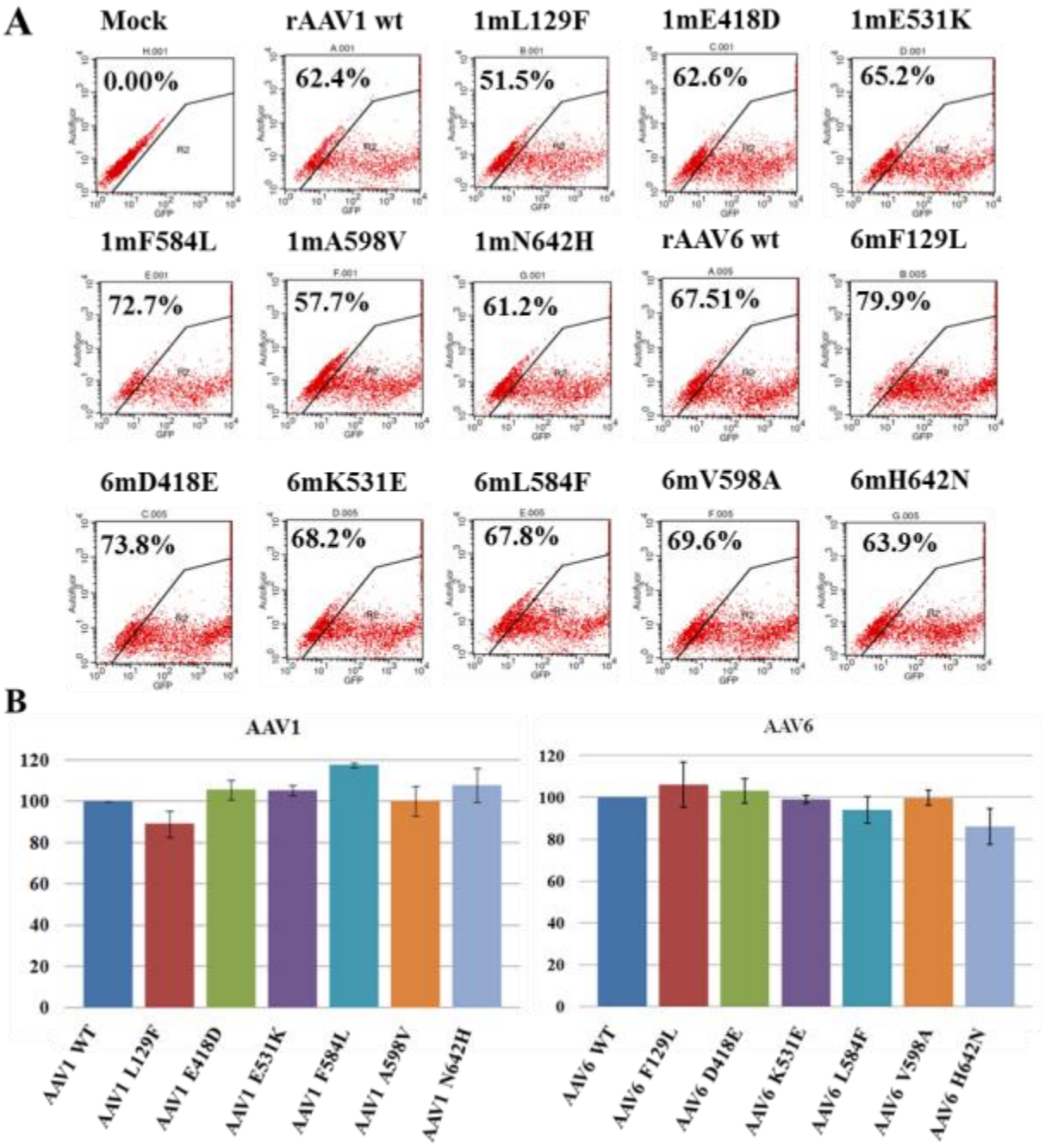

Figure 5-3. Green Fluorescence Protein (GFP) Infectivity Assay using HEK293 cells. (A) Representative FACS analysis of the GFP expression by recombinant AAV1 and AAV6 reciprocal mutants carrying pTRUF11 (GFP reporter gene). (B) The averaged result from the three independent GFP infectivity assays shown in panel A.

CHAPTER 6
SUMMARY AND FUTURE DIRECTIONS

The focuses of this study were to structurally characterize the glycan receptor interaction on the capsid surface of two related AAV serotypes, AAV1 and AAV6, and to identify the potential functional role of the six differing residues between these serotypes. In the effort to characterize the AAV capsid glycan receptor interaction, the structure of AAV6 was initially determined to 9.7 Å using cryo electron microscopy and image reconstruction (cryo-reconstruction). The AAV6 reconstruction map shows the characteristic features of AAV capsid topology; a depression at each 2-fold axis, protrusions surrounding each 3-fold axis, and a canyon-like depression surrounding the channel at each 5-fold axis. In this study, we were able to identify the location of five out of six AAV1/AAV6 different residues. However to better determined the orientation of a.a. side chains and potential interactions differ between these serotypes, we undertook X-ray crystallography approach. The crystal structure of AAV6 VLP was determined at 3.0 Å resolutions and this allows the completion of crystal structural library of the representative members of AAV phylogenetic clades (A-F and clonal isolates) (92, 119, 180, 223, 225, 232, 246, 291, 311, 312). Structural superposition and comparisons of crystallographic ordered VP region (218-736) between AAV6 and other serotypes identify the conserved core domain (βBIDG-βCHEF) among parvoviruses and nine variable regions (VRI - VRIX) which spread across the VP3 common region but are clustered on the AAV capsid surface. Comparison between AAV1 and AAV6 crystal structures enables us to annotate five of six different amino acids (E418D, E531K, F584L, A598V and N642H). The ordered five different residues are clustered surrounding the virus icosahedral three fold axis, residue 418 and 642 are located in the

interior surface and residue 531 (on VRVI) , 584, and 598 (on VRVIII) are located on the exterior capsid surface (Figure 6-1 and Figure 6-2). Based on previous mutagenesis, biochemical and in vivo studies, regions on the three fold symmetry of AAV capsid have been shown to exhibit functional role in receptor interaction, tissue transduction and antigenicities (5-7). For the assessment of capsid associated differential receptor interaction between these serotypes, efforts have been underway to obtain crystal diffraction data for AAV1/ AAV6 glycan complex.

Currently, we have obtained crystal structure of AAV1-3'SLDN (Neu5Acα2-3GalNacβ1-4GlcNAc) complex at 3.0 Å resolution. Using this X-ray data, we were able to calculated positive F_o-F_c difference electron density map and a SIA molecule was modeled and refined into the density map located in a pocket closed to the plateau at the outside wall of the 3-fold protrusion. These potential interacting residues are S268, D270 and N271 on VRI; N447, S472 and V473 on VRIV; and N500, T502 and W503 on VRV (Figure 6-1). Structural alignment between AAV1 and AAV6 shows 100% a.a. identity on this region suggesting that these serotypes utilize similar region for SIA interaction (Figure 6-2).

In the case of AAV6 - HS interaction, *in silico* DOCK6 program we were able to calculate the lowest and most stable interaction region between HS molecule onto AAV6 trimer crystal structure. The location of modeled HS molecule was calculated at proximity to basic residue patches, containing R485 and R488 on VRIV; R528 and K531 on VRVI; and R576 on VRVIII (Figure 6-1). This HS interacting capsid region is located on the outside shoulder of the protrusion surrounding the three-fold axis (Figure 6-2).

Mutagenesis studies of the AAV1 SIA contact residues to AAV2 corresponding a.a.; N447S, S472R, V473D, N500E, and T502S, are underway. In addition to these mutations, we also propose to generate W503A mutation which is shown to be important for AAV9 GAL interaction. Following the generation and expression of these mutations, immediate future of the project will focus on the biochemical characterization of these mutants using ELISA and qPCR to calculate and examine the possible effect of mutation on capsid assembly and genome packaging. In order to assess potential role of glycan interaction in cellular transduction, we propose to perform GFP infectivity and cell binding assays on these recombinant mutant AAVs against different cell lines (e.g., muscle, lung and liver), as well as on stably transformed CHO cell lines which are deficient in a series of glyco-transferases' activities; e.g, Lec-1, Lec-2, Lec-8, *pgs* D667, and A745. Based on the results of these assays, future efforts might be inevitable to generate double and triple mutations of the SIA contact residues to assess the cooperative properties of this SIA interacting region.

In addition to SIA interacting residues, a series of reciprocal mutations between AAV1 and AAV6 on their six differing residues were successfully expressed in HEK293 cells and purified using ion exchange chromatography. Using ELISA, qPCR and GFP infectivity assays, we were able to show that the recombinant wild-type AAV1 and AAV6 and their corresponding singletons exhibit no significant differences in capsid assembly, genome packaging, and HEK293 transduction properties. Provided with the current HEK293 transduction data, more efforts are necessary to better characterize the functional role of individual AAV1/AAV6 different residues in cellular interaction and transduction using different tissue types, including muscle, heart and lung cell line. In

addition, double and triple residue mutagenesis and biochemical studies are also necessary to address the role of the six AAV1/AAV6 differing residues in AAV cellular transduction.

In addition to receptor targeting or de-targeting, vector stability and antigenicity properties are also major concerns in vector generation for clinical application. Hence, comparative analysis of the thermal stability of the recombinant wild-types and all mutants (12 AAV1 / AAV6 SIA and 12 AAV1 / AAV6 reciprocal mutants) will be tested. Overall, data from these studies will provide the structural information on capsid regions involved in receptor binding, genome packaging, capsid assembly and stability as well as antigenicity which will aid in the development of superior AAV vectors with improved tissue specificity and transduction efficiency.

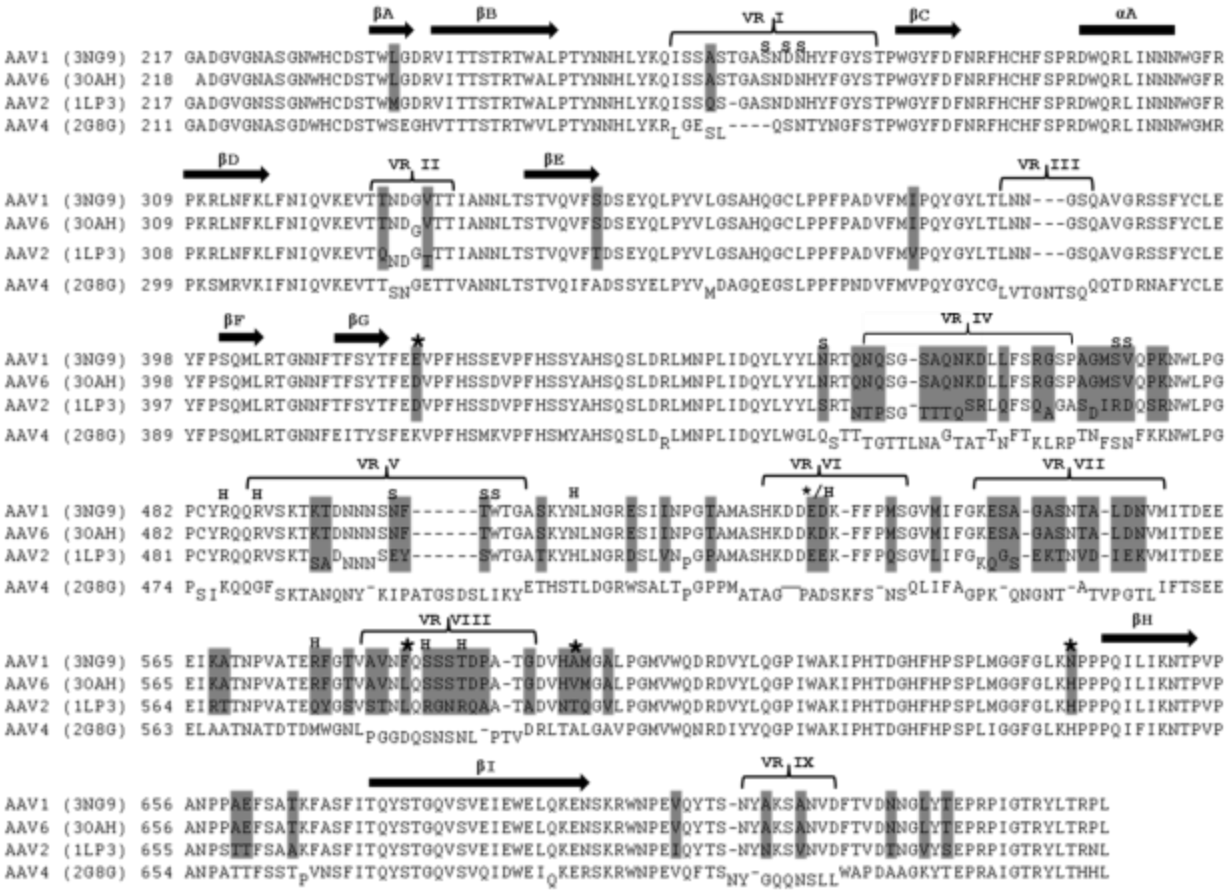

Figure 6-1. Structural alignment of crystallographic ordered VP amino acid sequences (~217-736) of AAV1, AAV2, AAV4 and AAV6. Non-identical amino acids (AAV1, AAV2 and AAV6) are highlighted in the figure. Secondary structure elements are labeled (α-A and βBIDG-βCHEF). Residues which Cα RMSD more than 1.0Å compared to AAV1 are subscripted. Roman numerals indicate residues on variable regions (6). Capsid regions identified for sialic acid (SIA) and heparan sulfate (HS) interactions are labeled (S and H, respectively). Asterisks indicate the different residues between AAV1 and AAV6.

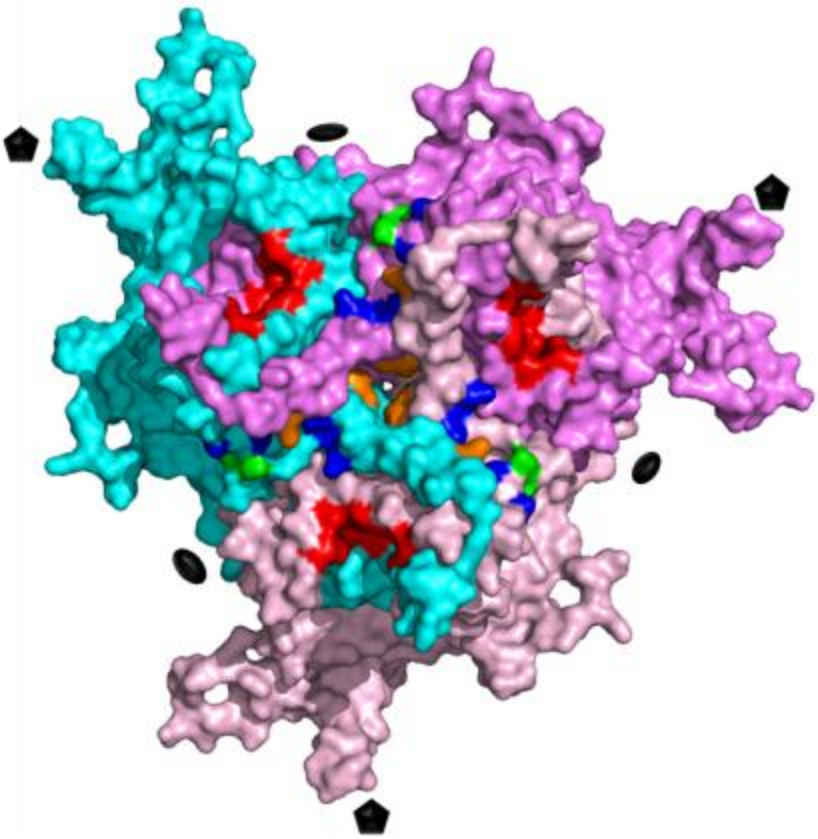

Figure 6-2. Trimer surface representation of AAV6 crystal structure showing glycan interacting regions. Different colors (cyan, purple and light purple) represent different VP monomers. Residue 584 and 598 are colored in orange. K531 is colored green. Heparan sulfate (HS) and sialic acid (SIA) interacting residue are colored as blue and red, respectively. Approximate positions of icosahedral 2-, 3- and 5-fold symmetry axes on the capsid are depicted as oval, triangle and pentagon, respectively.

LIST OF REFERENCES

1. Adams, P. D., P. V. Afonine, G. Bunkoczi, V. B. Chen, I. W. Davis, N. Echols, J. J. Headd, L. W. Hung, G. J. Kapral, R. W. Grosse-Kunstleve, A. J. McCoy, N. W. Moriarty, R. Oeffner, R. J. Read, D. C. Richardson, J. S. Richardson, T. C. Terwilliger, and P. H. Zwart. 2010. PHENIX: a comprehensive Python-based system for macromolecular structure solution. Acta Crystallogr D Biol Crystallogr 66:213-21.

2. Adams, P. D., P. V. Afonine, G. Bunkoczi, V. B. Chen, N. Echols, J. J. Headd, L. W. Hung, S. Jain, G. J. Kapral, R. W. Grosse Kunstleve, A. J. McCoy, N. W. Moriarty, R. D. Oeffner, R. J. Read, D. C. Richardson, J. S. Richardson, T. C. Terwilliger, and P. H. Zwart. 2011. The Phenix software for automated determination of macromolecular structures. Methods 55:94-106.

3. Adams, P. D., R. W. Grosse-Kunstleve, L. W. Hung, T. R. Ioerger, A. J. McCoy, N. W. Moriarty, R. J. Read, J. C. Sacchettini, N. K. Sauter, and T. C. Terwilliger. 2002. PHENIX: building new software for automated crystallographic structure determination. Acta Crystallogr D Biol Crystallogr 58:1948-54.

4. Adrian, M., J. Dubochet, J. Lepault, and A. W. McDowall. 1984. Cryo-electron microscopy of viruses. Nature 308:32-6.

5. Agbandje-Mckenna, M., and M. S. Chapman. 2006. Correlating Structure with Function in the Viral Capsid., p. 125. *In* J. R. Kerr, S. F. Cotmore, B. M.E., R. M. Linden, and C. R. Parrish (ed.), Parvoviruses. Hodder Arnold, New York.

6. Agbandje-McKenna, M., and J. Kleinschmidt. 2011. AAV capsid structure and cell interactions. Methods Mol Biol 807:47-92.

7. Agbandje-McKenna, M., A. L. Llamas-Saiz, F. Wang, P. Tattersall, and M. G. Rossmann. 1998. Functional implications of the structure of the murine parvovirus, minute virus of mice. Structure 6:1369-81.

8. Agbandje, M., R. McKenna, M. G. Rossmann, M. L. Strassheim, and C. R. Parrish. 1993. Structure determination of feline panleukopenia virus empty particles. Proteins 16:155-71.

9. Aiken, C. 1997. Pseudotyping human immunodeficiency virus type 1 (HIV-1) by the glycoprotein of vesicular stomatitis virus targets HIV-1 entry to an endocytic pathway and suppresses both the requirement for Nef and the sensitivity to cyclosporin A. J Virol 71:5871-7.

10. Aiuti, A., F. Cattaneo, S. Galimberti, U. Benninghoff, B. Cassani, L. Callegaro, S. Scaramuzza, G. Andolfi, M. Mirolo, I. Brigida, A. Tabucchi, F. Carlucci, M. Eibl, M. Aker, S. Slavin, H. Al-Mousa, A. Al Ghonaium, A. Ferster, A. Duppenthaler, L. Notarangelo, U. Wintergerst, R. H. Buckley, M. Bregni, S. Marktel, M. G. Valsecchi, P. Rossi, F. Ciceri, R. Miniero, C. Bordignon, and M. G. Roncarolo. 2009. Gene therapy for immunodeficiency due to adenosine deaminase deficiency. N Engl J Med 360:447-58.

11. Aiuti, A., S. Slavin, M. Aker, F. Ficara, S. Deola, A. Mortellaro, S. Morecki, G. Andolfi, A. Tabucchi, F. Carlucci, E. Marinello, F. Cattaneo, S. Vai, P. Servida, R. Miniero, M. G. Roncarolo, and C. Bordignon. 2002. Correction of ADA-SCID by stem cell gene therapy combined with nonmyeloablative conditioning. Science 296:2410-3.

12. Akache, B., D. Grimm, K. Pandey, S. R. Yant, H. Xu, and M. A. Kay. 2006. The 37/67-kilodalton laminin receptor is a receptor for adeno-associated virus serotypes 8, 2, 3, and 9. J Virol 80:9831-6.

13. Akinc, A., M. Thomas, A. M. Klibanov, and R. Langer. 2005. Exploring polyethylenimine-mediated DNA transfection and the proton sponge hypothesis. J Gene Med 7:657-63.

14. Alba, R., A. Bosch, and M. Chillon. 2005. Gutless adenovirus: last-generation adenovirus for gene therapy. Gene Ther 12 Suppl 1:S18-27.

15. Aldawsari, H., B. S. Raj, R. Edrada-Ebel, D. R. Blatchford, R. J. Tate, L. Tetley, and C. Dufes. 2011. Enhanced gene expression in tumors after intravenous administration of arginine-, lysine- and leucine-bearing polyethylenimine polyplex. Nanomedicine 7:615-23.

16. Anderson, L. M., S. Swaminathan, I. Zackon, A. K. Tajuddin, B. Thimmapaya, and S. A. Weitzman. 1999. Adenovirus-mediated tissue-targeted expression of the HSVtk gene for the treatment of breast cancer. Gene Ther 6:854-64.

17. Arbetman, A. E., M. Lochrie, S. Zhou, J. Wellman, C. Scallan, M. M. Doroudchi, B. Randlev, S. Patarroyo-White, T. Liu, P. Smith, H. Lehmkuhl, L. A. Hobbs, G. F. Pierce, and P. Colosi. 2005. Novel caprine adeno-associated virus (AAV) capsid (AAV-Go.1) is closely related to the primate AAV-5 and has unique tropism and neutralization properties. J Virol 79:15238-45.

18. Asokan, A., J. B. Hamra, L. Govindasamy, M. Agbandje-McKenna, and R. J. Samulski. 2006. Adeno-associated virus type 2 contains an integrin alpha5beta1 binding domain essential for viral cell entry. J Virol 80:8961-9.

19. Bahner, I., K. Kearns, Q. L. Hao, E. M. Smogorzewska, and D. B. Kohn. 1996. Transduction of human CD34+ hematopoietic progenitor cells by a retroviral vector expressing an RRE decoy inhibits human immunodeficiency virus type 1 replication in myelomonocytic cells produced in long-term culture. J Virol 70:4352-60.

20. Baker, A., M. Saltik, H. Lehrmann, I. Killisch, V. Mautner, G. Lamm, G. Christofori, and M. Cotten. 1997. Polyethylenimine (PEI) is a simple, inexpensive and effective reagent for condensing and linking plasmid DNA to adenovirus for gene delivery. Gene Ther 4:773-82.

21. Bantel-Schaal, U., I. Braspenning-Wesch, and J. Kartenbeck. 2009. Adeno-associated virus type 5 exploits two different entry pathways in human embryo fibroblasts. J Gen Virol 90:317-22.

22. Bantel-Schaal, U., B. Hub, and J. Kartenbeck. 2002. Endocytosis of adeno-associated virus type 5 leads to accumulation of virus particles in the Golgi compartment. J Virol 76:2340-9.

23. Bartlett, J. S., R. Wilcher, and R. J. Samulski. 2000. Infectious entry pathway of adeno-associated virus and adeno-associated virus vectors. J Virol 74:2777-85.

24. Basak, S., and H. Turner. 1992. Infectious entry pathway for canine parvovirus. Virology 186:368-76.

25. Batshaw, M. L., J. M. Wilson, S. Raper, M. Yudkoff, and M. B. Robinson. 1999. Recombinant adenovirus gene transfer in adults with partial ornithine transcarbamylase deficiency (OTCD). Hum Gene Ther 10:2419-37.

26. Behr, J. P. 1997. The proton sponge: a trick to enter cells the viruses did not exploit. Chimica 51:34-36.

27. Bell, C. L., B. L. Gurda, K. Van Vliet, M. Agbandje-McKenna, and J. M. Wilson. 2012. Identification of the galactose binding domain of the AAV9 capsid. J Virol.

28. Bell, C. L., L. H. Vandenberghe, P. Bell, M. P. Limberis, G. P. Gao, K. Van Vliet, M. Agbandje-McKenna, and J. M. Wilson. 2011. The AAV9 receptor and its modification to improve in vivo lung gene transfer in mice. J Clin Invest 121:2427-35.

29. Bergoin, M., J. Kleinschmidt, J. M. Almendral, K. Hedman, Y. Li, M. Agbandje-Mckenna, P. Tattersall, P. Tijssen, D. J. Pintel, and T. W. Flegel. 2011. Ninth Report of the International Committee on Taxonomy of Viruses, p. 1-1326. *In* A. M. Q. King, M. J. Adams, E. Lefkowitz, and E. B. Carstens (ed.), Virus Taxonomy. Academic Press.

30. Berk, A. J. 2012. Adenoviridae: The Viruses and Their Replication, p. 2355-2394. *In* D. M. Knipe, P. M. Howley, D. E. Griffin, M. A. Martin, R. A. Lamb, S. E. Straus, and B. Roizman (ed.), Fields Virology, 6th Edition ed, vol. 2. Lippincott Williams & Wilkins.

31. Berns, K. I., and C. R. Parrish. 2007. Parvoviridae, p. 2437. *In* D. M. Knipe, P. M. Howley, D. E. Griffin, M. A. Martin, R. A. Lamb, S. E. Straus, and B. Roizman (ed.), Fields Virology. Lippincott Williams & Wilkins.

32. Beutler, A. S. 2010. AAV provides an alternative for gene therapy of the peripheral sensory nervous system. Mol Ther 18:670-3.

33. Bharali, D. J., I. Klejbor, E. K. Stachowiak, P. Dutta, I. Roy, N. Kaur, E. J. Bergey, P. N. Prasad, and M. K. Stachowiak. 2005. Organically modified silica nanoparticles: a nonviral vector for in vivo gene delivery and expression in the brain. Proc Natl Acad Sci U S A 102:11539-44.

34. Biffi, A., C. C. Bartolomae, D. Cesana, N. Cartier, P. Aubourg, M. Ranzani, M. Cesani, F. Benedicenti, T. Plati, E. Rubagotti, S. Merella, A. Capotondo, J. Sgualdino, G. Zanetti, C. von Kalle, M. Schmidt, L. Naldini, and E. Montini. 2011. Lentiviral vector common integration sites in preclinical models and a clinical trial reflect a benign integration bias and not oncogenic selection. Blood 117:5332-9.

35. Biggs, R., A. S. Douglas, R. G. Macfarlane, J. V. Dacie, W. R. Pitney, and Merskey. 1952. Christmas disease: a condition previously mistaken for haemophilia. Br Med J 2:1378-82.

36. Bischoff, J. R., D. H. Kirn, A. Williams, C. Heise, S. Horn, M. Muna, L. Ng, J. A. Nye, A. Sampson-Johannes, A. Fattaey, and F. McCormick. 1996. An adenovirus mutant that replicates selectively in p53-deficient human tumor cells. Science 274:373-6.

37. Blackburn, S. D., R. A. Steadman, and F. B. Johnson. 2006. Attachment of adeno-associated virus type 3H to fibroblast growth factor receptor 1. Arch Virol 151:617-23.

38. Bleker, S., M. Pawlita, and J. A. Kleinschmidt. 2006. Impact of capsid conformation and Rep-capsid interactions on adeno-associated virus type 2 genome packaging. J Virol 80:810-20.

39. Bleker, S., F. Sonntag, and J. A. Kleinschmidt. 2005. Mutational analysis of narrow pores at the fivefold symmetry axes of adeno-associated virus type 2 capsids reveals a dual role in genome packaging and activation of phospholipase A2 activity. J Virol 79:2528-40.

40. Boussif, O., F. Lezoualc'h, M. A. Zanta, M. D. Mergny, D. Scherman, B. Demeneix, and J. P. Behr. 1995. A versatile vector for gene and oligonucleotide transfer into cells in culture and in vivo: polyethylenimine. Proc Natl Acad Sci U S A 92:7297-301.

41. Boutin, S., V. Monteilhet, P. Veron, C. Leborgne, O. Benveniste, M. F. Montus, and C. Masurier. 2010. Prevalence of serum IgG and neutralizing factors against adeno-associated virus (AAV) types 1, 2, 5, 6, 8, and 9 in the healthy population: implications for gene therapy using AAV vectors. Hum Gene Ther 21:704-12.

42. Bowles, D. E., J. E. Rabinowitz, and R. J. Samulski. 2006. The Genus Dependovirus. *In* J. R. Kerr, S. F. Cotmore, B. M.E., R. M. Linden, and C. R. Parrish (ed.), Parvoviruses. Hodder Arnold, London.

43. Boztug, K., M. Schmidt, A. Schwarzer, P. P. Banerjee, I. A. Diez, R. A. Dewey, M. Bohm, A. Nowrouzi, C. R. Ball, H. Glimm, S. Naundorf, K. Kuhlcke, R. Blasczyk, I. Kondratenko, L. Marodi, J. S. Orange, C. von Kalle, and C. Klein. 2010. Stem-cell gene therapy for the Wiskott-Aldrich syndrome. N Engl J Med 363:1918-27.

44. Brady, R. O., J. N. Kanfer, and D. Shapiro. 1965. Metabolism of Glucocerebrosides. Ii. Evidence of an Enzymatic Deficiency in Gaucher's Disease. Biochem Biophys Res Commun 18:221-5.

45. Brown, K. E. 2006. The Genus Erythrovirus, p. 25. *In* J. R. Kerr, S. F. Cotmore, B. M.E., R. M. Linden, and C. R. Parrish (ed.), Parvoviruses. Hodder Arnold.

46. Brownlie, A., I. F. Uchegbu, and A. G. Schatzlein. 2004. PEI-based vesicle-polymer hybrid gene delivery system with improved biocompatibility. Int J Pharm 274:41-52.

47. Brunetti-Pierri, N., and P. Ng. 2008. Progress and prospects: gene therapy for genetic diseases with helper-dependent adenoviral vectors. Gene Ther 15:553-60.

48. Brunger, A. T. 2007. Version 1.2 of the Crystallography and NMR system. Nat Protoc 2:2728-33.

49. Brunger, A. T., P. D. Adams, G. M. Clore, W. L. DeLano, P. Gros, R. W. Grosse-Kunstleve, J. S. Jiang, J. Kuszewski, M. Nilges, N. S. Pannu, R. J. Read, L. M. Rice, T. Simonson, and G. L. Warren. 1998. Crystallography & NMR system: A new software suite for macromolecular structure determination. Acta Crystallogr D Biol Crystallogr 54:905-21.

50. Buch, P. K., J. W. Bainbridge, and R. R. Ali. 2008. AAV-mediated gene therapy for retinal disorders: from mouse to man. Gene Ther 15:849-57.

51. Buckley, R. H. 2002. Gene therapy for SCID--a complication after remarkable progress. Lancet 360:1185-6.

52. Buning, H., S. A. Nicklin, L. Perabo, M. Hallek, and A. H. Baker. 2003. AAV-based gene transfer. Curr Opin Mol Ther 5:367-75.

53. Buning, H., M. U. Ried, L. Perabo, F. M. Gerner, N. A. Huttner, J. Enssle, and M. Hallek. 2003. Receptor targeting of adeno-associated virus vectors. Gene Ther 10:1142-51.

54. Byrnes, A. P. 2005. Challenges and future prospects in gene therapy. IDrugs 8:993-6.

55. Cai, X., S. M. Conley, and M. I. Naash. 2009. RPE65: role in the visual cycle, human retinal disease, and gene therapy. Ophthalmic Genet 30:57-62.

56. Carrillo-Tripp, M., C. M. Shepherd, I. A. Borelli, S. Venkataraman, G. Lander, P. Natarajan, J. E. Johnson, C. L. Brooks, 3rd, and V. S. Reddy. 2009. VIPERdb2: an enhanced and web API enabled relational database for structural virology. Nucleic Acids Res 37:D436-42.

57. Carter, B. J. 2005. Adeno-associated virus vectors in clinical trials. Hum Gene Ther 16:541-50.

58. Cartier, N., S. Hacein-Bey-Abina, C. C. Bartholomae, G. Veres, M. Schmidt, I. Kutschera, M. Vidaud, U. Abel, L. Dal-Cortivo, L. Caccavelli, N. Mahlaoui, V. Kiermer, D. Mittelstaedt, C. Bellesme, N. Lahlou, F. Lefrere, S. Blanche, M. Audit, E. Payen, P. Leboulch, B. l'Homme, P. Bougneres, C. Von Kalle, A. Fischer, M. Cavazzana-Calvo, and P. Aubourg. 2009. Hematopoietic stem cell gene therapy with a lentiviral vector in X-linked adrenoleukodystrophy. Science 326:818-23.

59. Cattoglio, C., G. Facchini, D. Sartori, A. Antonelli, A. Miccio, B. Cassani, M. Schmidt, C. von Kalle, S. Howe, A. J. Thrasher, A. Aiuti, G. Ferrari, A. Recchia, and F. Mavilio. 2007. Hot spots of retroviral integration in human CD34+ hematopoietic cells. Blood 110:1770-8.

60. Cattoglio, C., D. Pellin, E. Rizzi, G. Maruggi, G. Corti, F. Miselli, D. Sartori, A. Guffanti, C. Di Serio, A. Ambrosi, G. De Bellis, and F. Mavilio. 2010. High-definition mapping of retroviral integration sites identifies active regulatory elements in human multipotent hematopoietic progenitors. Blood 116:5507-17.

61. Cereseto, A., and M. Giacca. 2004. Integration site selection by retroviruses. AIDS Rev 6:13-21.

62. Chapman, M. S., and M. Agbandje-McKenna. 2006. Atomic Structures of Viral Particles, p. 107. *In* J. R. Kerr, S. F. Cotmore, B. M.E., R. M. Linden, and C. R. Parrish (ed.), Parvoviruses. Hodder Arnold, New York.

63. Chejanovsky, N., and B. J. Carter. 1989. Mutagenesis of an AUG codon in the adeno-associated virus rep gene: effects on viral DNA replication. Virology 173:120-8.

64. Chen, H., H. Zhang, D. Thor, R. Rahimian, and X. Guo. 2012. Novel pH-sensitive cationic lipids with linear ortho ester linkers for gene delivery. Eur J Med Chem 52:159-72.

65. Chen, K. C., B. C. Shull, E. A. Moses, M. Lederman, E. R. Stout, and R. C. Bates. 1986. Complete nucleotide sequence and genome organization of bovine parvovirus. J Virol 60:1085-97.

66. Chen, V. B., W. B. Arendall, 3rd, J. J. Headd, D. A. Keedy, R. M. Immormino, G. J. Kapral, L. W. Murray, J. S. Richardson, and D. C. Richardson. 2010. MolProbity: all-atom structure validation for macromolecular crystallography. Acta Crystallogr D Biol Crystallogr 66:12-21.

67. Cheng, B., C. Ling, Y. Dai, Y. Lu, L. G. Glushakova, S. W. Gee, K. E. McGoogan, G. V. Aslanidi, M. Park, P. W. Stacpoole, D. Siemann, C. Liu, and A. Srivastava. 2012. Development of optimized AAV3 serotype vectors: mechanism of high-efficiency transduction of human liver cancer cells. Gene Ther 19:375-84.

68. Chiorini, J. A., S. Afione, and R. M. Kotin. 1999. Adeno-associated virus (AAV) type 5 Rep protein cleaves a unique terminal resolution site compared with other AAV serotypes. J Virol 73:4293-8.

69. Chirmule, N., K. Propert, S. Magosin, Y. Qian, R. Qian, and J. Wilson. 1999. Immune responses to adenovirus and adeno-associated virus in humans. Gene Ther 6:1574-83.

70. Chuah, M. K., D. Collen, and T. VandenDriessche. 2004. Clinical gene transfer studies for hemophilia A. Semin Thromb Hemost 30:249-56.

71. Cideciyan, A. V. 2010. Leber congenital amaurosis due to RPE65 mutations and its treatment with gene therapy. Prog Retin Eye Res 29:398-427.

72. Cideciyan, A. V., T. S. Aleman, S. L. Boye, S. B. Schwartz, S. Kaushal, A. J. Roman, J. J. Pang, A. Sumaroka, E. A. Windsor, J. M. Wilson, T. R. Flotte, G. A. Fishman, E. Heon, E. M. Stone, B. J. Byrne, S. G. Jacobson, and W. W. Hauswirth. 2008. Human gene therapy for RPE65 isomerase deficiency activates the retinoid cycle of vision but with slow rod kinetics. Proc Natl Acad Sci U S A 105:15112-7.

73. Collaco, R. F., V. Kalman-Maltese, A. D. Smith, J. D. Dignam, and J. P. Trempe. 2003. A biochemical characterization of the adeno-associated virus Rep40 helicase. J Biol Chem 278:34011-7.

74. Condit, R. C. 2012. Principles of virology. *In* D. M. Knipe, P. M. Howley, D. E. Griffin, M. A. Martin, R. A. Lamb, S. E. Straus, and B. Roizman (ed.), Fields Virology, 6th Edition ed, vol. 1. Lippincott Williams & Wilkins.

75. Cotmore, S. F., and P. Tattersall. 2007. Parvoviral host range and cell entry mechanisms. Adv Virus Res 70:183-232.

76. Cotmore, S. F., and P. Tattersall. 2006. A Rolling-hairpin Strategy: Basic Mechanism of DNA Replication in the Parvoviruses, p. 171. *In* J. R. Kerr, S. F. Cotmore, B. M.E., R. M. Linden, and C. R. Parrish (ed.), Parvoviruses. Hodder Arnold, New York.

77. Cotmore, S. F., and P. Tattersall. 2006. Structure and Organization of the Viral Genome, p. 15. *In* J. R. Kerr, S. F. Cotmore, B. M.E., R. M. Linden, and C. R. Parrish (ed.), Parvoviruses. Hodder Arnold, London.

78. Coura Rdos, S., and N. B. Nardi. 2007. The state of the art of adeno-associated virus-based vectors in gene therapy. Virol J 4:99.

79. Cowtan, K., P. Emsley, and K. S. Wilson. 2011. From crystal to structure with CCP4. Acta Crystallogr D Biol Crystallogr 67:233-4.

80. Daniel, R., and J. A. Smith. 2008. Integration site selection by retroviral vectors: molecular mechanism and clinical consequences. Hum Gene Ther 19:557-68.

81. Danthinne, X., and M. J. Imperiale. 2000. Production of first generation adenovirus vectors: a review. Gene Ther 7:1707-14.

82. Dave, U. P., N. A. Jenkins, and N. G. Copeland. 2004. Gene therapy insertional mutagenesis insights. Science 303:333.

83. Davis, I. W., A. Leaver-Fay, V. B. Chen, J. N. Block, G. J. Kapral, X. Wang, L. W. Murray, W. B. Arendall, 3rd, J. Snoeyink, J. S. Richardson, and D. C. Richardson. 2007. MolProbity: all-atom contacts and structure validation for proteins and nucleic acids. Nucleic Acids Res 35:W375-83.

84. Davis, I. W., L. W. Murray, J. S. Richardson, and D. C. Richardson. 2004. MOLPROBITY: structure validation and all-atom contact analysis for nucleic acids and their complexes. Nucleic Acids Res 32:W615-9.

85. Debreczeni, J. E., and P. Emsley. 2012. Handling ligands with Coot. Acta Crystallogr D Biol Crystallogr 68:425-30.

86. Delano, W. L. 2002. The PyMOL molecular graphics system. *In* D. Scientific (ed.), San Carlos, CA.

87. Descamps, D., and K. Benihoud. 2009. Two key challenges for effective adenovirus-mediated liver gene therapy: innate immune responses and hepatocyte-specific transduction. Curr Gene Ther 9:115-27.

88. Di Pasquale, G., B. L. Davidson, C. S. Stein, I. Martins, D. Scudiero, A. Monks, and J. A. Chiorini. 2003. Identification of PDGFR as a receptor for AAV-5 transduction. Nat Med 9:1306-12.

89. Di Pasquale, G., N. Kaludov, M. Agbandje-McKenna, and J. A. Chiorini. 2010. BAAV transcytosis requires an interaction with beta-1-4 linked- glucosamine and gp96. PLoS One 5:e9336.

90. Di Scipio, R. G., K. Kurachi, and E. W. Davie. 1978. Activation of human factor IX (Christmas factor). J Clin Invest 61:1528-38.

91. Dickey, D. D., K. J. Excoffon, J. T. Koerber, J. Bergen, B. Steines, J. Klesney-Tait, D. V. Schaffer, and J. Zabner. 2011. Enhanced sialic acid-dependent endocytosis explains the increased efficiency of infection of airway epithelia by a novel adeno-associated virus. J Virol 85:9023-30.

92. Dimattia, M. A., H. J. Nam, K. Van Vliet, M. Mitchell, A. Bennett, B. L. Gurda, R. McKenna, N. H. Olson, R. S. Sinkovits, M. Potter, B. J. Byrne, G. Aslanidi, S. Zolotukhin, N. Muzyczka, T. S. Baker, and M. Agbandje-McKenna. 2012. Structural insight into the unique properties of Adeno-Associated Virus Serotype 9. J Virol.

93. DiPrimio, N., A. Asokan, L. Govindasamy, M. Agbandje-McKenna, and R. J. Samulski. 2008. Surface loop dynamics in adeno-associated virus capsid assembly. J Virol 82:5178-89.

94. Douar, A. M., K. Poulard, D. Stockholm, and O. Danos. 2001. Intracellular trafficking of adeno-associated virus vectors: routing to the late endosomal compartment and proteasome degradation. J Virol 75:1824-33.

95. Duan, D., Q. Li, A. W. Kao, Y. Yue, J. E. Pessin, and J. F. Engelhardt. 1999. Dynamin is required for recombinant adeno-associated virus type 2 infection. J Virol 73:10371-6.

96. Duan, D., Y. Yue, Z. Yan, J. Yang, and J. F. Engelhardt. 2000. Endosomal processing limits gene transfer to polarized airway epithelia by adeno-associated virus. J Clin Invest 105:1573-87.

97. Dubielzig, R., J. A. King, S. Weger, A. Kern, and J. A. Kleinschmidt. 1999. Adeno-associated virus type 2 protein interactions: formation of pre-encapsidation complexes. J Virol 73:8989-98.

98. Dubochet, J., M. Adrian, J. J. Chang, J. C. Homo, J. Lepault, A. W. McDowall, and P. Schultz. 1988. Cryo-electron microscopy of vitrified specimens. Q Rev Biophys 21:129-228.

99. Edelstein, M. L., M. R. Abedi, J. Wixon, and R. M. Edelstein. 2004. Gene therapy clinical trials worldwide 1989-2004-an overview. J Gene Med 6:597-602.

100. Edwards, N. L., and I. H. Fox. 1984. Disorders associated with purine and pyrimidine metabolism. Spec Top Endocrinol Metab 6:95-140.

101. Emsley, P., and K. Cowtan. 2004. Coot: model-building tools for molecular graphics. Acta Crystallogr D Biol Crystallogr 60:2126-32.

102. Emsley, P., B. Lohkamp, W. G. Scott, and K. Cowtan. 2010. Features and development of Coot. Acta Crystallogr D Biol Crystallogr 66:486-501.

103. Enquist, I. B., E. Nilsson, A. Ooka, J. E. Mansson, K. Olsson, M. Ehinger, R. O. Brady, J. Richter, and S. Karlsson. 2006. Effective cell and gene therapy in a murine model of Gaucher disease. Proc Natl Acad Sci U S A 103:13819-24.

104. Errington, F., L. Steele, R. Prestwich, K. J. Harrington, H. S. Pandha, L. Vidal, J. de Bono, P. Selby, M. Coffey, R. Vile, and A. Melcher. 2008. Reovirus activates human dendritic cells to promote innate antitumor immunity. J Immunol 180:6018-26.

105. Excoffon, K. J., J. T. Koerber, D. D. Dickey, M. Murtha, S. Keshavjee, B. K. Kaspar, J. Zabner, and D. V. Schaffer. 2009. Directed evolution of adeno-associated virus to an infectious respiratory virus. Proc Natl Acad Sci U S A 106:3865-70.

106. Fisher, A. J., B. R. McKinney, A. Schneemann, R. R. Rueckert, and J. E. Johnson. 1993. Crystallization of viruslike particles assembled from flock house virus coat protein expressed in a baculovirus system. J Virol 67:2950-3.

107. Folkman, J. 1996. Fighting cancer by attacking its blood supply. Sci Am 275:150-4.

108. Freed, E. O., and M. A. Martin. 2012. HIVs and Their Replications, p. 2106-2186. *In* D. M. Knipe, P. M. Howley, D. E. Griffin, M. A. Martin, R. A. Lamb, S. E. Straus, and B. Roizman (ed.), Fields Virology. Lippincott Williams & Wilkins.

109. Friedmann, T., and R. Roblin. 1972. Gene therapy for human genetic disease? Science 175:949-55.

110. Gabriel, N., R. Duraiswamy, R. A. Gadkari, S. Gocindarajan, B. Ramakrishna, A. Srivastava, N. Srinivasan, A. Srivastava, and G. Jayandharan. 2012. Targeted Mutagenesis of Ubiquitin-Binding Lysine Residues on the Adeno-Associated Virus (AAV)2 Capsid Improves Its Transduction Efficiency, p. S146, ASGCT 15th Annual Meeting, vol. 20. Nature Publishing Group, Philadelphia, PA.

111. Gamblin, S. J., L. F. Haire, R. J. Russell, D. J. Stevens, B. Xiao, Y. Ha, N. Vasisht, D. A. Steinhauer, R. S. Daniels, A. Elliot, D. C. Wiley, and J. J. Skehel. 2004. The structure and receptor binding properties of the 1918 influenza hemagglutinin. Science 303:1838-42.

112. Ganly, I., D. Kirn, G. Eckhardt, G. I. Rodriguez, D. S. Soutar, R. Otto, A. G. Robertson, O. Park, M. L. Gulley, C. Heise, D. D. Von Hoff, and S. B. Kaye. 2000. A phase I study of Onyx-015, an E1B attenuated adenovirus, administered intratumorally to patients with recurrent head and neck cancer. Clin Cancer Res 6:798-806.

113. Gao, G., L. H. Vandenberghe, M. R. Alvira, Y. Lu, R. Calcedo, X. Zhou, and J. M. Wilson. 2004. Clades of Adeno-associated viruses are widely disseminated in human tissues. J Virol 78:6381-8.

114. Garlatti, V., A. Chouquet, T. Lunardi, R. Vives, H. Paidassi, H. Lortat-Jacob, N. M. Thielens, G. J. Arlaud, and C. Gaboriaud. 2010. Cutting edge: C1q binds deoxyribose and heparan sulfate through neighboring sites of its recognition domain. J Immunol 185:808-12.

115. Gaucher, P. C. E. 1882. De l'epithelioma primitif de la rate, hypertrophie idiopathique de la rate sans leucemie, Paris, France.

116. Giacca, M. 2010. Gene Therapy, 1st Edition ed. Springer, Milan, Italy.

117. Giacca, M., and S. Zacchigna. 2012. Virus-mediated gene delivery for human gene therapy. J Control Release.

118. Goff, S. 2012. Retroviridae: The RetroViruses and Their Replication, p. 1999-2070. *In* D. M. Knipe, P. M. Howley, D. E. Griffin, M. A. Martin, R. A. Lamb, S. E. Straus, and B. Roizman (ed.), Fileds Virology, 6th Edition ed, vol. 2. Lippincott Williams & Wilkins.

119. Govindasamy, L., E. Padron, R. McKenna, N. Muzyczka, N. Kaludov, J. A. Chiorini, and M. Agbandje-McKenna. 2006. Structurally mapping the diverse phenotype of adeno-associated virus serotype 4. J Virol 80:11556-70.

120. Grieger, J. C., S. Snowdy, and R. J. Samulski. 2006. Separate basic region motifs within the adeno-associated virus capsid proteins are essential for infectivity and assembly. J Virol 80:5199-210.

121. Griesenbach, U., and E. W. Alton. 2012. Progress in gene and cell therapy for cystic fibrosis lung disease. Curr Pharm Des 18:642-62.

122. Griesenbach, U., S. Ferrari, D. M. Geddes, and E. W. Alton. 2002. Gene therapy progress and prospects: cystic fibrosis. Gene Ther 9:1344-50.

123. Grimm, D., and M. A. Kay. 2003. From virus evolution to vector revolution: use of naturally occurring serotypes of adeno-associated virus (AAV) as novel vectors for human gene therapy. Curr Gene Ther 3:281-304.

124. Grimm, D., S. Zhou, H. Nakai, C. E. Thomas, T. A. Storm, S. Fuess, T. Matsushita, J. Allen, R. Surosky, M. Lochrie, L. Meuse, A. McClelland, P. Colosi, and M. A. Kay. 2003. Preclinical in vivo evaluation of pseudotyped adeno-associated virus vectors for liver gene therapy. Blood 102:2412-9.

125. Gunzburg, W. H., and B. Salmons. 1995. Virus vector design in gene therapy. Mol Med Today 1:410-7.

126. Gurda, B. L., K. N. Parent, H. Bladek, R. S. Sinkovits, M. A. DiMattia, C. Rence, A. Castro, R. McKenna, N. Olson, K. Brown, T. S. Baker, and M. Agbandje-McKenna. 2010. Human bocavirus capsid structure: insights into the structural repertoire of the parvoviridae. J Virol 84:5880-9.

127. Hacein-Bey-Abina, S., A. Garrigue, G. P. Wang, J. Soulier, A. Lim, E. Morillon, E. Clappier, L. Caccavelli, E. Delabesse, K. Beldjord, V. Asnafi, E. MacIntyre, L. Dal Cortivo, I. Radford, N. Brousse, F. Sigaux, D. Moshous, J. Hauer, A. Borkhardt, B. H. Belohradsky, U. Wintergerst, M. C. Velez, L. Leiva, R. Sorensen, N. Wulffraat, S. Blanche, F. D. Bushman, A. Fischer, and M. Cavazzana-Calvo. 2008. Insertional oncogenesis in 4 patients after retrovirus-mediated gene therapy of SCID-X1. J Clin Invest 118:3132-42.

128. Hacein-Bey-Abina, S., C. von Kalle, M. Schmidt, F. Le Deist, N. Wulffraat, E. McIntyre, I. Radford, J. L. Villeval, C. C. Fraser, M. Cavazzana-Calvo, and A. Fischer. 2003. A serious adverse event after successful gene therapy for X-linked severe combined immunodeficiency. N Engl J Med 348:255-6.

129. Hacein-Bey-Abina, S., C. Von Kalle, M. Schmidt, M. P. McCormack, N. Wulffraat, P. Leboulch, A. Lim, C. S. Osborne, R. Pawliuk, E. Morillon, R. Sorensen, A. Forster, P. Fraser, J. I. Cohen, G. de Saint Basile, I. Alexander, U. Wintergerst, T. Frebourg, A. Aurias, D. Stoppa-Lyonnet, S. Romana, I. Radford-Weiss, F. Gross, F. Valensi, E. Delabesse, E. Macintyre, F. Sigaux, J. Soulier, L. E. Leiva, M. Wissler, C. Prinz, T. H. Rabbitts, F. Le Deist, A. Fischer, and M. Cavazzana-Calvo. 2003. LMO2-associated clonal T cell proliferation in two patients after gene therapy for SCID-X1. Science 302:415-9.

130. Halbert, C. L., J. M. Allen, and A. D. Miller. 2001. Adeno-associated virus type 6 (AAV6) vectors mediate efficient transduction of airway epithelial cells in mouse lungs compared to that of AAV2 vectors. J Virol 75:6615-24.

131. Halbert, C. L., A. D. Miller, S. McNamara, J. Emerson, R. L. Gibson, B. Ramsey, and M. L. Aitken. 2006. Prevalence of neutralizing antibodies against adeno-associated virus (AAV) types 2, 5, and 6 in cystic fibrosis and normal populations: Implications for gene therapy using AAV vectors. Hum Gene Ther 17:440-7.

132. Halder, S., R. Ng, and M. Agbandje-McKenna. 2012. Parvoviruses: structure and infection. Future Virology 7:253-278.

133. Hansen, J., K. Qing, and A. Srivastava. 2001. Adeno-associated virus type 2-mediated gene transfer: altered endocytic processing enhances transduction efficiency in murine fibroblasts. J Virol 75:4080-90.

134. Hansen, J., K. Qing, and A. Srivastava. 2001. Infection of purified nuclei by adeno-associated virus 2. Mol Ther 4:289-96.

135. Harbison, C. E., J. A. Chiorini, and C. R. Parrish. 2008. The parvovirus capsid odyssey: from the cell surface to the nucleus. Trends Microbiol 16:208-14.

136. Hasan, A., H. Ghebeh, C. Lehe, R. Ahmad, and S. Dermime. 2011. Therapeutic targeting of B7-H1 in breast cancer. Expert Opin Ther Targets 15:1211-25.

137. Hauck, B., and W. Xiao. 2003. Characterization of tissue tropism determinants of adeno-associated virus type 1. J Virol 77:2768-74.

138. Hauswirth, W. W., T. S. Aleman, S. Kaushal, A. V. Cideciyan, S. B. Schwartz, L. Wang, T. J. Conlon, S. L. Boye, T. R. Flotte, B. J. Byrne, and S. G. Jacobson. 2008. Treatment of leber congenital amaurosis due to RPE65 mutations by ocular subretinal injection of adeno-associated virus gene vector: short-term results of a phase I trial. Hum Gene Ther 19:979-90.

139. Heise, C., A. Sampson-Johannes, A. Williams, F. McCormick, D. D. Von Hoff, and D. H. Kirn. 1997. ONYX-015, an E1B gene-attenuated adenovirus, causes tumor-specific cytolysis and antitumoral efficacy that can be augmented by standard chemotherapeutic agents. Nat Med 3:639-45.

140. Heller, R., S. Shirley, S. Guo, A. Donate, and L. Heller. 2011. Electroporation based gene therapy--from the bench to the bedside. Conf Proc IEEE Eng Med Biol Soc 2011:736-8.

141. Hernando, E., A. L. Llamas-Saiz, C. Foces-Foces, R. McKenna, I. Portman, M. Agbandje-McKenna, and J. M. Almendral. 2000. Biochemical and physical characterization of parvovirus minute virus of mice virus-like particles. Virology 267:299-309.

142. Holscher, C., J. A. Kleinschmidt, and A. Burkle. 1995. High-level expression of adeno-associated virus (AAV) Rep78 or Rep68 protein is sufficient for infectious-particle formation by a rep-negative AAV mutant. J Virol 69:6880-5.

143. Hong, Y. B., E. Y. Kim, H. W. Yoo, and S. C. Jung. 2004. Feasibility of gene therapy in Gaucher disease using an adeno-associated virus vector. J Hum Genet 49:536-43.

144. Hooft, R. W., C. Sander, and G. Vriend. 1997. Objectively judging the quality of a protein structure from a Ramachandran plot. Comput Appl Biosci 13:425-30.

145. Huang, L., and E. Viroonchatapan. 1999. Introduction, p. 4-17. *In* L. Huang, M.-C. Hung, and E. Wagner (ed.), Nonviral Vectors for Gene Therapy, 1st Edition ed. Academic Press, New York.

146. Inoue, K., P. Perrotte, C. G. Wood, J. W. Slaton, P. Sweeney, and C. P. Dinney. 2000. Gene therapy of human bladder cancer with adenovirus-mediated antisense basic fibroblast growth factor. Clin Cancer Res 6:4422-31.

147. Jacobson, E. R., W. Kopit, F. A. Kennedy, and R. S. Funk. 1996. Coinfection of a bearded dragon, Pogona vitticeps, with adenovirus- and dependovirus-like viruses. Vet Pathol 33:343-6.

148. Jiang, H., D. Lillicrap, S. Patarroyo-White, T. Liu, X. Qian, C. D. Scallan, S. Powell, T. Keller, M. McMurray, A. Labelle, D. Nagy, J. A. Vargas, S. Zhou, L. B. Couto, and G. F. Pierce. 2006. Multiyear therapeutic benefit of AAV serotypes 2, 6, and 8 delivering factor VIII to hemophilia A mice and dogs. Blood 108:107-15.

149. Johnson, J. S., M. Gentzsch, L. Zhang, C. M. Ribeiro, B. Kantor, T. Kafri, R. J. Pickles, and R. J. Samulski. 2011. AAV exploits subcellular stress associated with inflammation, endoplasmic reticulum expansion, and misfolded proteins in models of cystic fibrosis. PLoS Pathog 7:e1002053.

150. Johnson, J. S., C. Li, N. DiPrimio, M. S. Weinberg, T. J. McCown, and R. J. Samulski. 2010. Mutagenesis of adeno-associated virus type 2 capsid protein VP1 uncovers new roles for basic amino acids in trafficking and cell-specific transduction. J Virol 84:8888-902.

151. Johnson, J. S., and R. J. Samulski. 2009. Enhancement of adeno-associated virus infection by mobilizing capsids into and out of the nucleolus. J Virol 83:2632-44.

152. Jones, T. A., and S. Thirup. 1986. Using known substructures in protein model building and crystallography. EMBO J 5:819-22.

153. Kaludov, N., K. E. Brown, R. W. Walters, J. Zabner, and J. A. Chiorini. 2001. Adeno-associated virus serotype 4 (AAV4) and AAV5 both require sialic acid binding for hemagglutination and efficient transduction but differ in sialic acid linkage specificity. J Virol 75:6884-93.

154. Karmali, P. P., and D. Simberg. 2011. Interactions of nanoparticles with plasma proteins: implication on clearance and toxicity of drug delivery systems. Expert Opin Drug Deliv 8:343-57.

155. Kashiwakura, Y., K. Tamayose, K. Iwabuchi, Y. Hirai, T. Shimada, K. Matsumoto, T. Nakamura, M. Watanabe, K. Oshimi, and H. Daida. 2005. Hepatocyte growth factor receptor is a coreceptor for adeno-associated virus type 2 infection. J Virol 79:609-14.

156. Katano, H., S. Afione, M. Schmidt, and J. A. Chiorini. 2004. Identification of adeno-associated virus contamination in cell and virus stocks by PCR. Biotechniques 36:676-80.

157. Kaufmann, B., P. R. Chipman, V. A. Kostyuchenko, S. Modrow, and M. G. Rossmann. 2008. Visualization of the externalized VP2 N termini of infectious human parvovirus B19. J Virol 82:7306-12.

158. Kaufmann, B., A. A. Simpson, and M. G. Rossmann. 2004. The structure of human parvovirus B19. Proc Natl Acad Sci U S A 101:11628-33.

159. Keating, A., and F. Toneguzzo. 1990. Gene transfer by electroporation: a model for gene therapy. Prog Clin Biol Res 333:491-8.

160. Kern, A., K. Schmidt, C. Leder, O. J. Muller, C. E. Wobus, K. Bettinger, C. W. Von der Lieth, J. A. King, and J. A. Kleinschmidt. 2003. Identification of a heparin-binding motif on adeno-associated virus type 2 capsids. J Virol 77:11072-81.

161. Khuri, F. R., J. Nemunaitis, I. Ganly, J. Arseneau, I. F. Tannock, L. Romel, M. Gore, J. Ironside, R. H. MacDougall, C. Heise, B. Randlev, A. M. Gillenwater, P. Bruso, S. B. Kaye, W. K. Hong, and D. H. Kirn. 2000. a controlled trial of intratumoral ONYX-015, a selectively-replicating adenovirus, in combination with cisplatin and 5-fluorouracil in patients with recurrent head and neck cancer. Nat Med 6:879-85.

162. Kichler, A., J. P. Behr, and P. Erbacher. 1999. Polyethylamines: A Family of Polymers for Nucleic Acid Delivery, p. 192-199. *In* L. Huang, M.-C. Hung, and E. Wagner (ed.), Nonviral Vectors for Gene Therapy, 1st Edition ed. Academic Press, New York.

163. King, J. A., R. Dubielzig, D. Grimm, and J. A. Kleinschmidt. 2001. DNA helicase-mediated packaging of adeno-associated virus type 2 genomes into preformed capsids. EMBO J 20:3282-91.

164. Kirn, D. 2001. Oncolytic virotherapy for cancer with the adenovirus dl1520 (Onyx-015): results of phase I and II trials. Expert Opin Biol Ther 1:525-38.

165. Klimczak, R. R., J. T. Koerber, D. Dalkara, J. G. Flannery, and D. V. Schaffer. 2009. A novel adeno-associated viral variant for efficient and selective intravitreal transduction of rat Muller cells. PLoS One 4:e7467.

166. Kogure, K., R. Moriguchi, K. Sasaki, M. Ueno, S. Futaki, and H. Harashima. 2004. Development of a non-viral multifunctional envelope-type nano device by a novel lipid film hydration method. J Control Release 98:317-23.

167. Kohn, D. B., M. Sadelain, and J. C. Glorioso. 2003. Occurrence of leukaemia following gene therapy of X-linked SCID. Nat Rev Cancer 3:477-88.

168. Kontou, M., L. Govindasamy, H. J. Nam, N. Bryant, A. L. Llamas-Saiz, C. Foces-Foces, E. Hernando, M. P. Rubio, R. McKenna, J. M. Almendral, and M. Agbandje-McKenna. 2005. Structural determinants of tissue tropism and in vivo pathogenicity for the parvovirus minute virus of mice. J Virol 79:10931-43.

169. Koonin, E. V., T. G. Senkevich, and V. V. Dolja. 2006. The ancient Virus World and evolution of cells. Biol Direct 1:29.

170. Kotchey, N. M., K. Adachi, M. Zahid, K. Inagaki, R. Charan, R. S. Parker, and H. Nakai. 2011. A potential role of distinctively delayed blood clearance of recombinant adeno-associated virus serotype 9 in robust cardiac transduction. Mol Ther 19:1079-89.

171. Kronenberg, S., B. Bottcher, C. W. von der Lieth, S. Bleker, and J. A. Kleinschmidt. 2005. A conformational change in the adeno-associated virus type 2 capsid leads to the exposure of hidden VP1 N termini. J Virol 79:5296-303.

172. Kronenberg, S., J. A. Kleinschmidt, and B. Bottcher. 2001. Electron cryo-microscopy and image reconstruction of adeno-associated virus type 2 empty capsids. EMBO Rep 2:997-1002.

173. Lacerda, S. H., J. J. Park, C. Meuse, D. Pristinski, M. L. Becker, A. Karim, and J. F. Douglas. 2010. Interaction of gold nanoparticles with common human blood proteins. ACS Nano 4:365-79.

174. Lairmore, M. D., and G. Franchini. 2012. Human T Cell Leukemia Virus Type 1 and 2, p. 2071-2106. *In* D. M. Knipe, P. M. Howley, D. E. Griffin, M. A. Martin, R. A. Lamb, S. E. Straus, and B. Roizman (ed.), Fields Virology, 6th Edition ed, vol. 2. Lippincott Williams & Wilkins.

175. Lang, P. T., S. R. Brozell, S. Mukherjee, E. F. Pettersen, E. C. Meng, V. Thomas, R. C. Rizzo, D. A. Case, T. L. James, and I. D. Kuntz. 2009. DOCK 6: combining techniques to model RNA-small molecule complexes. RNA 15:1219-30.

176. Lasic, D. D. 1999. Structure and Structure-Activity Relationships of Lipid-Based Gene Delivery Systems, p. 69-87. *In* L. Huang, M.-C. Hung, and E. Wagner (ed.), Nonviral Vectors for Gene Therapy, 1st Edition ed. Academic Press, New York.

177. Lee, K. M., I. S. Kim, Y. B. Lee, S. C. Shin, K. C. Lee, and I. J. Oh. 2005. Evaluation of transferrin-polyethylenimine conjugate for targeted gene delivery. Arch Pharm Res 28:722-9.

178. Lehrman, S. 1999. Virus treatment questioned after gene therapy death. Nature 401:517-8.

179. Lerch, T. F., and M. S. Chapman. 2011. Identification of the heparin binding site on adeno-associated virus serotype 3B (AAV-3B). virology 423:6-13.

180. Lerch, T. F., Q. Xie, and M. S. Chapman. 2010. The structure of adeno-associated virus serotype 3B (AAV-3B): insights into receptor binding and immune evasion. Virology 403:26-36.

181. Lesterhuis, W. J., J. B. Haanen, and C. J. Punt. 2011. Cancer immunotherapy--revisited. Nat Rev Drug Discov 10:591-600.

182. Lever, A. M., J. F. Kaye, E. McCann, D. Chadwick, N. Dorman, J. Thomas, and J. Zhao. 1999. Lentivirus vectors for gene therapy. Biochem Soc Trans 27:841-7.

183. Levy, H. C., V. D. Bowman, L. Govindasamy, R. McKenna, K. Nash, K. Warrington, W. Chen, N. Muzyczka, X. Yan, T. S. Baker, and M. Agbandje-McKenna. 2009. Heparin binding induces conformational changes in Adeno-associated virus serotype 2. J Struct Biol 165:146-56.

184. Li, S. D., and L. Huang. 2006. Gene therapy progress and prospects: non-viral gene therapy by systemic delivery. Gene Ther 13:1313-9.

185. Li, W., A. Asokan, Z. Wu, T. Van Dyke, N. DiPrimio, J. S. Johnson, L. Govindaswamy, M. Agbandje-McKenna, S. Leichtle, D. E. Redmond, Jr., T. J. McCown, K. B. Petermann, N. E. Sharpless, and R. J. Samulski. 2008. Engineering and selection of shuffled AAV genomes: a new strategy for producing targeted biological nanoparticles. Mol Ther 16:1252-60.

186. Li, W., L. Zhang, J. S. Johnson, W. Zhijian, J. C. Grieger, X. Ping-Jie, L. M. Drouin, M. Agbandje-McKenna, R. J. Pickles, and R. J. Samulski. 2009. Generation of novel AAV variants by directed evolution for improved CFTR delivery to human ciliated airway epithelium. Mol Ther 17:2067-77.

187. Limberis, M. P., L. H. Vandenberghe, L. Zhang, R. J. Pickles, and J. M. Wilson. 2009. Transduction efficiencies of novel AAV vectors in mouse airway epithelium in vivo and human ciliated airway epithelium in vitro. Mol Ther 17:294-301.

188. Ling, C., Y. Lu, J. K. Kalsi, G. R. Jayandharan, B. Li, W. Ma, B. Cheng, S. W. Gee, K. E. McGoogan, L. Govindasamy, L. Zhong, M. Agbandje-McKenna, and A. Srivastava. 2010. Human hepatocyte growth factor receptor is a cellular coreceptor for adeno-associated virus serotype 3. Hum Gene Ther 21:1741-7.

189. Liu, L., S. Wang, B. Shan, M. Sang, S. Liu, and G. Wang. 2010. Advances in viral-vector systemic cytokine gene therapy against cancer. Vaccine 28:3883-7.

190. Liu, Q., and D. A. Muruve. 2003. Molecular basis of the inflammatory response to adenovirus vectors. Gene Ther 10:935-40.

191. Llamas-Saiz, A. L., M. Agbandje-McKenna, W. R. Wikoff, J. Bratton, P. Tattersall, and M. G. Rossmann. 1997. Structure determination of minute virus of mice. Acta Crystallogr D Biol Crystallogr 53:93-102.

192. Lochrie, M. A., G. P. Tatsuno, A. E. Arbetman, K. Jones, C. Pater, P. H. Smith, J. W. McDonnell, S. Z. Zhou, S. Kachi, M. Kachi, P. A. Campochiaro, G. F. Pierce, and P. Colosi. 2006. Adeno-associated virus (AAV) capsid genes isolated from rat and mouse liver genomic DNA define two new AAV species distantly related to AAV-5. Virology 353:68-82.

193. Lochrie, M. A., G. P. Tatsuno, B. Christie, J. W. McDonnell, S. Zhou, R. Surosky, G. F. Pierce, and P. Colosi. 2006. Mutations on the external surfaces of adeno-associated virus type 2 capsids that affect transduction and neutralization. J Virol 80:821-34.

194. Loimas, S., M. R. Toppinen, T. Visakorpi, J. Janne, and J. Wahlfors. 2001. Human prostate carcinoma cells as targets for herpes simplex virus thymidine kinase-mediated suicide gene therapy. Cancer Gene Ther 8:137-44.

195. MacGregor, R. R. 2001. Clinical protocol. A phase 1 open-label clinical trial of the safety and tolerability of single escalating doses of autologous CD4 T cells transduced with VRX496 in HIV-positive subjects. Hum Gene Ther 12:2028-9.

196. Maguire, A. M., F. Simonelli, E. A. Pierce, E. N. Pugh, Jr., F. Mingozzi, J. Bennicelli, S. Banfi, K. A. Marshall, F. Testa, E. M. Surace, S. Rossi, A. Lyubarsky, V. R. Arruda, B. Konkle, E. Stone, J. Sun, J. Jacobs, L. Dell'Osso, R. Hertle, J. X. Ma, T. M. Redmond, X. Zhu, B. Hauck, O. Zelenaia, K. S. Shindler, M. G. Maguire, J. F. Wright, N. J. Volpe, J. W. McDonnell, A. Auricchio, K. A. High, and J. Bennett. 2008. Safety and efficacy of gene transfer for Leber's congenital amaurosis. N Engl J Med 358:2240-8.

197. Manfredsson, F. P., A. C. Rising, and R. J. Mandel. 2009. AAV9: a potential blood-brain barrier buster. Mol Ther 17:403-5.

198. Manilla, P., T. Rebello, C. Afable, X. Lu, V. Slepushkin, L. M. Humeau, K. Schonely, Y. Ni, G. K. Binder, B. L. Levine, R. R. MacGregor, C. H. June, and B. Dropulic. 2005. Regulatory considerations for novel gene therapy products: a review of the process leading to the first clinical lentiviral vector. Hum Gene Ther 16:17-25.

199. Mansilla-Soto, J., M. Yoon-Robarts, W. J. Rice, S. Arya, C. R. Escalante, and R. M. Linden. 2009. DNA structure modulates the oligomerization properties of the AAV initiator protein Rep68. PLoS Pathog 5:e1000513.

200. Marlhens, F., C. Bareil, J. M. Griffoin, E. Zrenner, P. Amalric, C. Eliaou, S. Y. Liu, E. Harris, T. M. Redmond, B. Arnaud, M. Claustres, and C. P. Hamel. 1997. Mutations in RPE65 cause Leber's congenital amaurosis. Nat Genet 17:139-41.

201. Marshall, E. 1999. Gene therapy death prompts review of adenovirus vector. Science 286:2244-5.

202. McCarty, D. M., T. H. Ni, and N. Muzyczka. 1992. Analysis of mutations in adeno-associated virus Rep protein in vivo and in vitro. J Virol 66:4050-7.

203. McCarty, D. M., D. J. Pereira, I. Zolotukhin, X. Zhou, J. H. Ryan, and N. Muzyczka. 1994. Identification of linear DNA sequences that specifically bind the adeno-associated virus Rep protein. J Virol 68:4988-97.

204. McCarty, D. M., J. H. Ryan, S. Zolotukhin, X. Zhou, and N. Muzyczka. 1994. Interaction of the adeno-associated virus Rep protein with a sequence within the A palindrome of the viral terminal repeat. J Virol 68:4998-5006.

205. McCormack, M. P., and T. H. Rabbitts. 2004. Activation of the T-cell oncogene LMO2 after gene therapy for X-linked severe combined immunodeficiency. N Engl J Med 350:913-22.

206. McCormick, F. 2000. Interactions between adenovirus proteins and the p53 pathway: the development of ONYX-015. Semin Cancer Biol 10:453-9.

207. McKenna, R., N. H. Olson, P. R. Chipman, T. S. Baker, T. F. Booth, J. Christensen, B. Aasted, J. M. Fox, M. E. Bloom, J. B. Wolfinbarger, and M. Agbandje-McKenna. 1999. Three-dimensional structure of Aleutian mink disease parvovirus: implications for disease pathogenicity. J Virol 73:6882-91.

208. McKenna, R., D. Xia, P. Willingmann, L. L. Ilag, S. Krishnaswamy, M. G. Rossmann, N. H. Olson, T. S. Baker, and N. L. Incardona. 1992. Atomic structure of single-stranded DNA bacteriophage phi X174 and its functional implications. Nature 355:137-43.

209. Michelfelder, S., and M. Trepel. 2009. Adeno-associated viral vectors and their redirection to cell-type specific receptors. Adv Genet 67:29-60.

210. Miller, D. G., M. A. Adam, and A. D. Miller. 1990. Gene transfer by retrovirus vectors occurs only in cells that are actively replicating at the time of infection. Mol Cell Biol 10:4239-42.

211. Miller, E. A., L. J. Smith, K. Van Vliet, K. K. Wong, M. Agbandje-McKenna, and S. Chatterjee. 2012. Role of AAVHSC15 Capsid Elements in In-Vivo Liver Transduction, p. S7, ASGCT 15th Annual Meeting, vol. 20. Nature Publishing Group, Philadelphia, PA.

212. Miller, E. B., B. Gurda-Whitaker, L. Govindasamy, R. McKenna, S. Zolotukhin, N. Muzyczka, and M. Agbandje-McKenna. 2006. Production, purification and preliminary X-ray crystallographic studies of adeno-associated virus serotype 1. Acta Crystallogr Sect F Struct Biol Cryst Commun 62:1271-4.

213. Mingozzi, F., and K. A. High. 2011. Therapeutic in vivo gene transfer for genetic disease using AAV: progress and challenges. Nat Rev Genet 12:341-55.

214. Minor, W., M. Cymborowski, Z. Otwinowski, and M. Chruszcz. 2006. HKL-3000: the integration of data reduction and structure solution--from diffraction images to an initial model in minutes. Acta Crystallogr D Biol Crystallogr 62:859-66.

215. Miyake, K., K. Inokuchi, N. Miyake, K. Dan, and T. Shimada. 2007. HIV vector-mediated targeted suicide gene therapy for adult T-cell leukemia. Gene Ther 14:1662-7.

216. Morgan, R. A., and W. F. Anderson. 1993. Human gene therapy. Annu Rev Biochem 62:191-217.

217. Mueller, C., and T. R. Flotte. 2008. Clinical gene therapy using recombinant adeno-associated virus vectors. Gene Ther 15:858-63.

218. Mulvihill, S., R. Warren, A. Venook, A. Adler, B. Randlev, C. Heise, and D. Kirn. 2001. Safety and feasibility of injection with an E1B-55 kDa gene-deleted, replication-selective adenovirus (ONYX-015) into primary carcinomas of the pancreas: a phase I trial. Gene Ther 8:308-15.

219. Munyon, W., E. Kraiselburd, D. Davis, and J. Mann. 1971. Transfer of thymidine kinase to thymidine kinaseless L cells by infection with ultraviolet-irradiated herpes simplex virus. J Virol 7:813-20.

220. Muruve, D. A. 2004. The innate immune response to adenovirus vectors. Hum Gene Ther 15:1157-66.

221. Naldini, L., U. Blomer, P. Gallay, D. Ory, R. Mulligan, F. H. Gage, I. M. Verma, and D. Trono. 1996. In vivo gene delivery and stable transduction of nondividing cells by a lentiviral vector. Science 272:263-7.

222. Nam, H. J., B. L. Gurda, R. McKenna, M. Potter, B. Byrne, M. Salganik, N. Muzyczka, and M. Agbandje-McKenna. 2011. Structural studies of adeno-associated virus serotype 8 capsid transitions associated with endosomal trafficking. J Virol 85:11791-9.

223. Nam, H. J., M. D. Lane, E. Padron, B. Gurda, R. McKenna, E. Kohlbrenner, G. Aslanidi, B. Byrne, N. Muzyczka, S. Zolotukhin, and M. Agbandje-McKenna. 2007. Structure of adeno-associated virus serotype 8, a gene therapy vector. J Virol 81:12260-71.

224. Nemunaitis, J., F. Khuri, I. Ganly, J. Arseneau, M. Posner, E. Vokes, J. Kuhn, T. McCarty, S. Landers, A. Blackburn, L. Romel, B. Randlev, S. Kaye, and D. Kirn. 2001. Phase II trial of intratumoral administration of ONYX-015, a replication-selective adenovirus, in patients with refractory head and neck cancer. J Clin Oncol 19:289-98.

225. Ng, R., L. Govindasamy, B. L. Gurda, R. McKenna, O. G. Kozyreva, R. J. Samulski, K. N. Parent, T. S. Baker, and M. Agbandje-McKenna. 2010. Structural characterization of the dual glycan binding adeno-associated virus serotype 6. J Virol 84:12945-57.

226. Nguyen, H. K., P. Lemieux, S. V. Vinogradov, C. L. Gebhart, N. Guerin, G. Paradis, T. K. Bronich, V. Y. Alakhov, and A. V. Kabanov. 2000. Evaluation of polyether-polyethyleneimine graft copolymers as gene transfer agents. Gene Ther 7:126-38.

227. Noguiez-Hellin, P., M. R. Meur, J. L. Salzmann, and D. Klatzmann. 1996. Plasmoviruses: nonviral/viral vectors for gene therapy. Proc Natl Acad Sci U S A 93:4175-80.

228. O'Donnell, J., K. A. Taylor, and M. S. Chapman. 2009. Adeno-associated virus-2 and its primary cellular receptor--Cryo-EM structure of a heparin complex. Virology 385:434-43.

229. Olia, A. S., P. E. Prevelige, Jr., J. E. Johnson, and G. Cingolani. 2011. Three-dimensional structure of a viral genome-delivery portal vertex. Nat Struct Mol Biol 18:597-603.

230. Opie, S. R., K. H. Warrington, Jr., M. Agbandje-McKenna, S. Zolotukhin, and N. Muzyczka. 2003. Identification of amino acid residues in the capsid proteins of adeno-associated virus type 2 that contribute to heparan sulfate proteoglycan binding. J Virol 77:6995-7006.

231. Owens, R. A., M. D. Weitzman, S. R. Kyostio, and B. J. Carter. 1993. Identification of a DNA-binding domain in the amino terminus of adeno-associated virus Rep proteins. J Virol 67:997-1005.

232. Padron, E., V. Bowman, N. Kaludov, L. Govindasamy, H. Levy, P. Nick, R. McKenna, N. Muzyczka, J. A. Chiorini, T. S. Baker, and M. Agbandje-McKenna. 2005. Structure of adeno-associated virus type 4. J Virol 79:5047-58.

233. Pan, J. G., X. Zhou, R. Luo, and R. F. Han. 2011. The adeno-associated virus-mediated HSV-TK/GCV suicide system: a potential strategy for the treatment of bladder carcinoma. Med Oncol.

234. Parker, J. S., and C. R. Parrish. 2000. Cellular uptake and infection by canine parvovirus involves rapid dynamin-regulated clathrin-mediated endocytosis, followed by slower intracellular trafficking. J Virol 74:1919-30.

235. Parks, R. J., L. Chen, M. Anton, U. Sankar, M. A. Rudnicki, and F. L. Graham. 1996. A helper-dependent adenovirus vector system: removal of helper virus by Cre-mediated excision of the viral packaging signal. Proc Natl Acad Sci U S A 93:13565-70.

236. Parrish, C. R. 2006. Autonomous Parvovirus Variation and Evolution, p. 27. *In* J. R. Kerr, S. F. Cotmore, B. M.E., R. M. Linden, and C. R. Parrish (ed.), Parvoviruses. Hodder Arnold.

237. Pettersen, E. F., T. D. Goddard, C. C. Huang, G. S. Couch, D. M. Greenblatt, E. C. Meng, and T. E. Ferrin. 2004. UCSF Chimera-a visualization system for exploratory research and analysis. . J. Comput. Chem 25:1605-1612.

238. Pires, P., S. Simoes, S. Nir, R. Gaspar, N. Duzgunes, and M. C. Pedroso de Lima. 1999. Interaction of cationic liposomes and their DNA complexes with monocytic leukemia cells. Biochim Biophys Acta 1418:71-84.

239. Plank, C., U. Schillinger, F. Scherer, C. Bergemann, J. S. Remy, F. Krotz, M. Anton, J. Lausier, and J. Rosenecker. 2003. The magnetofection method: using magnetic force to enhance gene delivery. Biol Chem 384:737-47.

240. Ponder, K. P. 2011. Merry christmas for patients with hemophilia B. N Engl J Med 365:2424-5.

241. Preuss, E., A. Muik, K. Weber, J. Otte, D. von Laer, and B. Fehse. 2011. Cancer suicide gene therapy with TK.007: superior killing efficiency and bystander effect. J Mol Med (Berl) 89:1113-24.

242. Prijic, S., L. Prosen, M. Cemazar, J. Scancar, R. Romih, J. Lavrencak, V. B. Bregar, A. Coer, M. Krzan, A. Znidarsic, and G. Sersa. 2012. Surface modified magnetic nanoparticles for immuno-gene therapy of murine mammary adenocarcinoma. Biomaterials 33:4379-91.

243. Pulicherla, N., S. Shen, S. Yadav, K. Debbink, L. Govindasamy, M. Agbandje-McKenna, and A. Asokan. 2011. Engineering liver-detargeted AAV9 vectors for cardiac and musculoskeletal gene transfer. Mol Ther 19:1070-8.

244. Qing, K., C. Mah, J. Hansen, S. Zhou, V. Dwarki, and A. Srivastava. 1999. Human fibroblast growth factor receptor 1 is a co-receptor for infection by adeno-associated virus 2. Nat Med 5:71-7.

245. Qiu, J., F. Cheng, and D. Pintel. 2006. Molecular characterization of caprine adeno-associated virus (AAV-Go.1) reveals striking similarity to human AAV5. Virology 356:208-16.

246. Quesada, O., B. Gurda, L. Govindasamy, R. McKenna, E. Kohlbrenner, G. Aslanidi, S. Zolotukhin, N. Muzyczka, and M. Agbandje-McKenna. 2007. Production, purification and preliminary X-ray crystallographic studies of adeno-associated virus serotype 7. Acta Crystallogr Sect F Struct Biol Cryst Commun 63:1073-6.

247. Rabinowitz, J. E., F. Rolling, C. Li, H. Conrath, W. Xiao, X. Xiao, and R. J. Samulski. 2002. Cross-packaging of a single adeno-associated virus (AAV) type 2 vector genome into multiple AAV serotypes enables transduction with broad specificity. J Virol 76:791-801.

248. Ratjen, F., and G. Doring. 2003. Cystic fibrosis. Lancet 361:681-9.

249. Richter, S. N., I. Frasson, and G. Palu. 2009. Strategies for inhibiting function of HIV-1 accessory proteins: a necessary route to AIDS therapy? Curr Med Chem 16:267-86.

250. Rolling, F. 2010. AAV-mediated gene therapy for the treatment of retinal diseases. Curr Gene Ther 10:318.

251. Ros, C., C. Baltzer, B. Mani, and C. Kempf. 2006. Parvovirus uncoating in vitro reveals a mechanism of DNA release without capsid disassembly and striking differences in encapsidated DNA stability. Virology 345:137-47.

252. Ros, C., C. J. Burckhardt, and C. Kempf. 2002. Cytoplasmic trafficking of minute virus of mice: low-pH requirement, routing to late endosomes, and proteasome interaction. J Virol 76:12634-45.

253. Rosenberg, S. A., P. Aebersold, K. Cornetta, A. Kasid, R. A. Morgan, R. Moen, E. M. Karson, M. T. Lotze, J. C. Yang, S. L. Topalian, and et al. 1990. Gene transfer into humans--immunotherapy of patients with advanced melanoma, using tumor-infiltrating lymphocytes modified by retroviral gene transduction. N Engl J Med 323:570-8.

254. Rothmann, T., A. Hengstermann, N. J. Whitaker, M. Scheffner, and H. zur Hausen. 1998. Replication of ONYX-015, a potential anticancer adenovirus, is independent of p53 status in tumor cells. J Virol 72:9470-8.

255. Rutledge, E. A., C. L. Halbert, and D. W. Russell. 1998. Infectious clones and vectors derived from adeno-associated virus (AAV) serotypes other than AAV type 2. J Virol 72:309-19.

256. Sanlioglu, S., P. K. Benson, J. Yang, E. M. Atkinson, T. Reynolds, and J. F. Engelhardt. 2000. Endocytosis and nuclear trafficking of adeno-associated virus type 2 are controlled by rac1 and phosphatidylinositol-3 kinase activation. J Virol 74:9184-96.

257. Sasaki, K., K. Kogure, S. Chaki, Y. Nakamura, R. Moriguchi, H. Hamada, R. Danev, K. Nagayama, S. Futaki, and H. Harashima. 2008. An artificial virus-like nano carrier system: enhanced endosomal escape of nanoparticles via synergistic action of pH-sensitive fusogenic peptide derivatives. Anal Bioanal Chem 391:2717-27.

258. Schmidt, M., L. Govindasamy, S. Afione, N. Kaludov, M. Agbandje-McKenna, and J. A. Chiorini. 2008. Molecular characterization of the heparin-dependent transduction domain on the capsid of a novel adeno-associated virus isolate, AAV(VR-942). J Virol 82:8911-6.

259. Schmitz, V., M. Kornek, T. Hilbert, C. Dzienisowicz, E. Raskopf, C. Rabe, T. Sauerbruch, C. Qian, and W. H. Caselmann. 2005. Treatment of metastatic colorectal carcinomas by systemic inhibition of vascular endothelial growth factor signaling in mice. World J Gastroenterol 11:4332-6.

260. Schneider-Schaulies, J. 2000. Cellular receptors for viruses: links to tropism and pathogenesis. J Gen Virol 81:1413-29.

261. Schneidman-Duhovny, D., Y. Inbar, R. Nussinov, and H. J. Wolfson. 2005. PatchDock and SymmDock: servers for rigid and symmetric docking. Nucleic Acids Res 33:W363-7.

262. Schuttelkopf, A. W., and D. M. van Aalten. 2004. PRODRG: a tool for high-throughput crystallography of protein-ligand complexes. Acta Crystallogr D Biol Crystallogr 60:1355-63.

263. Seiler, M. P., A. D. Miller, J. Zabner, and C. L. Halbert. 2006. Adeno-associated virus types 5 and 6 use distinct receptors for cell entry. Hum Gene Ther 17:10-9.

264. Shen, S., K. D. Bryant, S. M. Brown, S. H. Randell, and A. Asokan. 2011. Terminal N-linked galactose is the primary receptor for adeno-associated virus 9. J Biol Chem 286:13532-40.

265. Shen, X., T. Storm, and M. A. Kay. 2007. Characterization of the relationship of AAV capsid domain swapping to liver transduction efficiency. Mol Ther 15:1955-62.

266. Simpson, A. A., B. Hebert, G. M. Sullivan, C. R. Parrish, Z. Zadori, P. Tijssen, and M. G. Rossmann. 2002. The structure of porcine parvovirus: comparison with related viruses. J Mol Biol 315:1189-98.

267. Sinn, P. L., S. L. Sauter, and P. B. McCray, Jr. 2005. Gene therapy progress and prospects: development of improved lentiviral and retroviral vectors--design, biosafety, and production. Gene Ther 12:1089-98.

268. Smith, R. H., and R. M. Kotin. 2000. An adeno-associated virus (AAV) initiator protein, Rep78, catalyzes the cleavage and ligation of single-stranded AAV ori DNA. J Virol 74:3122-9.

269. Sonntag, F., S. Bleker, B. Leuchs, R. Fischer, and J. A. Kleinschmidt. 2006. Adeno-associated virus type 2 capsids with externalized VP1/VP2 trafficking domains are generated prior to passage through the cytoplasm and are maintained until uncoating occurs in the nucleus. J Virol 80:11040-54.

270. Sonntag, F., K. Kother, K. Schmidt, M. Weghofer, C. Raupp, K. Nieto, A. Kuck, B. Gerlach, B. Bottcher, O. J. Muller, K. Lux, M. Horer, and J. A. Kleinschmidt. 2011. The assembly-activating protein promotes capsid assembly of different adeno-associated virus serotypes. J Virol 85:12686-97.

271. Sonntag, F., K. Schmidt, and J. A. Kleinschmidt. 2010. A viral assembly factor promotes AAV2 capsid formation in the nucleolus. Proc Natl Acad Sci U S A 107:10220-5.

272. Stahnke, S., K. Lux, S. Uhrig, F. Kreppel, M. Hosel, O. Coutelle, M. Ogris, M. Hallek, and H. Buning. 2011. Intrinsic phospholipase A2 activity of adeno-associated virus is involved in endosomal escape of incoming particles. Virology 409:77-83.

273. Steele, T. A. 2000. Recent developments in the virus therapy of cancer. Proc Soc Exp Biol Med 223:118-27.

274. Summerford, C., J. S. Bartlett, and R. J. Samulski. 1999. AlphaVbeta5 integrin: a co-receptor for adeno-associated virus type 2 infection. Nat Med 5:78-82.

275. Summerford, C., and R. J. Samulski. 1998. Membrane-associated heparan sulfate proteoglycan is a receptor for adeno-associated virus type 2 virions. J Virol 72:1438-45.

276. Sun, Y., A. Y. Chen, F. Cheng, W. Guan, F. B. Johnson, and J. Qiu. 2009. Molecular characterization of infectious clones of the minute virus of canines reveals unique features of bocaviruses. J Virol 83:3956-67.

277. Susa, T., T. Kato, and Y. Kato. 2008. Reproducible transfection in the presence of carrier DNA using FuGENE6 and Lipofectamine2000. Mol Biol Rep 35:313-9.

278. Suzuki, Y., and R. Craigie. 2007. The road to chromatin - nuclear entry of retroviruses. Nat Rev Microbiol 5:187-96.

279. Swisher, S. G., J. A. Roth, J. Nemunaitis, D. D. Lawrence, B. L. Kemp, C. H. Carrasco, D. G. Connors, A. K. El-Naggar, F. Fossella, B. S. Glisson, W. K. Hong, F. R. Khuri, J. M. Kurie, J. J. Lee, J. S. Lee, M. Mack, J. A. Merritt, D. M. Nguyen, J. C. Nesbitt, R. Perez-Soler, K. M. Pisters, J. B. Putnam, Jr., W. R. Richli, M. Savin, D. S. Schrump, D. M. Shin, A. Shulkin, G. L. Walsh, J. Wait, D. Weill, and M. K. Waugh. 1999. Adenovirus-mediated p53 gene transfer in advanced non-small-cell lung cancer. J Natl Cancer Inst 91:763-71.

280. Tang, G. P., J. M. Zeng, S. J. Gao, Y. X. Ma, L. Shi, Y. Li, H. P. Too, and S. Wang. 2003. Polyethylene glycol modified polyethylenimine for improved CNS gene transfer: effects of PEGylation extent. Biomaterials 24:2351-62.

281. Thompson, L. F., and J. E. Seegmiller. 1980. Adenosine deaminase deficiency and severe combined immunodeficiency disease. Adv Enzymol Relat Areas Mol Biol 51:167-210.

282. Tong, L., and M. G. Rossmann. 1997. Rotation function calculations with GLRF program. Methods Enzymol 276:594-611.

283. Trapani, S., and J. Navaza. 2008. AMoRe: classical and modern. Acta Crystallogr D Biol Crystallogr 64:11-6.

284. Tsao, J., M. S. Chapman, M. Agbandje, W. Keller, K. Smith, H. Wu, M. Luo, T. J. Smith, M. G. Rossmann, R. W. Compans, and et al. 1991. The three-dimensional structure of canine parvovirus and its functional implications. Science 251:1456-64.

285. Uhrig, S., O. Coutelle, T. Wiehe, L. Perabo, M. Hallek, and H. Buning. 2012. Successful target cell transduction of capsid-engineered rAAV vectors requires clathrin-dependent endocytosis. Gene Ther 19:210-8.

286. Urzhumtseva, L., P. V. Afonine, P. D. Adams, and A. Urzhumtsev. 2009. Crystallographic model quality at a glance. Acta Crystallogr D Biol Crystallogr 65:297-300.

287. van Aalten, D. M., R. Bywater, J. B. Findlay, M. Hendlich, R. W. Hooft, and G. Vriend. 1996. PRODRG, a program for generating molecular topologies and unique molecular descriptors from coordinates of small molecules. J Comput Aided Mol Des 10:255-62.

288. van Heel, M., and M. Schatz. 2005. Fourier shell correlation threshold criteria. J Struct Biol 151:250-62.

289. Vihinen-Ranta, M., A. Kalela, P. Makinen, L. Kakkola, V. Marjomaki, and M. Vuento. 1998. Intracellular route of canine parvovirus entry. J Virol 72:802-6.

290. Wagner, D. E., and S. B. Bhaduri. 2012. Progress and outlook of inorganic nanoparticles for delivery of nucleic acid sequences related to orthopedic pathologies: a review. Tissue Eng Part B Rev 18:1-14.

291. Walters, R. W., M. Agbandje-McKenna, V. D. Bowman, T. O. Moninger, N. H. Olson, M. Seiler, J. A. Chiorini, T. S. Baker, and J. Zabner. 2004. Structure of adeno-associated virus serotype 5. J Virol 78:3361-71.

292. Walters, R. W., S. M. Yi, S. Keshavjee, K. E. Brown, M. J. Welsh, J. A. Chiorini, and J. Zabner. 2001. Binding of adeno-associated virus type 5 to 2,3-linked sialic acid is required for gene transfer. J Biol Chem 276:20610-6.

293. Wang, Q., and M. H. Finer. 1996. Second-generation adenovirus vectors. Nat Med 2:714-6.

294. Wang, Z. X., H. B. Bian, J. S. Yang, W. De, and X. H. Ji. 2009. Adenovirus-mediated suicide gene therapy under the control of Cox-2 promoter for colorectal cancer. Cancer Biol Ther 8:1480-8.

295. Ward, P., N. Clement, and R. M. Linden. 2007. cis effects in adeno-associated virus type 2 replication. J Virol 81:9976-89.

296. Wasungu, L., and D. Hoekstra. 2006. Cationic lipids, lipoplexes and intracellular delivery of genes. J Control Release 116:255-64.

297. Wei, W., Y. Mu, X. Li, M. Gou, H. Zhang, S. Luo, K. Men, Y. Mao, Z. Qian, and L. Yang. 2011. Adenoviral vectors modified by heparin-polyethyleneimine nanogels enhance targeting to the lung and show therapeutic potential for pulmonary metastasis in vivo. J Biomed Nanotechnol 7:768-75.

298. Weller, M. L., P. Amornphimoltham, M. Schmidt, P. A. Wilson, J. S. Gutkind, and J. A. Chiorini. 2010. Epidermal growth factor receptor is a co-receptor for adeno-associated virus serotype 6. Nat Med 16:662-4.

299. Whiteside, T. L. 2010. Inhibiting the inhibitors: evaluating agents targeting cancer immunosuppression. Expert Opin Biol Ther 10:1019-35.

300. Winn, M. D., C. C. Ballard, K. D. Cowtan, E. J. Dodson, P. Emsley, P. R. Evans, R. M. Keegan, E. B. Krissinel, A. G. Leslie, A. McCoy, S. J. McNicholas, G. N. Murshudov, N. S. Pannu, E. A. Potterton, H. R. Powell, R. J. Read, A. Vagin, and K. S. Wilson. 2011. Overview of the CCP4 suite and current developments. Acta Crystallogr D Biol Crystallogr 67:235-42.

301. Wobus, C. E., B. Hugle-Dorr, A. Girod, G. Petersen, M. Hallek, and J. A. Kleinschmidt. 2000. Monoclonal antibodies against the adeno-associated virus type 2 (AAV-2) capsid: epitope mapping and identification of capsid domains involved in AAV-2-cell interaction and neutralization of AAV-2 infection. J Virol 74:9281-93.

302. Wold, W. S. M., and M. S. Horwitz. 2012. Adenovirus, p. 2395-2436. *In* D. M. Knipe, P. M. Howley, D. E. Griffin, M. A. Martin, R. A. Lamb, S. E. Straus, and B. Roizman (ed.), Fields Virology, vol. 2. Lippincott Williams & Wilkins.

303. Wriggers, W., R. A. Milligan, and J. A. McCammon. 1999. Situs: A package for docking crystal structures into low-resolution maps from electron microscopy. J Struct Biol 125:185-95.

304. Wu, H., W. Keller, and M. G. Rossmann. 1993. Determination and refinement of the canine parvovirus empty-capsid structure. Acta Crystallogr D Biol Crystallogr 49:572-9.

305. Wu, P., W. Xiao, T. Conlon, J. Hughes, M. Agbandje-McKenna, T. Ferkol, T. Flotte, and N. Muzyczka. 2000. Mutational analysis of the adeno-associated virus type 2 (AAV2) capsid gene and construction of AAV2 vectors with altered tropism. J Virol 74:8635-47.

306. Wu, Z., A. Asokan, J. C. Grieger, L. Govindasamy, M. Agbandje-McKenna, and R. J. Samulski. 2006. Single amino acid changes can influence titer, heparin binding, and tissue tropism in different adeno-associated virus serotypes. J Virol 80:11393-7.

307. Wu, Z., E. Miller, M. Agbandje-McKenna, and R. J. Samulski. 2006. Alpha2,3 and alpha2,6 N-linked sialic acids facilitate efficient binding and transduction by adeno-associated virus types 1 and 6. J Virol 80:9093-103.

308. Xiang, J. J., J. Q. Tang, S. G. Zhu, X. M. Nie, H. B. Lu, S. R. Shen, X. L. Li, K. Tang, M. Zhou, and G. Y. Li. 2003. IONP-PLL: a novel non-viral vector for efficient gene delivery. J Gene Med 5:803-17.

309. Xiao, C., and M. G. Rossmann. 2007. Interpretation of electron density with stereographic roadmap projections. J. Struct. Biol. 158:182-187.

310. Xiao, W., K. H. Warrington, Jr., P. Hearing, J. Hughes, and N. Muzyczka. 2002. Adenovirus-facilitated nuclear translocation of adeno-associated virus type 2. J Virol 76:11505-17.

311. Xie, Q., W. Bu, S. Bhatia, J. Hare, T. Somasundaram, A. Azzi, and M. S. Chapman. 2002. The atomic structure of adeno-associated virus (AAV-2), a vector for human gene therapy. Proc Natl Acad Sci U S A 99:10405-10.

312. Xie, Q., T. F. Lerch, N. L. Meyer, and M. S. Chapman. 2011. Structure-function analysis of receptor-binding in adeno-associated virus serotype 6 (AAV-6). Virology 420:10-9.

313. Xie, Q., T. Somasundaram, S. Bhatia, W. Bu, and M. S. Chapman. 2003. Structure determination of adeno-associated virus 2: three complete virus particles per asymmetric unit. Acta Crystallogr D Biol Crystallogr 59:959-70.

314. Yamauchi, J., Y. Hayashi, K. Kajimoto, H. Akita, and H. Harashima. 2010. Comparison between a multifunctional envelope-type nano device and lipoplex for delivery to the liver. Biol Pharm Bull 33:926-9.

315. Yan, X., R. S. Sinkovits, and T. S. Baker. 2007. AUTO3DEM--an automated and high throughput program for image reconstruction of icosahedral particles. J Struct Biol 157:73-82.

316. Yang, Q., and J. P. Trempe. 1993. Analysis of the terminal repeat binding abilities of mutant adeno-associated virus replication proteins. J Virol 67:4442-7.

317. Yee, J. K., T. Friedmann, and J. C. Burns. 1994. Generation of high-titer pseudotyped retroviral vectors with very broad host range. Methods Cell Biol 43 Pt A:99-112.

318. Yoon-Robarts, M., and R. M. Linden. 2003. Identification of active site residues of the adeno-associated virus type 2 Rep endonuclease. J Biol Chem 278:4912-8.

319. Youjin, S., and Y. Jun. 2009. The treatment of hemophilia A: from protein replacement to AAV-mediated gene therapy. Biotechnol Lett 31:321-8.

320. Zadori, Z., J. Szelei, M. C. Lacoste, Y. Li, S. Gariepy, P. Raymond, M. Allaire, I. R. Nabi, and P. Tijssen. 2001. A viral phospholipase A2 is required for parvovirus infectivity. Dev Cell 1:291-302.

321. Zhao, J., Y. Guo, Z. Yan, J. Zhang, Y. Bushkin, and P. Liang. 2011. Soluble MHC I and soluble MIC molecules: potential therapeutic targets for cancer. Int Rev Immunol 30:35-43.

322. Zhdanov, R. I., O. V. Podobed, and V. V. Vlassov. 2002. Cationic lipid-DNA complexes-lipoplexes-for gene transfer and therapy. Bioelectrochemistry 58:53-64.

323. Zhong, L., B. Li, G. Jayandharan, C. S. Mah, L. Govindasamy, M. Agbandje-McKenna, R. W. Herzog, K. A. Weigel-Van Aken, J. A. Hobbs, S. Zolotukhin, N. Muzyczka, and A. Srivastava. 2008. Tyrosine-phosphorylation of AAV2 vectors and its consequences on viral intracellular trafficking and transgene expression. Virology 381:194-202.

324. Zhong, L., B. Li, C. S. Mah, L. Govindasamy, M. Agbandje-McKenna, M. Cooper, R. W. Herzog, I. Zolotukhin, K. H. Warrington, Jr., K. A. Weigel-Van Aken, J. A. Hobbs, S. Zolotukhin, N. Muzyczka, and A. Srivastava. 2008. Next generation of adeno-associated virus 2 vectors: point mutations in tyrosines lead to high-efficiency transduction at lower doses. Proc Natl Acad Sci U S A 105:7827-32.

325. Zhong, L., S. Li, M. Li, J. Xie, Q. Su, R. He, Y. Zhang, H. Li, J. Goetzmann, T. Flotte, and G. Gao. 2012. Critical Amino Acid Residues Contribute to Crossing Vascular Barier, p. S6, ASGCT 15th Annual Meeting, vol. 20. Nature Publlishing Group, Philadephia, PA.

326. Zincarelli, C., S. Soltys, G. Rengo, and J. E. Rabinowitz. 2008. Analysis of AAV serotypes 1-9 mediated gene expression and tropism in mice after systemic injection. Mol Ther 16:1073-80.

327. Zolotukhin, S., M. Potter, I. Zolotukhin, Y. Sakai, S. Loiler, T. J. Fraites, Jr., V. A. Chiodo, T. Phillipsberg, N. Muzyczka, W. W. Hauswirth, T. R. Flotte, B. J. Byrne, and R. O. Snyder. 2002. Production and purification of serotype 1, 2, and 5 recombinant adeno-associated viral vectors. Methods 28:158-67.

BIOGRAPHICAL SKETCH

Robert Ng was born in 1984 in Medan, Indonesia. He spent most of his childhood and schooling years in Medan. He completed his high school education at Sutomo-1, Medan in 2002. Towards the later years of his high school education, he became very interested in biotechnology, and wanted to study abroad and become a scientist. After graduating from high school, he enrolled in Bachelors in Science (B.Sc.) at National Taiwan University, Taipei, Taiwan and graduated in 2006 with an honor in agricultural chemistry. During this time he conducted two-year research at National Taiwan University, Taipei, taiwan gaining experience in molecular biology and proteomics techniques under the guidance of Dr. Whi-Fin Wu. This experience kindled within him a keen interest for further research. He then continued to do his master in biochemistry and molecular biology at University of Florida, Gainesville, FL. During his master's program Robert developed deep passion for serious scientific research and work under the supervision of Dr. Thomas O'Brien, he was working on the characterization of interactions between mitochondria ribosomal proteins. Without completion of his master's program, Robert decided to explore new, broader and better opportunities and decided to apply to the PhD degree in Interdisciplinary program (IDP) in University of Florida. In the fall of 2007 he started the IDP program and spent his first year completing the core courses and lab rotations, finally began research as a graduate assistant in Agbandje-McKenna Laboratory in summer 2008. While pursuing his PhD program Robert started working under the supervision of Dr. Mavis Agbandje-McKenna (Professor, Department of Biochemistry and Molecular Biology, UFL). Robert was initiated to some very interesting and challenging problems in the field of virus crystallography and cryo-electron microscopy reconstruction.